CHARACTERISTICS AND POZZOLANIC REACTIVITY OF REACTIVE TREATED RICE STRAW ASH (TRSA) FOR INTERFACIAL TRANSITIONAL ZONE (ITZ) IMPROVEMENT IN CEMENT MORTAR

BY

AIDA NABILA BINTI JAMALUDDIN

A thesis submitted in fulfillment of the requirement for the degree of Master of Science in Engineering.

Kulliyyah of Engineering

International Islamic University Malaysia

APRIL 2024

ABSTRACT

For utilizing rice straw as pozzolan in the mortar production, it is required to develop an amorphous silica rich material to replace cement. At the same time, it is an excellent alternative, instead of burning the rice straw after the harvesting process. Silica is a beneficial additive to cement mix by accelerating the cement hydration process due to its high reactivity to improve the mortar strength. Thus, the research aims to develop rice straw ash (RSA) as a highly reactive silica-rich pozzolan. This study focuses on extracting the high amorphous silica through thermochemical pretreatment using a low concentration of hydrochloric acid (HCl) and continued with the incineration process at a controlled temperature. The response surface methodology (RSM) through the Design Expert software was used to determine the sample number involved in the thermochemical pretreatment and incineration process since both processes had a few factors with a large range. Then, the treated RSA (TRSA) undergoing the grinding process using a ball mill. Lastly, the minimum amount of TRSA was evaluated in the mortar with partial replacement levels varying from 1% to 5. As a result, the TRSA is a highly reactive pozzolan since the total percentage of reactive compound content (silicon dioxide (SiO_2), aluminium oxide (Al_2O_3), and iron (III) oxide (Fe_2O_3)) fulfilled the ASTM C618 standard requirement (>70%) when treated using 0.06 M of HCl solution heated at 70℃ for about 2 hours and incinerated at 600℃ for about 1 hour. TRSA was achieved to be an amorphous silica rich pozzolan through XRD and FTIR analysis. TEM analysis also conducted and further confirmed the TRSA had a high amorphous silica content. TRSA with the nano-sized (4.505 nm to 6.278 nm) in the high amorphous silica state produces a good pozzolan and causes an excellent pozzolanic reaction in developing the mortar strength. The strength activity index (SAI) test for pozzolanic reactivity proves the TRSA meets the requirement of ASTM C311, having more than 75% of the SAI value. In addition, the composition of 4% TRSA as cement replacement material was the highest and improved by 60.27% in mortar strength and ITZ gap compared to the conventional mortar throughout 90 days. Overall, the strength of TRSA-based cement mortar showed an excellent performance compared to the conventional mortar and non-treated RSA (NTRSA). Hence, the TRSA is considered a high-quality pozzolanic material incorporated with a small amount of concrete production.

ملخص البحث

لاستخدام قش الأرز كالبوزولان في إنتاج الملاط، يلزم تطوير مادة غنية بالسيليكا غير المتبلورة لتحل محل الأسمنت. في الوقت نفسه، هو بديل ممتاز، بدلا من حرق قش الأرز بعد عملية الحصاد .تعتبر السيليكا مادة مضافة مفيدة لخليط الأسمنت عن طريق تسريع عملية ترطيب الأسمنت بسبب تفاعلها العالي لتحسين قوة الملاط. وبالتالي، يهدف البحث إلى تطوير رماد قش الأرز باعتباره بوزولان عالي التفاعل وغني بالسيليكا. تركز هذه الدراسة على استخلاص السيليكا غير المتبلورة العالية من خلال المعالجة الحرارية الكيميائية باستخدام تركيز منخفض من حمض الهيدر وكلوريك وتستمر عملية الترميد عند درجة حرارة متحكم فيها .تم استخدام منهجية سطح الاستجابة من خلال برنامج خبير التصميم لتحديد رقم العينة المشاركة في عملية المعالجة والحرق الكيميائية الحرارية نظرًا لأن كلا العمليتين لهما عوامل قليلة ذات نطاق كبير.بعد ذلك، يخضع رماد قش الأرز المعالج لعملية الطحن باستخدام مطحنة كروية .وأخيرًا، تم تقييم الحد الأدنى من رماد قش الأرز المعالج في الملاط بمستويات استبدال جزئي تتراوح من ١% إلى ٥ %.ونتيجة لذلك، يعتبر رماد قش الأرز المعالج عبارة عن بوزولان شديد التفاعل لأن النسبة المئوية الإجمالية لمحتوى المركب التفاعلي (ثاني أكسيد السيليكون وأكسيد الألومنيوم وأكسيد الحديد) تلبي متطلبات معيار الجمعية الأمريكية للاختبار والمواد >(٧٠ %) عند معالجته بمحلول ٠.٠٦ مولار وتم تسخين حمض الهيدر وكلوريك عند ٧٠ درجة مئوية لمدة ساعتين تقريبًا، ثم يتم حرقها عند ٦٠٠ درجة مئوية لمدة ساعة تقريبًا .تم التحقق من أن رماد قش الأرز المعالج عبارة عن بوزولان غير متبلور غني بالسيليكا عن طريق تحليل حيود الأشعة السينية ومطيافية تحويل فورييه للأشعة تحتالحمراء .تم إجراء تحليل المجهر الإلكتروني للإرسال أيضًا وأكد أيضًا أن رماد قش الأرز المعالج يحتوي على نسبة عالية من السيليكا غير المتبلورة. رماد قش الأرز المعالج بحجم النانو (٤.٥٠٥ نانومتر إلى ٦.٢٧٨) نانومتر في حالة السيليكا غير المتبلورة العالية ينتج بوزولان جيد ويسبب تفاعل بوزولاني ممتاز في تطوير قوة الملاط

APPROVAL PAGE

I certify that I have supervised and read this study and that in my opinion, it conforms to acceptable standards of scholarly presentation and is fully adequate, in scope and quality, as a thesis for the degree of Master of Science in Engineering.

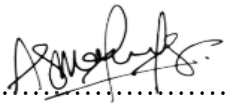

…….
Siti Asmahani Saad
Supervisor

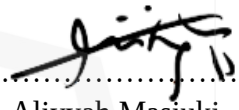

…….
Siti Aliyyah Masjuki
Co-Supervisor

I certify that I have read this study and that in my opinion it conforms to acceptable standards of scholarly presentation and is fully adequate, in scope and quality, as a thesis for the degree of Master of Science in Engineering.

…….
Wan Nur Firdaus Wan Hassan
Internal Examiner

…….
Hamidah Mohd Saman @ Hj. Mohamed
External Examiner

This thesis was submitted to the Department of Civil Engineering and is accepted as a fulfilment of the requirement for the degree of Master of Science in Engineering.

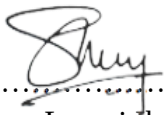

…….

Saerahany Legori Ibrahim
Head, Department of Civil Engineering

This thesis was submitted to the Kulliyyah of Engineering and is accepted as a fulfillment of the requirement for the degree of Master of Science in Engineering.

…….

Khairul Azami Sidek
Dean, Kulliyyah of Engineering

DECLARATION

I hereby declare that this thesis is the result of my own investigations, except where otherwise stated. I also declare that it has not been previously or concurrently submitted as a whole for any other degrees at IIUM or other institutions.

Aida Nabila Jamaluddin

Signature…… Date……01/04/2024……

INTERNATIONAL ISLAMIC UNIVERSITY MALAYSIA

DECLARATION OF COPYRIGHT AND AFFIRMATION OF FAIR USE OF UNPUBLISHED RESEARCH

CHARACTERISTICS AND POZZOLANIC REACTIVITY OF REACTIVE TREATED RICE STRAW ASH (TRSA) FOR INTERFACIAL TRANSITIONAL ZONE (ITZ) IMPROVEMENT IN CEMENT MORTAR

I declare that the copyright holder of this thesis is jointly owned by the student and IIUM.

By signing this form, I acknowledged that I have read and understand the IIUM Intellectual Property Right and Commercialization policy.

Affirmed by Aida Nabila Jamaluddin

…… Signature

….01/04/2024….. Date

This thesis is dedicated to:

My mother (Hamidah Binti Ibrahim) for laying the foundation of what I turned out to be in life and never fail even once to pray for my success in life

and

my siblings (Nurul Asyhikin, Muhammad Syaiful Azhar, Muhammad Hafiz Syahmi, and Muhammad Taufik Hidayat) for believing in me

and

all lecturers for their guidance

ACKNOWLEDGEMENTS

All praise is due to Allah, SWT the Almighty, whose Grace and Mercies have been with me throughout my study.

I am most indebted to my supervisor, Dr. Siti Asmahani Saad, and my co-supervisor, Dr. Siti Aliyyah Masjuki, those who pushed me hard to overcome the difficulties of this study with all their knowledge, experience, and critical thinking. I put on record and appreciate their detailed comments, valuable suggestions, and inspiring queries, which have considerably improved this thesis.

I appreciate the moral and financial support of my beloved mother and siblings, who have encouraged and supported me whenever I faced problems throughout my study. They always are my backbone through thick and thin in this journey.

Thanks, and gratitude goes to all the lecturers of Civil Engineering who help me a lot upon completing my project for guiding and helping me use the equipment during my laboratory work. A special thanks to my friends, especially Mudrikah Sofia, for her countless valuable opinion regarding this research work, Najlah Sakinah, Nurain Asrin, and Farah Salwana for your support of this research.

TABLE OF CONTENTS

LIST OF TABLES

LIST OF FIGURES

LIST OF EQUATIONS

LIST OF SYMBOLS

ºC	Degree Celsius
%	Per cent

LIST OF ABBREVIATIONS

AAS	Atomic Absorption Spectrophotometer
Al	Aluminium
Al_2O_3	Aluminium Oxide
Al-O	Alumina Bond
ASTM	American Society for Testing and Materials
BBD	Box-Behnken Design
BET	Brunauer-Emmet-Teller
BJH	Barret-Joyner-Halenda
BS	British Standard
C	Carbon
C/S	Cement to Sand
C_3S	Tricalcium Silicate
Ca^{2+}	Calcium Cation
CaO	Calcium Oxide
CaOH	Calcium Hydroxide
CCD	Central Composite Design
CEM-I	Ordinary Portland Cement
Cl	Chlorine
CNC	Cellulose Nanocrystals
CO_2	Carbon Dioxide
CRM	Cement Replacement Material
C-S-H	Calcium Silicate Hydrated
EN	European Standard
Fe_2O_3	Iron (III) Oxide
FESEM	Field Emission Scanning Electron Microscopy
FTIR	Fourier Transforms Infrared Spectroscopy

H_2O	Water
$H2SiO^{-2}$	Silicic Acid
H_2SO_4	Sulphuric Acid
HCl	Hydrochloric Acid
HNO_3	Nitric Acid
ITZ	Interfacial Transitional Zone
IUPAC	International Union of Pure and Applied Chemistry
K_2O	Potassium Oxide
K_2SiO_3	Potassium Polysilicate
MgO	Magnesium Oxide
Na_2O	Sodium Dioxide
NaOH	Sodium Hydroxide
NH_3	Ammonia
NTRSA	Non-Treated Rice Straw Ash
O_2	Oxygen
OH^-	Hydroxide Ion
OPC	Ordinary Portland Cement
P_2O_5	Phosphorus Pentoxide
PI	Prediction Index
PSD	Particle Size Distribution
RHA	Rice Husk Ash
RS	Rice Straw
RSA	Rice Straw Ash
RSM	Response Surface Methodology
S	Sulphide
S_6	Hexathiane
SAED	Selected Area Electron Diffraction
SAI	Strength Activity Index
SCM	Supplementary Cementitious Material
Si	Silicon

Si-O	Silica Bond
SiO_2	Silicon Dioxide
SSA	Specific Surface Area
TEM	Transmission Electron Microscopy
TRSA	Treated Rice Straw Ash
XRD	X-Ray Diffraction Analysis
XRF	X-Ray Fluorescence Analysis

COMMON ABBREVIATIONS

i.e.	That is

CHAPTER ONE

INTRODUCTION

1.1 OVERVIEW

The first chapter describes the background of the study, problem statement, research objectives, scope of research, significance of the study, and thesis organization.

1.2 BACKGROUND OF STUDY

Nowadays, ordinary Portland cement (OPC) is a popular essential substance in the construction sector. OPC is the primary substance used for producing concrete and mortar. OPC is used as a binder material in concrete production. However, OPC production required a lot of energy and produced an enormous amount of carbon dioxide (CO_2) (Yadav et al., 2020; Benhelal et al., 2021). The manufacture of cement is emitted CO_2 into the atmosphere. The increased CO_2 and other harmful gases exposed to the atmosphere will cause global warming (Venkatesan & Pazhani, 2016; N. B. Singh & Middendorf, 2020).

On the other hand, waste materials continue to be produced daily due to fast economic growth (Zahib et al., 2018). The underutilization of waste is becoming an alarming issue nowadays. Commonly, wastes are dumped in landfills. The development of the populace, expanding urbanization and increasing the standard of life cause the expansion of waste through industrial, domestic, and agricultural activities. So, it requires a proper landfilling technique to manage waste to avoid landfill problems or dispose of it through burning. Indeed, this practice will lead to air and environmental pollution, such as soil and water contamination. Sadef et al. (2016) mentioned that 90% of the collected

wastes disposed of at the landfill do not undergo treatment. Besides, increasing waste needs more landfill areas to dispose of and reduces air quality.

Due to those problems, most research has been conducted to find suitable cement replacement material (CRM) by utilizing the wastes to create a sustainable construction material. Pandey and Kumar (2019a), and Katare and Madurwar (2020) also stated that waste is converted into construction material to reduce pollution and avoid global warming. The amount of CO_2 exposed to the air will be reduced by substituting cement with agricultural waste to resolve environmental pollution (Lal et al., 2019). Agricultural wastes can also be used as a CRM in concrete production. Most agricultural wastes have the same pozzolanic properties as cementitious materials. Thus, it helps to enhance the quality of the construction materials.

Previous studies show that most researchers use industrial wastes to partially or solely replace cement instead of agricultural wastes. Examples of industrial wastes are wastepaper sludge ash, slag, fly ash, and red mud. But, those industrial wastes are not easy to get at low prices (Ataie & Riding, 2016; Kauldhar & Yadav, 2018). However, agricultural wastes can also be used as a CRM in concrete production. Nagashree et al. (2017) stated that many farming wastes have similar properties to cement and are mainly disposed into landfills.

Unlike industrial wastes, agricultural wastes are easily obtained at a low price. According to Ataie and Riding (2016), agricultural wastes, i.e., corn stoves, rice straws, sugarcane bagasse ash, and rice husk are produced around a million tonnes yearly. Madurwar et al. (2013) also stated that the most wastes generated are rice straw, rice husk, sugarcane bagasse, and coconut husk. Among all agricultural wastes, rice straws and husks are produced in significant amounts in every country. Both are agricultural waste from the rice production process.

For this research, the rice straw ash (RSA), a leftover from the open burning of rice straw after harvesting process, partially replace cement in mortar and studied the mechanical and microstructure properties of RSA in cement mortar. The RSA undergoes a pretreatment process to increase the silica content and decrease other impurities. Then, the highly reactive RSA incorporate in cement mortar improves the pozzolanic reactivity, hydration, and performance of cement mortar's interfacial transitional zone (ITZ).

1.3 PROBLEM STATEMENT

For agricultural wastes, the disposing of rice wastes, i.e., rice straw and rice husk, raises safety concerns and resources waste and creates environmental pollution. The amount of rice waste increases because rice is an important crop worldwide. Yao et al. (2016) stated that the annual rice production is around 10.8 million tons globally. More than 75 countries contributed to producing rice, while China manufactures the most rice. Karim et al. (2012) and Farirai et al. (2020) mentioned that paddy production is about 500 million tons annually. Thus, the common method to dispose rice wastes is the open burning caused air pollution and produced abundant number of wastes. However, agricultural wastes can be used in the cementing system as an alternative way to reduce air pollution and decrease waste materials (El-Sayed et al., 2017).

Many past studies used rice husk ash (RHA) as a partial replacement to cement in concrete production rather than rice straw ash (RSA). Then, Munshi and Sharma (2018), and Vieira et al. (2020) mentioned that past researchers are proven that the RHA has been successfully utilized in many building materials. But, only a few researchers focus on utilizing the RSA as a cement replacement material. Thus, this research used RSA to partially replace cement in mortar since the RSA has high pozzolanic properties (El-Sayed et al., 2017; Naveed & Sharma, 2020). According to Munshi and Sharma (2018), the amorphous silica of RSA helps to increase the pozzolanic reactivity and reduce porosity.

In producing the RSA as a good pozzolan, most past researchers used a high concentration of acid in the pretreatment process to enhance the silica content in RSA (Qudoos 2018, Wong 2019, Hu 2019, Rajan 2020, Uda 2020). At the same time, some past researchers focused on producing pozzolan by incinerating process without undergoing pretreatment process. Still, the amorphous silica of RSA can be produced through pretreatment and incineration processes at a controlled temperature since both processes diminish impurities that might disturb its performance in the mortar and increase the silica amount in RSA.

Therefore, this research aimed to find the effect of low concentration of hydrochloric acid (HCl) used in the pretreatment continued with the controlled temperature of incineration and grinding process to produce the highly treated RSA.

1.4 RESEARCH OBJECTIVES

Considering the previously discussed circumstances, the objectives are:

i. To establish the effect of the pretreatment and incineration process using a low concentration of acid on the reactive compound content of the treated rice straw ash (TRSA).
ii. To determine the characteristics of non-treated rice straw ash (NTRSA) and treated rice straw ash (TRSA).
iii. To evaluate the mechanical properties of cement mortar incorporating treated rice straw ash (TRSA).

1.5 SCOPE OF STUDY

To achieve all the objectives, the following scope of work shall be covered:

i. The rice straw ash (RSA) undergoes acid pretreatment before using it as the supplementary cementing material to enhance a high amount of silica.
ii. The RSA undergoes incineration process at a controlled temperature with proper grinding to produce a highly reactive RSA.
iii. The chemical composition of RSA powder identifies through x-ray fluorescence (XRF) analysis.
iv. Analyzing the chemical composition of RSA and cement to ensure the pozzolanic properties of RSA as cement replacement material in mortar.
v. Performing the x-ray diffraction (XRD) analysis to study mineralogical phases of RSA in cement mortar.
vi. The transmission electron microscopy (TEM) analysis analyzes the RSA particle size used in cement mortar.
vii. The field emission scanning electron microscope (FESEM) analysis determines the microstructure properties of RSA in mortar.
viii. Determination of structural elucidation of RSA in mortar through Fourier transforms infrared spectroscopy (FTIR) analysis.
ix. The compressive strength test identifies the strength development of RSA in cement mortar.
x. Observation of interfacial transitional zone (ITZ) of RSA in cement mortar to justify the bonding incorporated of RSA in cement mortar.

1.6 SIGNIFICANCE OF STUDY

This study is significant in promoting the usage of rice straw ash (RSA) as reactive silica-rich agriculture waste that can act as cement replacement material (CRM) in the concrete industry. Thus, the goal of this research is examining the suitability of paddy harvesting by-product namely rice straw to be used as CRM after treatment process using a low concentration of acid, continued with incineration at controlled temperature and grinding.

1.7 THESIS ORGANIZATION

This research is focused on developing the highly reactive treated rice straw ash as a cement replacement material in the mortar production. There are a total of five chapters in this thesis.

The first chapter has the framework of the research, problem statements, objectives, and the scope of the research involved in this research. However, chapter two covered the relevant literature regarding this study and was concerned with the research gap. Finally, there is an elaboration on the essential processes and methods required to produce highly reactive additive material in concrete production.

Next, there is an explanation of the methodology of this experimental work conducted in producing highly reactive additive material in chapter three. This chapter encompasses the material selection and preparation, the treatment processes, and the test procedure to examine the mechanical and microstructures of the additive material used in the concrete.

1.8 SUMMARY

This chapter discussed the introduction and the background of this study. The problem statement was clearly explained in the reason for conducting this experiment. Furthermore, there is a justification for the treatments involved to produce the highly reactive additive material in this study since past studies have preliminary findings. This chapter also covered the research objectives, the significance of study, and the study scope. Finally, the structure of this thesis was presented accordingly.

CHAPTER TWO

LITERATURE REVIEW

2.1 OVERVIEW

The second chapter focuses on the literature review of past research concerning this study. This part begins with an overview of the construction industry. Then, there is a close-up explanation regarding cement as a well-known material in the construction sector. Since cement usage in concrete production had more disadvantages than advantages, most researchers suggested pozzolan to replace cement. The pozzolan must contain a high silica content to enhance the performance of mortar regarding its microstructure and mechanical properties. Therefore, agricultural waste is selected to be the material used as pozzolan because it has amorphous silica due to the silica extraction from the soil during the growth process. Rice straw had a high potential to be pozzolan in the cementitious system. Besides, it also covers the past research on the testing method involved in this study.

2.2 POZZOLAN AS SUPPLEMENTARY CEMENTITIOUS MATERIAL IN THE CONSTRUCTION INDUSTRY

Pozzolan is an alternative to lessen the demand for cement in the construction industry. It will reduce the usage of energy and carbon dioxide (CO_2) exposures to the atmosphere during cement production. It is also known as a mineral additive in concrete production. Most pozzolans are by-products from industrial activities, i.e., fly ash, silica fumes, and slag (Ataie & Riding, 2016; Zareei et al., 2017). Some agricultural wastes, such as rice straw ash, sugarcane bagasse ash, and rice husk ash, have also been thoroughly investigated as prospective substitutes for cement in manufacturing concrete. However, fly ash, slag,

and rice husk ash have all been thoroughly examined by earlier studies (Pandey & Kumar, 2019a).

Madurwar et al. (2013) mentioned that the primary indicator required for utilizing waste materials such as pozzolan depends on the amount of silica. The pozzolan is divided into three classes had chemical content and physical properties conditions, as stated in Table 2.1 and Table 2.2 ("ASTM C618," 2014). However, a good pozzolan must meet a requirement expressed by ASTM C618, which is the total percentage of aluminium oxide (Al_2O_3), silicon dioxide (SiO_2), and iron (III) oxide (Fe_2O_3) must be more than 70% in the material (L. Singh et al., 2013; Raheem & Kareem, 2017b).

Table 2.1 Chemical Content Needs for Different Classes of Pozzolans ("ASTM C618," 2014).

	Class		
	N	F	C
Silicon dioxide (SiO_2), Aluminium Oxide (Al_2O_3), and Iron (III) Oxide (Fe_2O_3), min (%)	70	70	50
Sulphur Trioxide (SO_3), max (%)	4	5	5
Moisture Content, max, (%)	3	3	3
Loss on Ignition, max, (%)	10	6	6

Table 2.2 Physical Properties Needs for Different Classes of Pozzolans ("ASTM C618," 2014).

	Class		
	N	F	C
Fineness of pozzolan:	34	34	34

	Class		
	N	F	C
Amount retained when wet-sieved on 45μm (No. 325) sieve, max (%)			
Strength activity index/cement of pozzolan: At 7 and 28 days, min (% control)	75	75	75
Soundness: Autoclave expansion or contraction, max (%)	3	3	3
Uniformity requirements:			
Density of pozzolan: Maximum variation from average, (%)	5	5	5
Percentage of pozzolan retained on 45μm (No. 325) sieve: Maximum variation, (% average points)	5	5	5

Pozzolan aims to be produced as ultra-fine additives to improve the performance of concrete. The ultra-fine additive is a nano-sized particle-like nano-silica in cementitious materials for the construction industry. Nano-sized silica filled the void formed between aggregates and cement paste, and in turn, the porous structure in the concrete is reduced. Besides, nano-scaled silica also has higher pozzolanic reactivity compared to silica fumes. Therefore, both effects of nano-scaled silica are significant in producing a high concrete performance (L. Singh et al., 2013; Yang et al., 2021).

Pozzolans improved the performance of concrete regarding its microstructure and mechanical properties (Venkatanarayanan & Rangaraju, 2015). The pozzolan is a fine material with high silica amount involved in the first reaction caused by the chemical reaction due to the hydration process. Then, it is continued with the pozzolanic reaction. The additional calcium silicate hydrates (C-S-H) formed during pozzolanic reaction helps increase the concrete strength, decrease porosity in concrete, and dense concrete microstructure (Zareei et al., 2017).

Next, Figure 2.1 shows the primary reaction for the conventional concrete, whereby the water (H_2O) reacts with cement to form C-S-H (L. Singh et al., 2013). The primary reaction is the cement hydration process. At this stage, only C-S-H is beneficial to enhance the concrete strength (Saad et al., 2015). However, portlandite is unused in the primary reaction and forms C-S-H phases and visible capillary pores structures. And hence, it reduces the concrete strength. Portlandite is the formation of calcium hydroxide ($Ca(OH)_2$) from the primary reaction.

In contrast, when the pozzolan is added to the cement mixture, as shown in Figure 2.2, the primary reaction will occur same as the conventional concrete. Still, it continued with the secondary reaction, which is the pozzolanic reaction. In the pozzolanic reaction, pozzolan with a high silica react to the portlandite form an additional C-S-H, and the area of capillary pores is reduced (Saad et al., 2015). Forming an additional C-S-H is crucial and beneficial for further concrete strength development. Thus, the mixture becomes densified and less pore structure. It shows that the strength of concrete with pozzolan is greater than that without pozzolans.

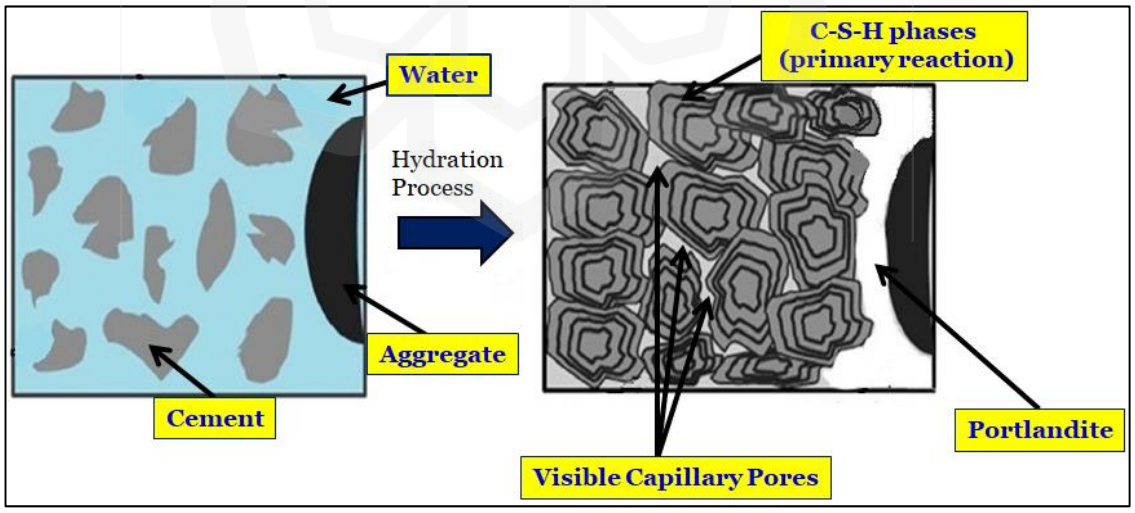

Figure 2.1 The Hydration Process of Conventional Concrete (L. Singh et al., 2013).

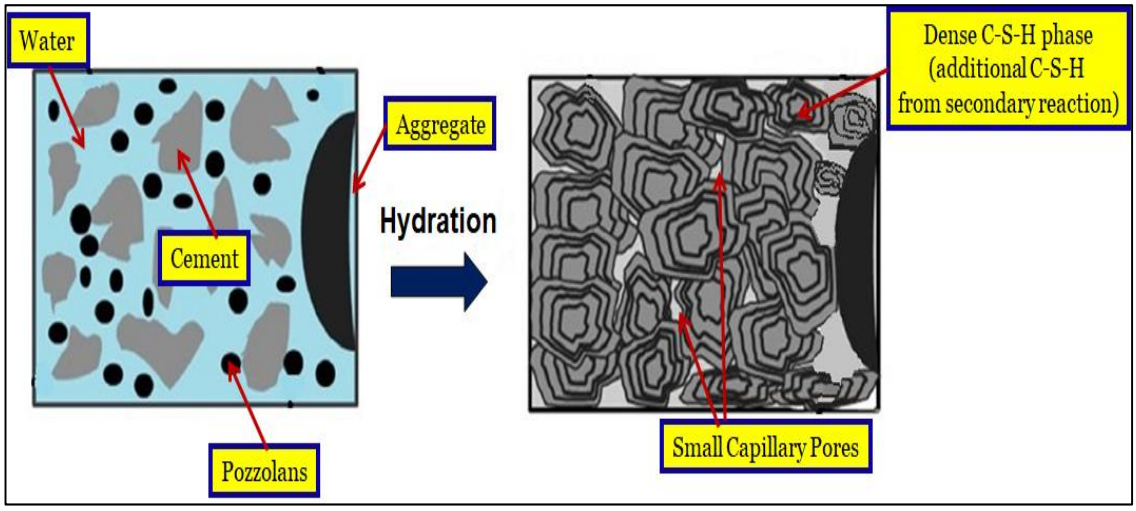

Figure 2.2 The Hydration Process of Concrete with Pozzolans (L. Singh et al., 2013).

2.3 SILICA-RICH POZZOLAN

Silica (SiO_2) is an important inorganic material. However, silica production harms the environment and requires high-energy manufacturing. Lu and Hsieh (2012) reported around 10% to 20% of hydrated silica per dry rice residue weight, rice husk, and rice straw had potentially about 60 to 120 million tonnes. Thus, extensive reports of silica from rice husks are used in the construction industry. And then, Munshi and Sharma (2018), and Vieira et al. (2020) mentioned that past researchers are proven that the rice straw, especially rice straw ash (RHA) has been successfully utilized in many building materials.

In contrast, there has been little information on using rice straw in the construction industry. Lu and Hsieh (2012) also reported that the silica obtained from rice straw has a greater potential than rice husk used as mineral additives in the construction industry. Parallel to this issue, the rice straw with high silica will be used in concrete production since silica in the rice straw is expected to be higher than in rice husk. Rice plants extract the silica content during the growth process. The polymerization process occurred when water reacted with silicic acid ($H_2SiO_4^{-2}$) absorbed from the soil, formed amorphous silica, and placed on the exterior cell wall of rice plants. Therefore, agricultural waste with a high

amount of silica is used in concrete production because it helps to increase pozzolanic reactivity and become a good filler.

Silica acted as an additive to expedite the cement hydration process. Silica is a filler that fills the void and becomes a dense microstructure, and in turn, the formation of the weak zone in concrete will be reduced. When the rate of the hydration process increases and weak zone formation decreases, the concrete strength will increase. The inclusion of silica in cement can accelerate the hydration process. Then, the pozzolanic reaction occurs when the reactive silica is in an amorphous state. The details of the pozzolanic reaction chemical equations 2.1 to 2.3 are shown below (L. Singh et al., 2013).

$$\text{Nano-SiO}_2 + \text{H}_2\text{O} \longrightarrow \text{H}_2\text{SiO}^{2-}_4 \quad (2.1)$$

$$\text{Ca(OH)}_2 + \text{H}_2\text{O} \longrightarrow \text{Ca}^{2+} + \text{OH}^- \quad (2.2)$$

$$\text{H}_2\text{SiO}^{2-}_4 + \text{Ca}^{2+} \longrightarrow \text{C—S—H (Additional C—S—H)} \quad (2.3)$$

When nano-silica is incorporated with cement particles, $H_2SiO_4^{-2}$ is formed and reacted with calcium cation (Ca^{2+}) to form additional calcium–silicate–hydrate (C–S–H) particles. These C–S–H particles are distributed in the water (H_2O) between the cement particles and function as agents to create a dense C–S–H phase. As a result, the C–S–H phase development is no longer restricted to the grain surface only, as it is in pure tri-calcium silicate (C_3S) and forms in the area of the pores structure. As a result, early cement hydration is accelerated because of the high development of C-S-H particles (L. Singh et al., 2013; Yang et al., 2021).

In this regard, pozzolan with a high amount of silica is significant in replacing part of the quantity of cement in the mixture as the mineral additives of supplementary cementitious material (SCM). Moreover, pozzolan improved the quality of concrete produced regarding its microstructure and mechanical properties. Thus, silica-rich

pozzolan incorporated in cement paste is the best alternative since it improves the cementitious systems, as shown in Figure 2.3. Yang et al. (2021) also stated that nanotechnology and nanomaterials are having a major impact on the macroscopic properties of concrete. For example, nanomaterials, i.e., nano-silica, improve cement hydration by filling concrete pore structures and increasing strength and durability. The size of nano-silica is from 10 to 200 nm.

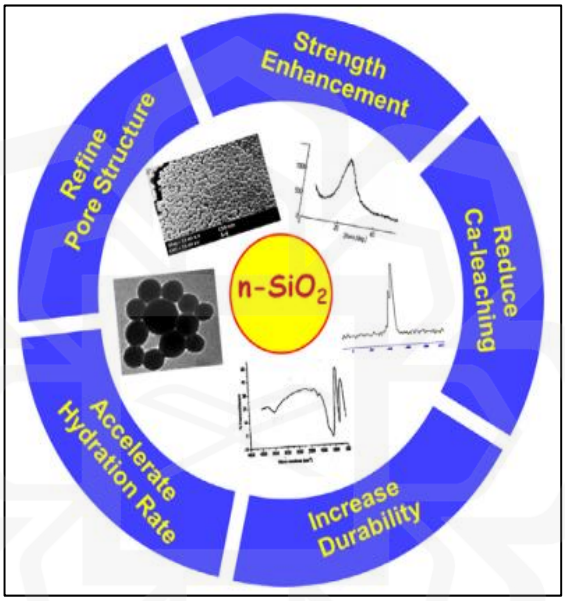

Figure 2.3 Advantages of Nano-Silica in the Cementitious System (L. Singh et al., 2013).

2.4 AGRICULTURE WASTE: RICE STRAW ASH (RSA) FROM PADDY CROPS

Rice is an important grain crop widely produced by all countries, with around 10.8 million tonnes of rice production yearly (Yao et al., 2016). Karim et al. (2012) mentioned that paddy production is about 500 million tons annually. There are more than 75 countries that contribute to produce rice, while China manufactures the most amount of rice. However, rice production is one of the major industries for Southeast Asia countries, and it is the

activity that contributes to the rural economy and as a staple of food. Farmers can easily plant paddy crops because those land areas are suitable for rice cultivation. Unfortunately, a huge amount of rice straw is produced as crop residue from rice production (Oladosu et al., 2016). Beidaghy Dizaji et al. (2019) also emphasize paddy rice production in more than 50 countries over ten years, from 2004 until 2018, as shown in Figure 2.4. Asia was the highest area producing paddy rice while Oceania made the lowest.

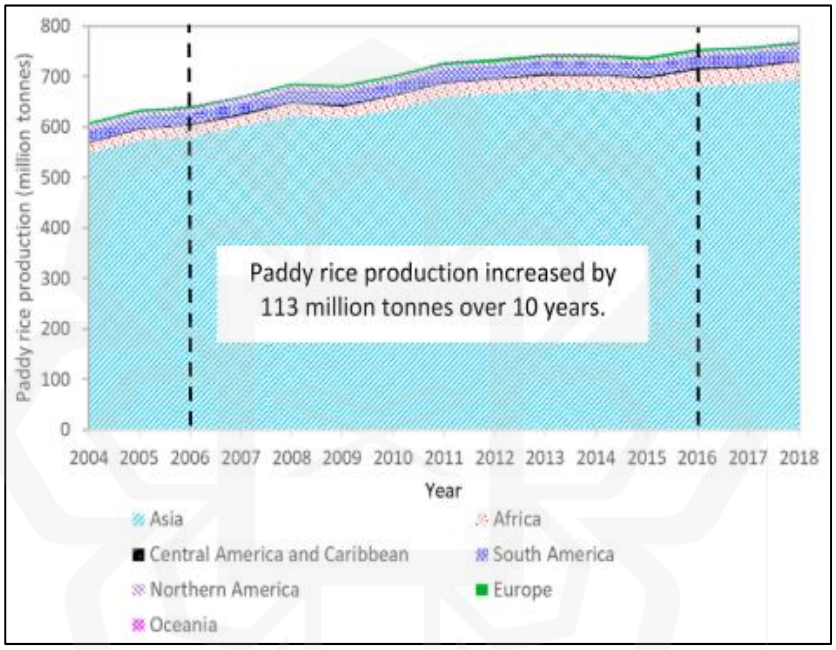

Figure 2.4 The Production of Paddy Rice for Over 50 Countries (Beidaghy Dizaji et al., 2019).

The development of the paddy field in Malaysia is more than 700,000 hectares, and then there were 2 million tonnes of rice straw in every cultivation season (Rosmiza et al., 2019). Rice straw is one of the significant crop leftovers produced worldwide, but it is only known as a residue by farmers. Traditionally, farmers diminish the straw after harvesting by burning the paddy field. The field must be free of straw for the replanting process of the paddy (Rosmiza et al., 2019). The open burning of rice straw is the cheapest and fastest way to remove it from the field.

However, the open burning of rice straw is improper, leading to environmental pollution because the rice straw is burnt under uncontrolled temperatures in an open space. Athira et al. (2019) stated that the combustion from the open burning of rice straw at the paddy field emitted harmful gases that caused pollution. The open burning at the paddy field is one of the reasons that cause the city to have low-quality air. This method also causes soil contamination and the greenhouse effect.

Some farmers practice the natural decomposition method to dispose of rice straw to produce organic compost. This method is widely famous in Japan. The natural decomposition method is another way to dispose of the rice straw without undergoing the burning process (Athira et al., 2019; Goodman, 2020). But, the natural composting method takes three to four weeks to decompose the rice straw before replanting. However, open burning and natural decomposition of rice straw methods to dispose of rice straw causes global warming and environmental pollution.

Basically, rice straw ash (RSA) is a residue left after the open burning of it at the paddy field. Athira et al. (2019) mentioned that the colour of RSA burnt at the paddy field is darker than cement, which the colour of RSA is black due to the unburnt carbon content, while OPC is grey. Generally, rice straw contains silica, cellulose, hemicellulose, lignin, proteins, and vitamins. The silica in the rice straw is absorbed from the soil during the growth process of the paddy plant (Munshi et al., 2013). The high amount silica makes the RSA have a high pozzolanic and can replace cement in concrete production. The pozzolan material helps improve the essential material characteristics in concrete or mortar production (Miller et al., 2019).

2.5 COMPARISON BETWEEN RICE HUSK ASH (RHA) AND RICE STRAW ASH (RSA)

First, rice husk as well as rice straw are rice waste produced abundantly worldwide. The rice husk is the outer part of the rice cover and consists of two interlocking, but the rice straw is a stem of the paddy plant. The rice husk residue remains after the grain has been extracted at the factory. The rice husk ash (RHA) is obtained after burning rice husk, which seems to be the primary waste material of the rice milling process (Raheem & Kareem, 2017b). On the other hand, rice straw is a stem of the paddy plant. The rice straw is a residue leftovers after the harvesting process, and the rice straw ash (RSA) is obtained after the open burning process of rice straw at the paddy field (Munshi & Sharma, 2018). Burning rice straw is the standard method for farmers to dispose of and replant it.

Both have different structures through scanning electron microscopy (SEM) analysis. The rice husk has a rough surface and looks like a net strip with typical cone-shaped protuberances (Xu et al., 2012; Bie et al., 2015) and the rice straw has needle-like structures (Pandey & Kumar, 2019b), as shown in Figure 2.5 and Figure 2.6, respectively. In addition, Xu et al. (2012) highlighted that rice straw and rice husk had a high amount of silica among other plant residues, as compared in Table 2.3.

Table 2.3 The Percentage of Silica Contained in Plant Residues (Xu et al., 2012).

Types of plant	Part of plant	Silica content (%)
Rice husk	Grain outer part	93.0
Rice straw	The stem of the paddy plant	82.0
Breadfruit tree	The stem of the tree	81.8
Corn	Leaf	64.3
Bamboo tree	The inner part of the tree	57.4

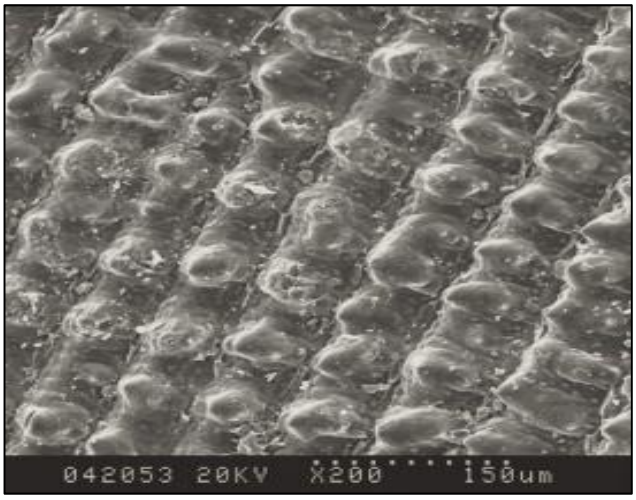

Figure 2.5 SEM Image of RHA (Bie et al., 2015).

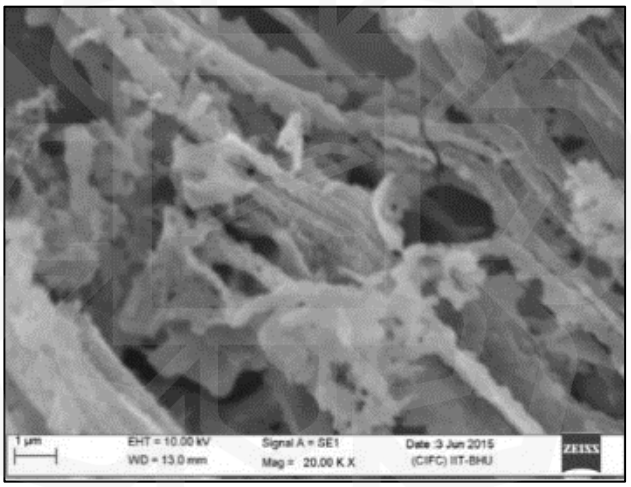

Figure 2.6 SEM Image of RSA (Pandey & Kumar, 2019b).

2.6 TREATED RICE STRAW ASH (TRSA) INCORPORATION IN CEMENT MORTAR

In recent years, the rice straw has been continuously increasing as rice production increases due to the increasing human population and urbanization. Hence, the common alternative to dispose of it is burning it in the paddy field to reduce rice straw waste. Some people use

rice straw as the primary need, which is the consumption of rice straw for cooking purposes that have been practiced for a long time. However, unique admixtures from agricultural waste are used in cement mortar to ensure sustainable construction material, the cost of construction is affordable, and the improved cement mortar and concrete cement characteristics nowadays (Morsy & Rashwan, 2015).

Agricultural waste is utilized to improve the performance of construction materials, decrease the expense of the construction materials and raise a concern about the environment (Naveed & Sharma, 2020). Rice straw is one of the agricultural wastes and is easy to get in all parts of the world. Alternatively, the residues of rice straw ash (RSA) left after the open burning of rice straw at the paddy field can partially replace cement in concrete or mortar production. The rice straw converted the RSA waste into a pozzolan in cement mortar or concrete (Roselló et al., 2017). This alternative can be one of the solutions to decrease RSA waste production to reduce pollution.

Most past researchers used RSA to partially replace the amount of cement between 5% to 30% (Agwa et al., 2020; John, 2020; Mahmuda et al., 2020; Naveed & Sharma, 2020). According to Munshi et al. (2013) and Munshi and Sharma (2016), the RSA is used to replace the cement content of about 5%, 10%, and 15% in concrete production. The performance of RSA incorporated in concrete production is great compared to the conventional mixture with 100% of cement. Miller et al. (2019) mentioned that several tests must be conducted for RSA to enhance the excellent performance of cement mortar or cement concrete production, as shown in Figure 2.7.

In this research, the RSA must undergo acid pretreatment to eliminate impurities and improve its silica content. Silica is one of the nanomaterials, a cementitious material that helps increase the quality of construction materials (Munshi et al., 2013). Silica is a fundamental substance needed for pozzolanic reaction to develop the strength (Roselló et al., 2017). The incineration process at a controlled high temperature also must be conducted to ensure the removal of organic materials presented in RSA, which can disturb the

performance of RSA in cement mortar. The proper and efficient pretreatment process and incineration at the controlled temperature of RSA can help cement mortar have a good pozzolanic reactivity and improve the performance of interfacial transitional zone (ITZ) of cement mortar.

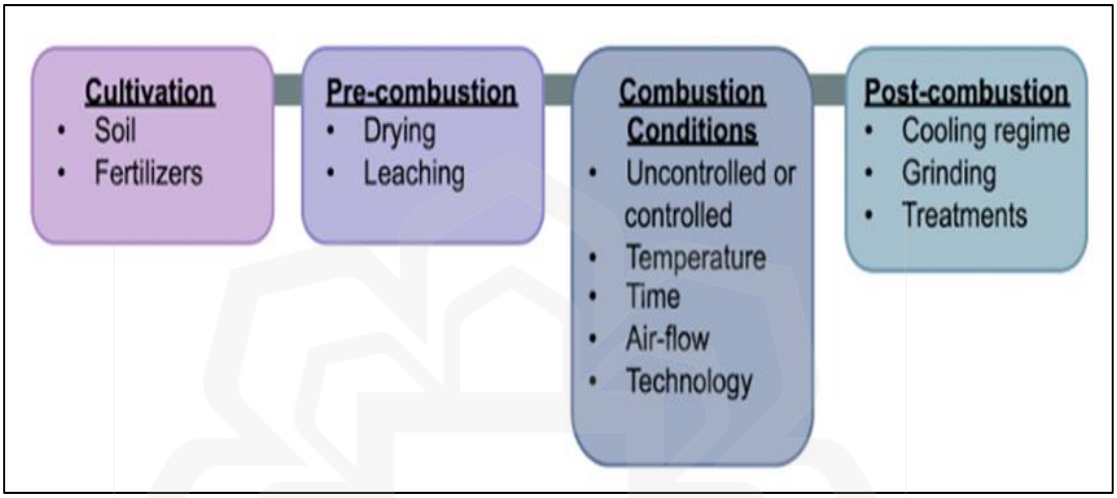

Figure 2.7 The Flowchart for the Production of RSA (Miller et al., 2019).

2.7 PREPARATION OF HIGHLY TREATED RICE STRAW ASH (TRSA) IN CEMENT MORTAR

The high quality of rice straw ash (RSA) can be obtained through pretreatment, incineration, and grinding operations. However, the type of pretreatment process, the incineration method, and the degree of grinding process affected the production of valuable RSA.

2.7.1 Pretreatment Process of Rice Straw

Concrete or mortar production properties can be improved by using pozzolanic materials to replace cement. Rice straw has natural constituents, which are cellulose, hemicellulose, lignin, and sand ash, as shown in Table 2.4. But, rice straw also consists of several minerals, including silica, alumina, and iron oxides. So, rice straw cannot be directly used to replace cement because it contains organic materials that can disturb the performance of cement mortar or cement concrete. Based on the standard of ASTM C618, the total percentage of iron oxide (Fe_2O_3), silicon dioxide (SiO_2), and aluminium oxide (Al_2O_3) must be greater than 70% of before using it to replace cement (Munshi et al., 2013; Olonade et al., 2017; Raheem & Kareem, 2017a).

Table 2.4 Major Components of Rice Straw (Goodman, 2020).

Significant elements of rice straw (%)			
Hemicellulose	Cellulose	Lignin	Ash
19.7-35.7	32.0-38.6	13.5-22.3	10-17

According to Roselló et al. (2017), silica is the essential component. There are several techniques of the pretreatment process to enhance the amount of silica in the ash to increase the pozzolanic reactivity of rice straw ash (RSA) in cement mortar. Goodman (2020) reported that biological pretreatment is slow, but some chemical and physical pretreatment methods are expensive, while environmentally friendly pretreatments are usually ineffective.

Oladosu et al. (2016) stated that chemical pretreatment could improve the amount of nutrition in rice straws, which the straws treated with alkaline solutions, for example, ammonia (NH_3), sodium hydroxide (NaOH), and calcium hydroxide ($Ca(OH)_2$). Urea is

the most famously utilized pretreatment rice straw since it is harmless and acts as a removal agent in ammonification. In contrast, Nazopatul et al. (2018) used acid solution in the chemical pretreatment to treat rice straws and mentioned that the hydrochloric acid (HCl) is more effective than sulphuric acid (H_2SO_4), and nitric acid (HNO_3) in enhancing silica content in rice straws. The chemical solution reacts to SiO_2 content in the rice straw. However, the hemicellulose and cellulose structure of the rice straw can be removed by utilizing the aqueous solution of azide ion (N_3), followed by the pretreatment of dilute H_2SO_4 (Goodman, 2020).

Furthermore, Vayghan et al. (2013), Xu et al. (2018), and Librea et al. (2019) stated that acid leaching pretreatment is the best way to apply for agricultural waste to remove metallic impurities and improve its performance as a supplementary cementitious material (SCM). There are metallic impurities and harmful materials presented in the farm waste, which are calcium oxide (CaO), magnesium oxide (MgO), and potassium oxides (K_2O). This is because of the great ionic bonding formation was happened in the HCl treatment process. Basically, the ionic bonding is the electrostatic attraction between positive and negative charged ions. An ion was formed when an electron was transferred from one atom to another atom. Then, the metallic impurities were removed when reacted with HCl. The HCl treatment hydrolyzes the hemicellulose structure to obtain high-quality pozzolan by removing the metal cations, especially potassium ion (K^+), from K_2O (Chen et al., 2013).

When the acid leaching pretreatment is conducted towards waste, all metallic impurities and harmful material will be eliminated and continued with the incineration process to produce ashes. In addition, the major silica crystallization catalyst is removed during the incineration process, and no surface melting occurs in the silica structure. Thus, carbon presented in the burning ash does not become volatile. At last, there is the least amount of unburnt carbon in the ash compared to non-acid leached ash. Commonly, inorganic acids are used in the acid leaching pretreatment process. Examples are potassium hydroxide (KOH), HCl, H_2SO_4, and HNO_3. Most previous researchers used a high concentration of inorganic acids, i.e., more than 1 N, for the acid leaching pretreatment

process of waste as SCM. However, a high concentration of acid leads to harm to the environment. According to Ataie and Riding (2016), using the thermochemical pretreatment technique, such as dilute acid pretreatment, RSA can increase the surface area and amorphous, making them highly reactive pozzolanic substances. Munshi and Sharma (2018) also mentioned that dilute acid pretreatment is effective since it removes the hemicellulose in the ashes. Acid pretreatment increases the amount of silica by lowering the sodium (Na) contents from RSA.

2.7.2 Incineration Process of Rice Straw at Controlled Temperature

The rice straw is the residue from the stem of the paddy plant after the harvesting process, and it contains organic and inorganic materials. Several organic materials in the rice straw are hemicellulose, cellulose, and lignin. In addition, the rice plant has absorbed important inorganic materials such as silica from the soil during its growth. Silica is extracted from the soil and gathered in the straw where the cellulose is formed. However, rice straw ash (RSA) is formed by burning rice straw before replanting. This method remains a common practice among farmers, despite their contributions to environmental problems resulting from air pollution.

When the cellulose undergoes the burning process, the silica is only left, and then it is ground to create a fine powder that can be used as pozzolanic (Munshi et al., 2013). But, the rice straw is not preferred to be burnt under uncontrolled temperature because the fibrous materials are not fully diminished and create carbon. The RSA produced through uncontrolled temperature consists of high unburnt carbon. When there is a high amount of unburnt carbon, a high amount of water needed can cause the strength of the concrete to be low. The ash with a high amount of carbon required a high amount of pozzolan to replace cement with high energy in the grinding process and then showed poor performance than the ash with low carbon content (Venkatanarayanan & Rangaraju, 2015).

Pandey and Kumar (2019a) stated that proper incineration at a controlled temperature is required to obtain a good quality of RSA by making it highly reactive. RSA must be prepared at over 400℃ with an appropriate grinding method that might reasonably utilize the ash as a pozzolan (Munshi & Sharma, 2018). In contrast, Bie et al. (2015) mentioned that the suitable temperature for the incineration process is 600℃ to produce amorphous silica in the form of nano-sized particles, which is about 90% of its presence in the ash. Bazargan et al. (2015) recorded that the reaction of the temperature of the combustion process (400℃ to 1000℃) on potassium oxides (K_2O) presented in the ash. There will be an interaction between potassium in the K_2O compound and silica in silicon dioxide (SiO_2) while both have different melting points and form potassium polysilicate (K_2SiO_3). The melting point of K_2O is below 350℃ compared to silica is above 1400℃, where the K_2O induces the surface melting of amorphous silica between 400℃ to 1000℃ during the combustion process.

In addition, the metal oxides and salts can interact with silica and form eutectic mixtures. The eutectic combinations are formed when those melting points of components are involved below 800℃. So, the more minerals are reduced from the material's composition, the more problems will be diminished, i.e., aggregation and clog and the pozzolanic reactivity of the ashes will increase. Silica is the vital material that must be presented in the ashes because silica will react with the lime to form calcium silicate hydrate (C-S-H), which is responsible for developing the mechanical and microstructural characteristics of cement mortar or concrete. Therefore, the incineration process at a controlled temperature makes the ashes have high silica to become valuable material.

2.7.3 Grinding Process of Rice Straw

The mechanical activation process is the grinding process, including the sieving and air separation processes (Hela & Orsakova, 2013). However, most researchers preferred the grinding process to the sieving and air separation process. In addition, both sieving and air

separation processes produced coarse particles of around 60% to 70%, which is not encouraged in the cement mixture.

The proper grinding process is required to obtain a good quality of rice straw ash (RSA). The grinding process converted the ashes into powder material. It plays a vital role in producing highly reactive RSA, although it requires high energy and cost compared to unground ash. But, besides the acid pretreatment and incineration processes, the grinding process is also essential to ensure that the finer particles become a filler to the structure of the concrete. Then, the porosity will be reduced, and increased reactivity of the ashes. Thus, the grinding process significantly assists in producing reactive mineral additives in concrete production (Venkatanarayanan & Rangaraju, 2013).

According to Qudoos et al. (2018), the grinding process helped reduce the size of particles, increased the specific surface area, and produced the ashes in an amorphous state. Most past researchers do not recommend unground ashes as cement replacement material (Venkatanarayanan & Rangaraju, 2015; Mangi et al., 2019). The unground ashes have a low bulk density which might affect the cement mixture's density when used in a large amount. It consists of more coarse particles than ground ashes which have a low tendency to obtain a uniform size of the particle of the ashes in the wet mixture than finer particles. And then, the distance between particles in the cementitious matrix increased and decreased the uniformity of the composition.

The distribution size of particles of ashes will be wide due to the irregular shape of particles and the non-homogeneous size. Therefore, the unground ashes obtained poor development of concrete strength. The coarse particles of unground ashes cause the formation of porous structures. Thereby, the total volume of pores in the structures will be increased. Then, the distribution of the large particles in the mixture does not much influence the permeability of the mixtures (Venkatanarayanan & Rangaraju, 2015). Hela and Orsakova (2013) stated that the coarse, porous, and rough particles would be reduced through the grinding process, thus increasing the specific gravity, fineness, and pozzolanic

reactivity. As shown in Figure 2.8, the reactive and less reactive small particles formed through the grinding process. Both less reactive and reactive particles can be a good filler in the voids between the cement particles; several grinding machines, i.e., ball mills, hammer mills, jet mills, and attrition mills.

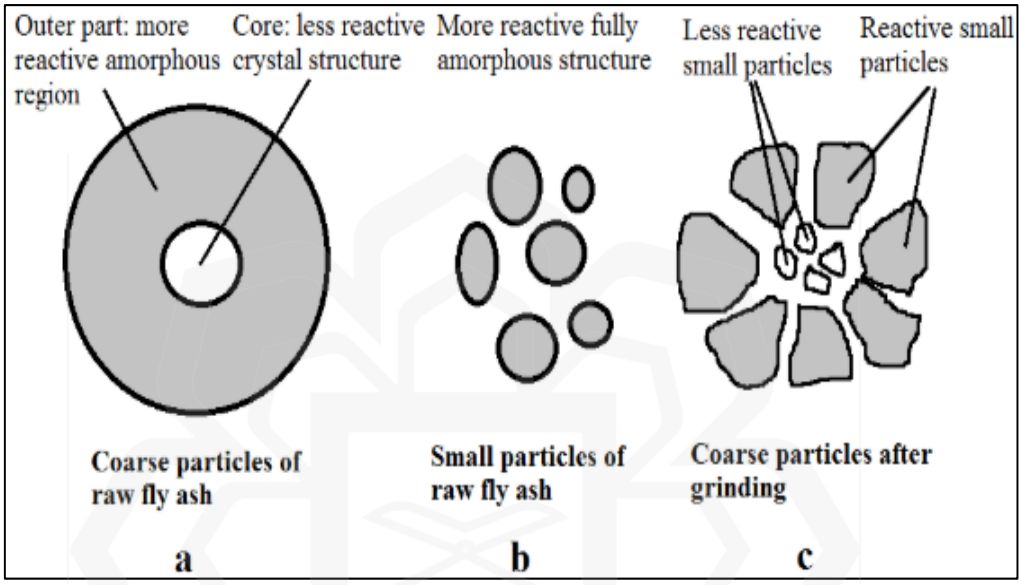

Figure 2.8 The Simulation of the Effectiveness of the Grinding Process from the Viewpoint of Pozzolanic Reactivity for (a) Coarse particles of raw ash (b) Tiny particles of raw ash (c) Small particles formed after grinding activity (Hela & Orsakova, 2013).

But, ball mills are often grinding machines used for the mechanical activation process of ashes (Venkatanarayanan & Rangaraju, 2015; Xu et al., 2015). Venkatanarayanan and Rangaraju (2015) conducted a grinding process using a ball mill with a 250-rpm speed for specific durations, which are about 0, 5, 10, 15, 30, and 60 minutes to obtain ground ashes with varying particle sizes. The grinding process emphasized that the average length of ashes particles decreases when the grinding time increases from 0 to 15 minutes. However, the minimal size of ashes particles reduces after the grinding duration is about 15 minutes, and it requires high energy to reduce the particle

size further. Saad et al. (2016) also used a ball mill to produce fine ashes at 15 minutes with 300 rpm of milling speed and a 15:1 ratio of ball-to-powder.

The high energy used to grind ashes is avoided since it increases the internal surface area of ashes instead of reducing the size of ash particles. Furthermore, Xu et al. (2015) also conducted a grinding process using a ball mill to reduce the size of particles after controlled incineration in the furnace. The grinding process at a speed of 1000 rpm with 20:1 for a ball-to-powder ratio but at 5, 10, 30, 60, 90, and 120 minutes of grinding durations. At last, they concluded that the fineness of ashes increased at the grinding duration between 5 to 30 minutes. The prolonged grinding duration is not encouraged because the grinding duration above 30 minutes caused the agglomeration particles.

In addition, Qudoos et al. (2018) obtained the fineness ashes after the incineration process at 670°C by grinding process using ball mill for about 30, 60, and 120 min. The ball mill is rotated at a speed of 350 rpm. As a result, the fineness of particles obtained when the grinding duration is 60 minutes and 120 minutes compared to 30 minutes. The cellular structure of ashes particles is completely broken when the grinding duration is 120 minutes. Thus, the parameters of grinding media influence the grinding process to obtain fine materials particles. Based on past research, different speeds, and the ratio of ball to powder are different; the grinding duration to get fine particles will differ. The grinding process is seen to be longer when there is no pretreatment process in producing ashes.

Table 2.5 shows most relevant past researchers that focused on the incineration process of materials to produce highly reactive substitute material instead of conducting all three operations which are the acid pretreatment process, the incineration process, and the grinding process.

Table 2.5 Summary of Past Research on the Preparation of Highly Reactive Treated Agricultural Waste.

Authors	Material	Preparation for highly treated material	Summary
Xu et al. (2012)	Rice husk	**Pretreatment:** Not involved. **Combustion process:** 500, 600, 700, and 800°C for about 2 hours. **Grinding process:** Ground rice husk ash using the vertical globe mill for about 2 hours.	The optimum combustion temperature is 600°C to produce highly reactive RHA.
Vayghan et al. (2013)	Rice husk	**Pretreatment:** Acid leaching treatment (boiled the rice husk with 0.01 N to 6 N of HCl solution for about 1 hour). **Combustion process:** 700°C for about 15 minutes, 1, 4, 8, and 16 hours. **Grinding process:** Ground in the 5 liters of porcelain mill for about 20 minutes.	0.01 N of HCl for acid leaching treatment was sufficient to enhance the reactivity of RHA by improving the high amount of silica and low impurities.
Van et al. (2013)	Rice husk	**Pretreatment:** Not included. **Combustion process:** Rice husk burnt under uncontrolled temperature. **Grinding process:** Ground in a ball mill for about 15, 30, 45, 120, and 540 minutes.	The optimum grinding time is 120 minutes for RHA to produce the maximum compressive strength of RHA incorporated in cement mortar.

Authors	Material	Preparation for highly treated material	Summary
Xu et al. (2015)	Rice husk	**Pretreatment:** Not involved. **Combustion process:** 600℃ for about 2 hours in an electronic oven. **Grinding process:** Use a ball mill to grind ashes at about 5, 10, 30, 60, 90, and 120 minutes with a BPR of 20:1 and rotation speed at 1000 rpm.	The optimum reactive RHA can be obtained when a grinding process is 30 minutes long. However, particle agglomeration might happen when the excessive time of grinding process (above 30 minutes).
Wong et al. (2019)	Rice husk	**Pretreatment:** Acid leaching treatment (1.0 M, 0.1 M and 0.01 M of HCl solution used to leach rice husk for about 2 hours at 80°C) **Combustion process:** 800℃ for about 2 hours by using an electric furnace to produce ashes **Grinding process:** Not involved.	1.0 M of HCl was used to leach rice husk ash for 2 hours at 80℃ and then combusted at 800°C for 2 hours, removing impurities and enhancing more than 98% of the amount of amorphous silica. The unburnt carbon content was reduced by around 5.24% compared to non-treated rice husk ash (RHA).
Rajan et al. (2020)	Rice husk	**Pretreatment:** Thermochemical pretreatment (1 M of HCl used to leach rice husk for an hour at 80°C). **Combustion process:** 700℃ for about 5 hours using the furnace. **Grinding process:** Not involved.	Remove the impurities and carbonaceous material and retain the amount of silica present in the ashes.

Authors	Material	Preparation for highly treated material	Summary
Hu et al. (2020)	Rice husk	**Pretreatment:** Rice husk soaked in the 5mol/L of dilute HCl solution for 7 days. **Combustion process:** 500-750℃ of combustion temperature for 2 hours. **Grinding process:** Ground for about 20 minutes using the planetary high energy pulverizing mill.	The HCl pretreatment with the combustion process at 600℃ produced highly reactive RHA.
H. B. Dizaji et al.(2022)	Rice husk Rice straw	**Pretreatment:** Waste treated using dilute citric acid. **Combustion process:** burnt at 700℃ of combustion temperature. **Grinding process:** Sieved using mesh sieve.	The size of particle is less than 3.15 mm. The treated waste recorded in the amorphous state.
Agwa et al. (2020)	Cotton stalk Rice straw	**Pretreatment:** Not involved. **Combustion process:** burnt at (550℃-600℃), then, continued with (600℃ to 1100℃) of combustion temperature using a muffle furnace. **Grinding process:** Sieved using mesh sieve.	The size of particle is less than 75 µm. The percentage of rice straw ash (RSA) more than 10% in concrete production has denser structure than control.
Morsy and Rashwan (2015)	Rice straw	**Pretreatment:** Not included. **Combustion process:** Rice straw burnt under uncontrolled temperature.	The amount of silica presented is 69.20%, and the total for reactive compound content is 75.40%.

Authors	Material	Preparation for highly treated material	Summary
		Grinding process: Not included. Only sieved through a 200 µm sieve.	
Roselló et al. (2017)	Rice straw	**Pretreatment process:** 50% of sodium hypochlorite (NaOCl) solution heated for about 24 hours at 105℃ was used to clarify the raw rice straw **Combustion process:** Burnt at various temperatures (450℃, 550℃, and 650℃) for about 1 hour. **Grinding process:** Not included.	The RSA burnt at 550℃ and above completely removed the impurities.
Munshi and Sharma (2018)	Rice straw	**Pretreatment:** Not included. **Combustion process:** Rice straw burnt under uncontrolled temperature, 400℃, 500℃, 600℃, and 750℃ for 6 hours. **Grinding process:** Ground the rice straw ash for about 30 minutes.	Rice straw's incineration process at controlled temperature performs better than at uncontrolled temperature. The rice straw burnt at 750℃ has 82% of amorphous silica.
Nazopatul et al. (2018)	Rice straw	**Pretreatment:** Rice straw is treated using a 3% concentration of HCl at 900℃ with a heating rate of 1.7 s for 1 hour.	The treated RSA has 80.40% of silicon dioxide.

Authors	Material	Preparation for highly treated material	Summary
		Combustion process: Rice straw burnt at 400℃ to 900℃ at a heating rate of 1.7 s for 2 hours. (Before the pretreatment process) **Grinding process**: Not included.	
Uda et al. (2020)	Rice straw	**Pretreatment:** RSA mixed with 2.5 M of NaOH at 100℃ for about 4 hours, then titrated using 2 M of sulphuric acid until it reached pH 7 and continued stirring for 18 hours. Continued with centrifugation and washed three times using ethanol solution and tap water twice. **Combustion process:** Rice straw burnt under uncontrolled temperature. **Grinding process:** Not included.	The size of the nanoparticle of silica was between 0.08 to 0.09 μm.
Ataie and Riding (2013)	Rice straw and Wheat straw	**Pretreatment process:** Distilled water and 0.1 N HCl were used at 23, 50, and 80°C for about 0.5, 1, 2, 4, 8, and 24 hours. **Combustion process:** Burnt at 500, 650, 700, and 800°C for about 1, 2 and 3 hours. **Grinding process:** Ground for 1 hour with a rotation speed of 85 rpm.	The thermochemical pretreatment process was effective in removing the impurities in the ashes. The RSA was treated with 0.1 N HCl at 80℃ for about 24 hours and continued with the incineration process at 650℃ for about 1 hour, obtaining 89.14% amorphous silica.

Authors	Material	Preparation for highly treated material	Summary
Qudoos et al. (2018)	Wheat straw	**Pretreatment process:** Not included. **Combustion process:** Burnt at 670℃ for about 5 hours. **Grinding process:** Ground using the ball mill for about 30, 60, and 120 minutes with the rotation speed at 350 rpm.	The grinding process helps reduce the particle size and increase the surface area of the ashes. The 60 minutes is the minimum duration of the grinding process to improve the quality of the ashes.
Embong et al. (2016)	Sugarcane	**Pretreatment process:** Treated the sugarcane with 0.1 M, 0.5 M, and 1.0 M of HCl for about 1, 2, 3, 4, 5, and 6 hours. **Combustion process:** Burnt at 600, 700, and 800℃ for about 1, 2 and 3 hours. **Grinding process:** Not included.	The sugarcane was treated with 0.1 M HCl at 1 hour of soaking duration and continued with the incineration process at 800℃ for about 1 hour had high silica content and increased the pozzolanic reactivity.
Rodier et al. (2017)	Bamboo stem	**Pretreatment process:** Not included. **Combustion process:** Burnt at 600℃ with the heating rate of 30℃/minutes for about 3 hours. **Grinding process:** Ground the bamboo stem by using the ball mill at 500 tr/min for about 2 minutes.	The bamboo stem ash (BSA) contained amorphous silica of about 68.74%.

2.8 CHARACTERIZATION PROPERTIES OF RICE STRAW ASH (RSA) AS POZZOLAN

The finding of characterization properties of rice straw ash (RSA) as pozzolan is important because it influences the performance of pozzolanic reactivity, the interfacial transitional zone (ITZ), and the development of mechanical properties of RSA in cement mortar. RSA microstructures were identified through field scanning electron microscopy (FESEM) analysis. The particle size of material and morphology can be determined through FESEM analysis (Munshi & Sharma, 2018; Záleská et al., 2018). From the FESEM analysis, Munshi and Sharma (2018) determined that the morphology of RSA changes with temperature. The morphology of RSA is different when it is burnt at 400℃, 600℃, and 750℃ and continued with the grinding process. As a result, the FESEM analysis shows that most RSA particles have heterogeneous shapes and amorphous porosity, and the average particle size of RSA is about 500 nm. For example, the RSA has non-agglomerated particles and a smooth surface texture at 600℃, as shown in FESEM analysis in Figure 2.9.

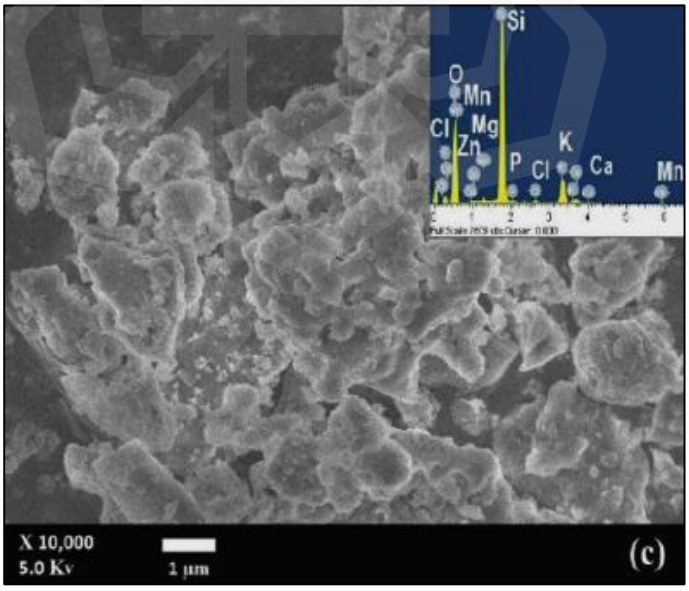

Figure 2.9 FESEM Image of RSA Burnt at 600℃ (Munshi & Sharma, 2018).

On the other hand, Uda et al., (2020) stated that the unground RSA is recorded between 0.08 to 0.09 µm in the FESEM test. The ground RSA has smaller particles size than unground RSA. It has been proven that the grinding process helps to obtain the nano-sized particle to be as pozzolan. The nanomaterial can be considered with the size of particles is less than 100 nm. However, Pandey and Kumar (2019b) also conducted FESEM analysis to identify the particle shape and size of RSA. FESEM investigation was done to support the evaluation on the RSA particles. From this analysis, RSA particles seem smaller than cement particles. The typical size of RSA particles is around five times that of cement particles. RSA particles are nearly more permeable and needle-like structures, as shown in Figure 2.10.

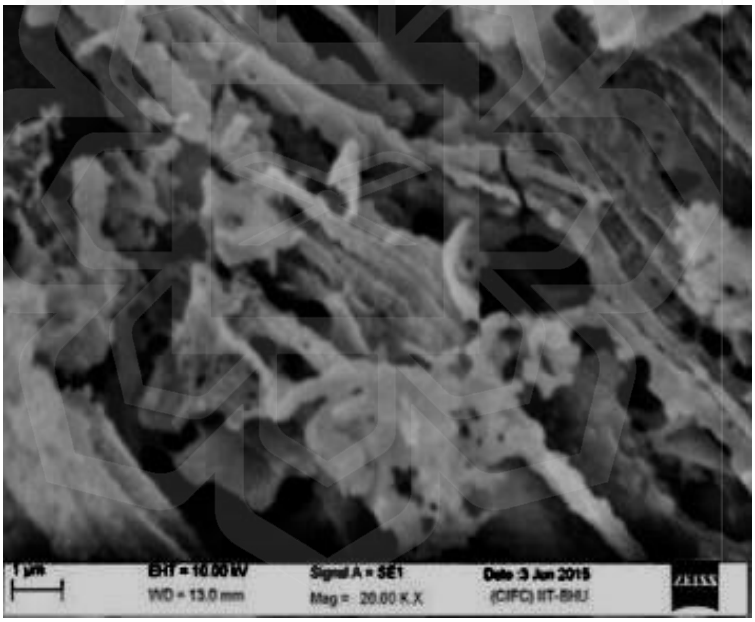

Figure 2.10 FESEM Image of RSA (Pandey & Kumar, 2019b).

Secondly, transmission electron microscopy (TEM) analysis is a flexible method for finding the size of materials, morphology, and chemical composition. TEM analysis can analyze the size of particles in the range from 1 to 100 nm (Farirai et al., 2020; Mast et al., 2019). Thus, the physical properties of nanoparticles can be easily interpreted through TEM

analysis. The procedure of TEM is the electron beam generates through the sample and forms the TEM image of the sample. Like Wang et al. (2012), TEM analysis is considered in the research for further analysis of the characterization properties of particles.

For example, Lu and Hsieh (2012) conducted a TEM analysis to determine the diameter and particle size distribution (PSD) of the material involved in the experiment. The size of nanoparticles of rice straw is between 50 to 80 nm, but most of them are close to 60 nm. As a result, the particle size distribution of silica from treated RSA seems like a circle (Lu & Hsieh, 2012), while the non-treated RSA look like agglomerate particles (Uda et al., 2021), as illustrated in Figure 2.11 and Figure 2.12, respectively. Additionally, the TEM test also analyzes the crystalline of nanomaterial is possible with selected area electron diffraction (SAED). The SAED pattern indicates whether a material has an amorphous structure or not (Lu and Hsieh, 2012; Uda et al., 2021). Figure 2.13 illustrates the SAED pattern formed when the material particles merged into rings, demonstrating the amorphous (Uda et al., 2021). The SAED pattern is vital to support the evaluation of material as pozzolan in concrete production.

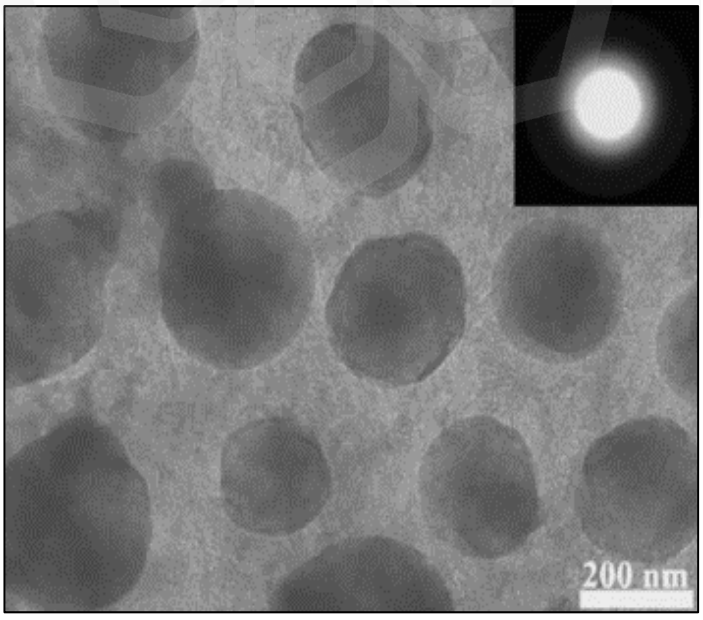

Figure 2.11 TEM Result of Silica from Treated RSA (Lu & Hsieh, 2012).

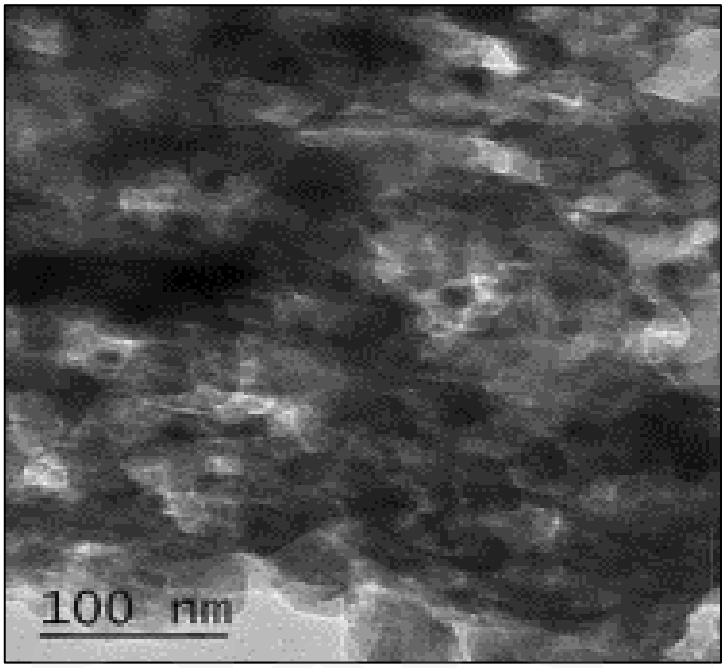

Figure 2.12 TEM Result of Silica from Non-Treated RSA (Uda et al., 2021).

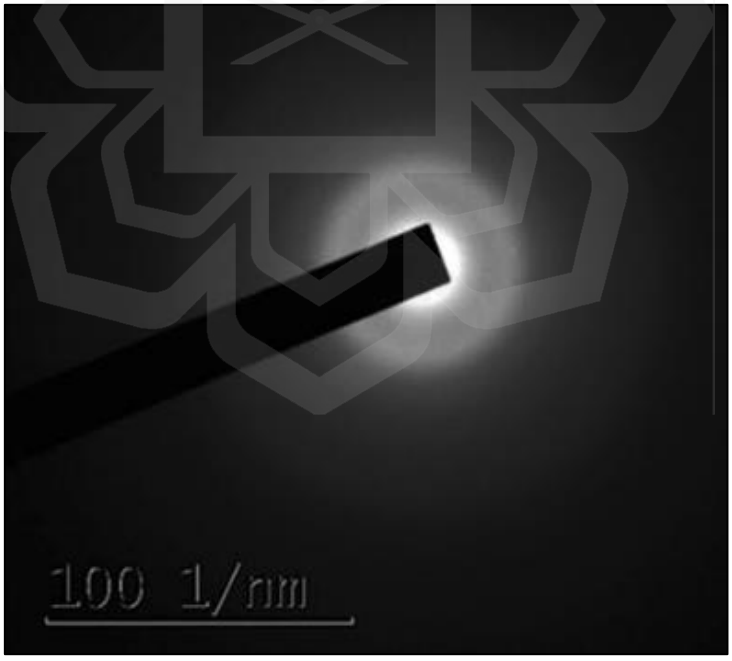

Figure 2.13 SAED Pattern (Uda et al., 2021).

In addition, the grinding process also affects the specific surface area (SSA) and pore structure of the material, where the Brunauer-Emmet-Teller (BET) test and Barret-Joyner-Halenda (BJH) test are conducted to find those properties, respectively. According to Das et al., (2020), the grinding process has reduced the pore size and increased the SSA of material which can be compacted hard, with less void ratio, and hence the water absorption is reduced. Miller et al. (2019) stated that the large SSA and high silica content create a highly reactive pozzolanic material. Van et al. (2013) also recorded that the mesoporous material has high SSA, volume of the pore, and water absorption proportion compared to silica fume. The difference in the BET test to indicate the SSA and pore volume are depended on reduction of pore volume, new open pore, and size of particles as demonstrated in Figure 2.14.

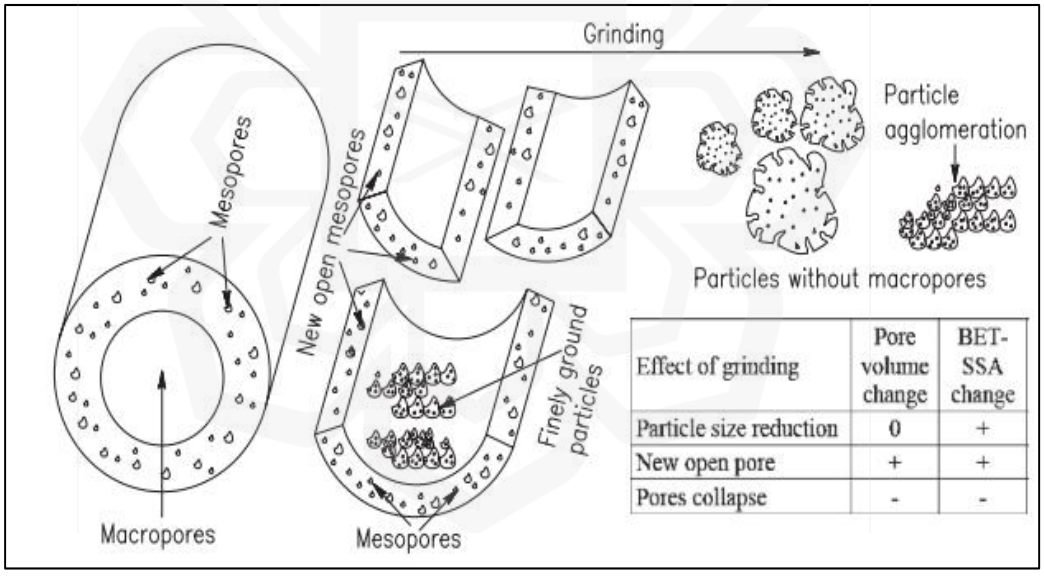

Effect of grinding	Pore volume change	BET-SSA change
Particle size reduction	0	+
New open pore	+	+
Pores collapse	-	-

Figure 2.14 The Effect of BET Result of Ash During Grinding Process (Van et al., 2013).

Since raw rice straw consists of impurities that disturb its performance as a cement replacement material, the chemical composition of RSA is discovered through x-ray fluorescence (XRF) analysis (Khorsand et al., 2013; Pandey & Kumar, 2019a). Lal et al. (2019) also stated that a significant ash component is a silica obtained from XRF analysis.

Based on ASTM C618, the combination of chemical compositions of silicon dioxide (SiO_2), aluminium oxide (Al_2O_3), and iron (III) oxide (Fe_2O_3) is more than 70% to be used as pozzolanic material (Raheem & Kareem, 2017a). Thus, many past researchers conducted XRF tests to indicate whether the amount of those chemical compositions meet the requirement of ASTM C618 (Morsy & Rashwan, 2015; Munshi & Sharma, 2018; Pandey & Kumar, 2019a, 2019b; Naveed & Sharma, 2020). According to the XRF results from those past researchers, the RSA has high SiO_2 content, while calcium oxide (CaO) is the lowest, and the material used had more than 70% of that chemical composition (SiO_2, Al_2O_3, and Fe_2O_3).

Next, the X-Ray Diffraction (XRD) analysis is another test that demonstrates evidence to prove that the pozzolan has high amorphous silica or not, so the mineralogical phases are presented in materials through XRD analysis (Lu & Hsieh, 2012). XRD analysis carried out to distinguish the existence of crystalline or amorphous silica structure. Based on the XRD result, a board and no sharp peak usually lie in between 2θ of 22° to 24° shows amorphous silica, while sharp peak of spectra at 2θ of 10° to 14° shows crystalline (Wong et al., 2019). Munshi and Sharma, (2016) also mentioned that the XRD analysis helps to monitor the presence of quartz as major components in the pozzolan and the lesser amount of calcite. For example, Pandey and Kumar (2019b) reported that XRD analysis shows the mineral phases present in the material. Three peaks were distinguished from the XRD analysis. Quartz (SiO_2) presented at peaks 1 and 3 while hexathiane (S_6) at peak two, as shown in Figure 2.15. Those peaks formed are amorphous silica. In addition, Xu et al. (2015) indicated that the grinding process does not affect the amount of chemical composition of ashes according to XRD analysis.

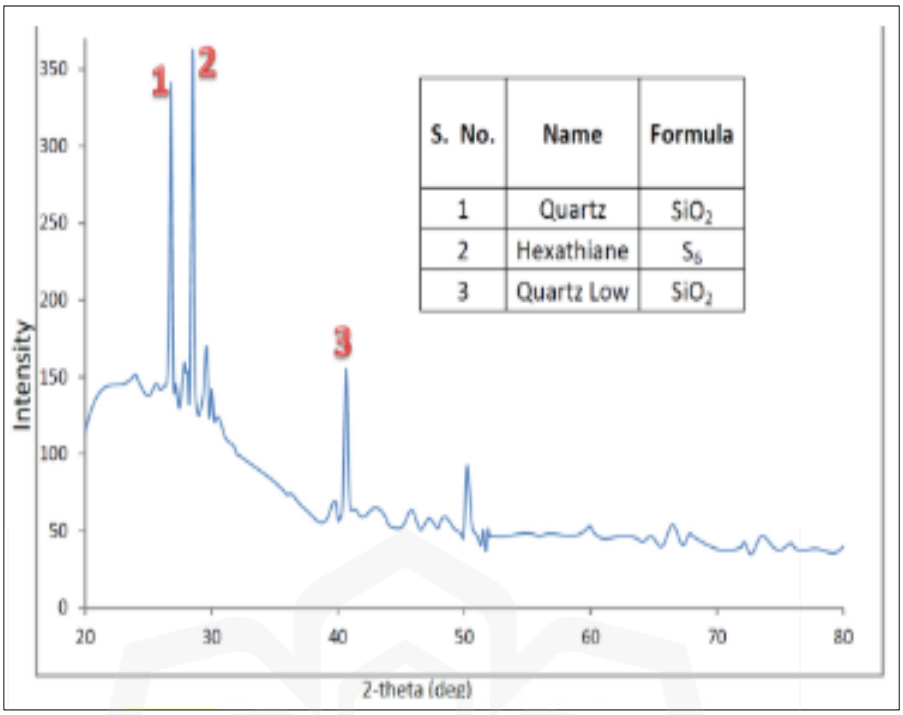

Figure 2.15 XRD Result of RSA (Pandey & Kumar, 2019b).

Furthermore, the Fourier transforms infrared spectroscopy (FTIR) analysis determines the functional groups and atomic arrangements of pozzolan in the cement mortar. The FTIR analysis is usually recorded between wavenumber 4000 cm^{-1} to 450 cm^{-1} (Parande et al., 2011; Roselló et al., 2017). The FTIR analysis was used to analyze whether the ash can replace cement or not as a binder in cement mortar (Parande et al., 2011). The FTIR analysis shows the presence of crucial peaks, which are carbonate and the vibration of bonds C-O, Si-O-Si/Al, and Al-O (Villca et al., 2021). Munshi and Sharma (2018) illustrated FTIR result in Figure 2.16 that two prominent absorption peaks (Al–O and Si–O bonds) are between wavenumber 466 cm^{-1} to 1087 cm^{-1}. Both bonds are essential for the ash and can be used as a pozzolanic material. The predominant absorbance peak at wavenumber 1080 cm^{-1} to 1090 cm^{-1} is siloxane bonds (Si–O–Si).

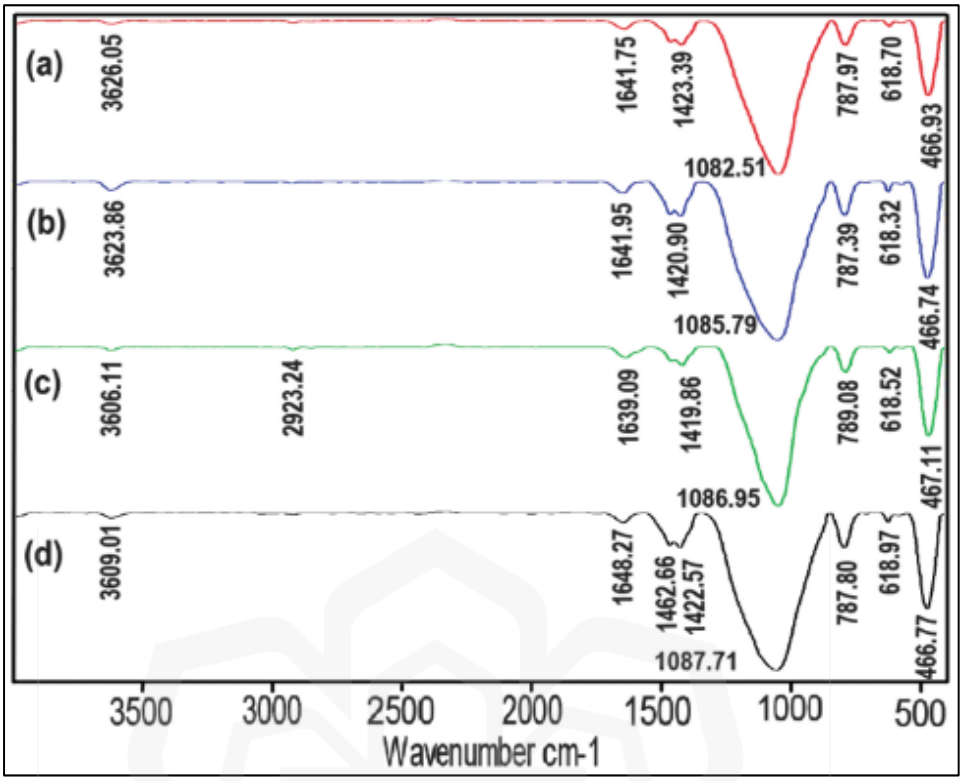

Figure 2.16 FTIR Analysis of Different Ashes (Munshi & Sharma, 2018).

2.9 MECHANICAL PROPERTIES OF RICE STRAW ASH (RSA) AS POZZOLAN IN CEMENT MORTAR

Many researchers have done this test to know the development strength of the samples. A compression test is used to test the strength of hardened concrete. The compression test is easy to perform to test the mechanical properties of cement mortar or concrete. Mahmuda et al., (2020) used rice straw ash (RSA) to replace the OPC content in the mortar for about 10%, 20%, and 30%, and then compared it with the conventional mortar (100% OPC) when the curing process reached 7 days, as illustrated in Figure 2.17. As a result, the strength of mortar incorporated with RSA was higher than the conventional mortar, and the mortar with 30% of RSA as cement replacement material (CRM) was reported as the highest strength value with 27.32 kN.

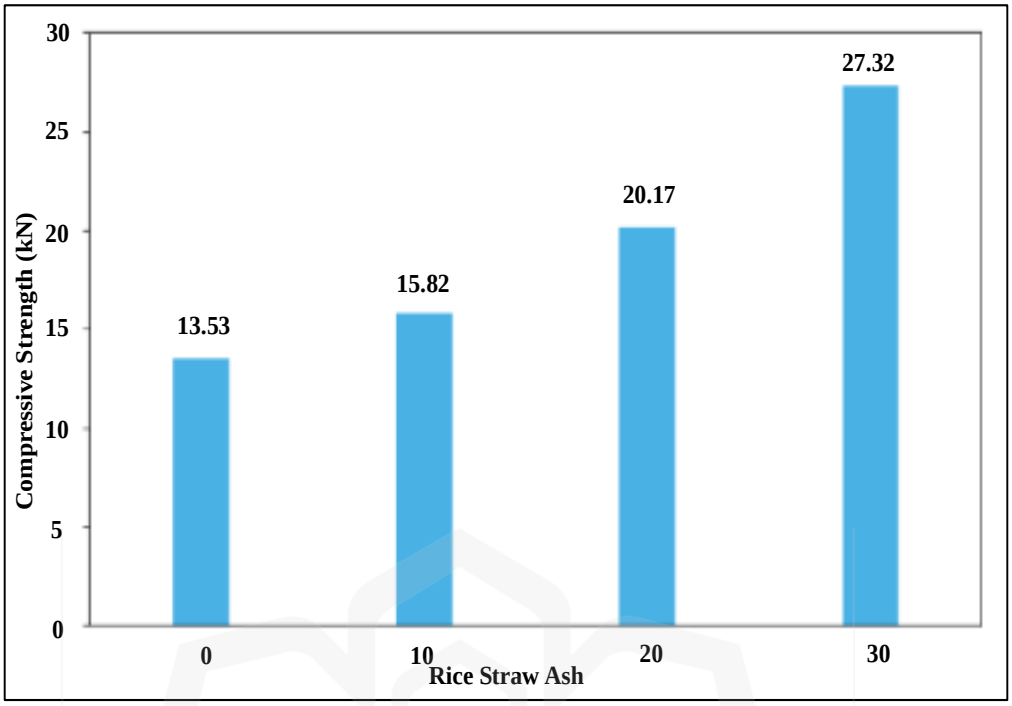

Figure 2.17 The Compressive Strength of RSA Incorporated in Cement Mortar at 7 Days of Curing Process (Mahmuda et al., 2020).

According to an experiment conducted by Ataie and Riding (2016), the strength of standard mortar specimens when the aged of it reached 7, 28, and 91 days for RSA is obtained to indicate the development of the strength of mortar. It was concluded that the compressive strength of 10% of RSA incorporated in the cement mortar is higher than the control samples (OPC). The presence of the RSA in the mixture helps develop the mortar strength. Therefore, the compressive strength of the mortar will be increased. The authors also found that the high specific surface area (SSA) of ashes influences the compressive strength value. The high SSA value of ashes improved mortar performance during 91 days. Dabai and Muhammad, (2017) conducted a compressive strength test when the aged cement mortar with 2%, 4%, 6%, 8%, and 10% of RSA achieved 2, 7, and 28 days. The authors perceived that the performance of compressive strength throughout 28 days for each percentage is increased but the decline pattern recorded for the 10% of RSA used as CRM in cement mortar.

Munshi et al. (2013) replaced 5%, 10%, and 15% of RSA by the weight of cement to form mortar. As illustrated in Figure 2.18, they reported that with 10% cement substitution in a mortar with RSA, the compressive strength improves up to 12.5%. At the same time, the value of initial and final setting time for mortar with the substitution of RSA up to 10% increased. On the other hand, the 15% of RSA replaced cement showed an opposite compressive strength value pattern with 5% and 10%. In 2019, Munshi and Sharma (2019) observed the performance of RSA as an admixture in construction work. They performed a compressive strength test to determine the improvement in the strength value of 10% RSA-replaced cement in mortar production for 56 days. As demonstrated in Figure 2.19, they mentioned that the compressive strength of mortar containing RSA is lesser than the control sample (OPC) at 7 days of curing process, but the strength increases when the cured age of mortar reaches 14 days. At last, the strength of mortar containing RSA increases by 6% to the control sample.

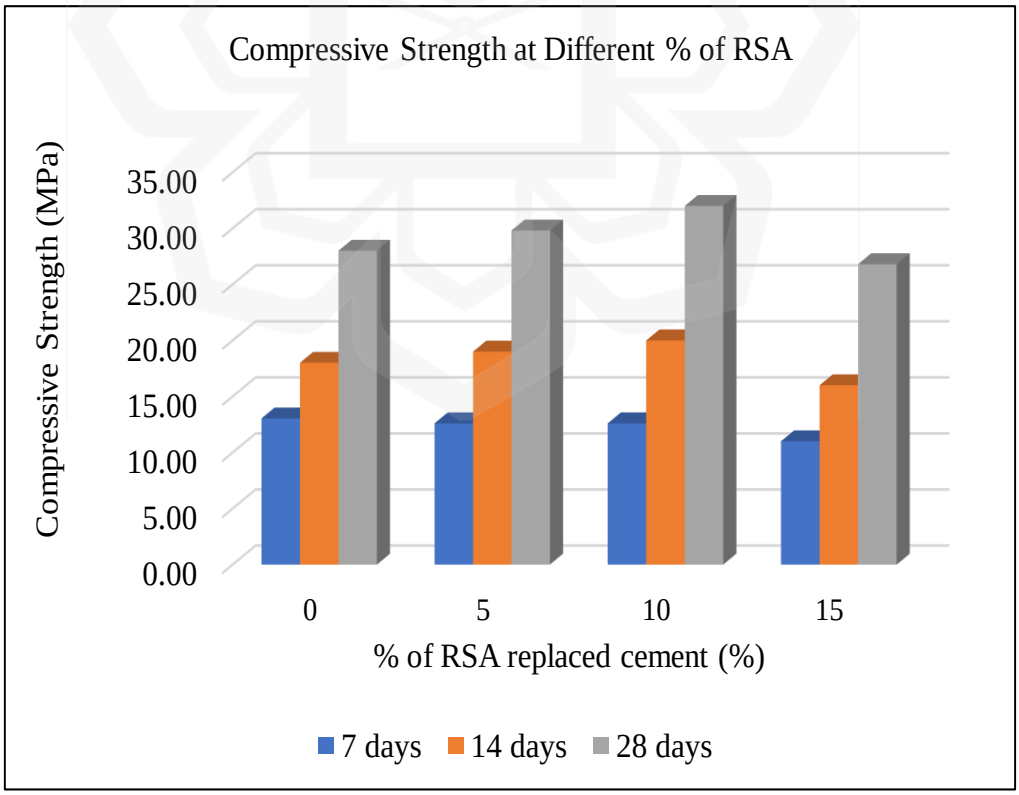

Figure 2.18 Compressive Strength at Different Percentages of RSA (Munshi et al., 2013).

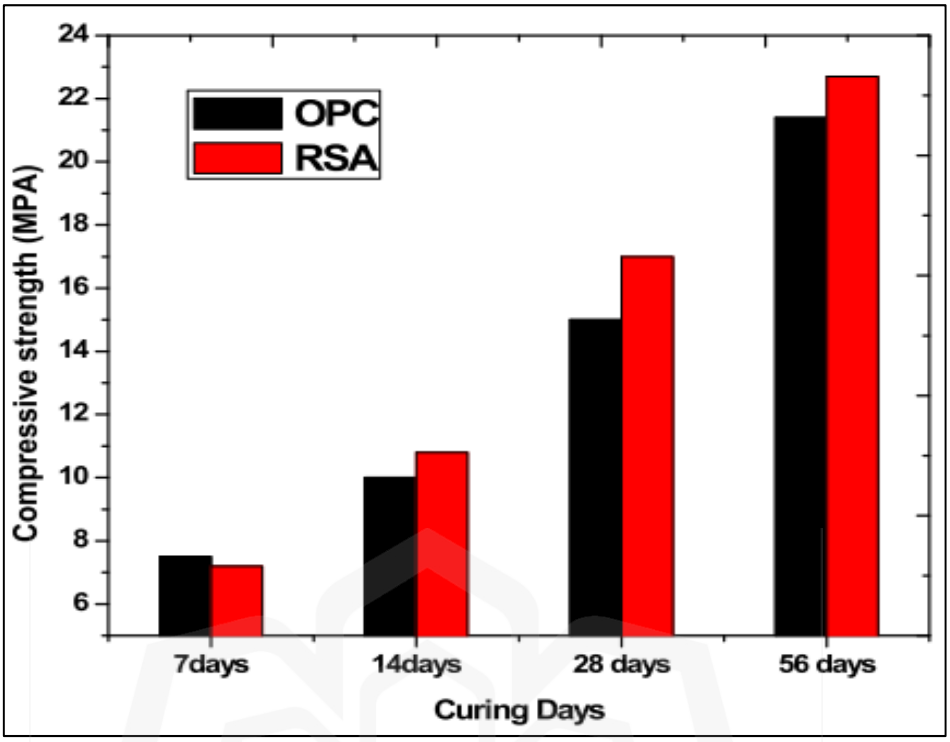

Figure 2.19 Compressive Strength of Mortar throughout 56 Days (Munshi & Sharma, 2019).

2.10 POZZOLANIC REACTIVITY OF RICE STRAW ASH (RSA) IN CEMENT MORTAR

As the utilization and henceforth the concrete production is expanded, one of the ways to decrease carbon dioxide (CO_2) emitted into the air is to utilize the pozzolan as a substitution for concrete. The pozzolanic reactivity of cement mortar or concrete depends on the silica content in rice straw ash (RSA) (Kumar & Pandey, 2014). However, Athira et al. (2019) reported that silica is the predominant material to increase the reactivity of concrete production. The high pozzolanic reactivity of mortar or concrete production causes high mechanical and microstructure performance (Kang et al., 2019).

Pozzolan tends to be one of the admixtures used in the cementing system. First, it is a fine powder material added to the cement mix. It then will be reacted with lime and

enhance the mechanical and microstructure properties of concrete or mortar. Finally, the hydration process of the cement will release it to form calcium silicate hydrated (C-S-H) (Goodman, 2020). The mineralogy, the surface area, and the presence of carbon in the materials affect the performance of pozzolan in the cement matrices. When the strength of specimens increased, the water content reduced, and the pozzolanic reaction increased. The fineness of pozzolan particles contributes to a more significant pozzolanic reaction and fills voids of mixtures. Thus, the compressive strength of mortar or concrete increases, mentioning that the silica content is a factor, but small particles and amorphous states are required.

2.10.1 Evaluation of Pozzolanic Reactivity of Rice Straw Ash (RSA) in Cement Mortar

The performance of the pozzolanic reactivity of any material incorporated with cement is important in the concrete technology. The formation of additional calcium-silicate-hydrate (C-S-H) was contributed to increase strength of concrete (M. Meddah et al., 2020). The first method to evaluate the pozzolanic reactivity is conductivity measurement test. For the conductivity measurement test, the rapid evaluation method was reported by Luxan et al. in 1989 to find the reactivity of ashes used in the study. First, the calcium hydroxide ($Ca(OH)_2$) was added to the saturated solution containing the ash. Then, the conductivity level will be measured using a direct current over a certain period. Most past researchers have conducted it to obtain the reactivity of the ashes such as sugarcane and rice husk ash (Hosseini & Aziz, 2013; Kusbiantoro et al., 2017).

Furthermore, the pozzolanic reactivity of the ashes in the strength activity index (SAI) test is calculated based on ASTM C311 (Abdulmatin et al., 2018; Athira et al., 2019; Khan et al., 2020). ASTM C311 is the standard procedure specification in preparing the specimen for the SAI test (“ASTM C311”, 2005). The sample of mortar prepared for this test is the same as the control mortar, with 20% of pozzolan replacing the cement content.

After a day, the mortar will be demoulded and cured in tap water for about 7 and 28 days. Then, the mortar undergoes the compression test to indicate the compressive strength for both cured ages. Based on ASTM C311, the good pozzolanic reactivity of the mortar is defined when the average SAI result increase about 75% after the age of the mortar reaches 28 days ("ASTM C311", 2005). The SAI result was determined as equation 2.4. Both Athira et al., (2019) and Khan et al., (2020) used this test to indicate the pozzolanic reactivity of rice straw ash (RSA).

$$SAI = (A/B) \times 100\% \quad (2.4)$$

Where: A = mean compressive strength of mortar with pozzolan

B = mean compressive strength of control mortar

The Frattini test is conducted based on EN 196-1, whereby the chemical titration is done to determine the dilution of calcium ion (Ca^{2+}) and hydroxide ion (OH^-) in the solution either with the presence of pozzolan or CEM-I (ordinary Portland cement) ("EN 196-1:1995", 2005). First, the 100 ml of purified water was mixed with 20 g of the specimen with 20% of pozzolan as a replacement for cement. Next, the specimen was placed in a sealed plastic bottle for about 8 days inside the oven at 80℃. The specimen was cooled under room temperature and vacuum filtered using the 2.7 µm nominal pore size of filter paper. Thus, OH^- is analyzed through titration process using dilute hydrochloric (HCl) acid combined with methyl orange indicator and the Ca^{2+} use Patton and Reeder indicator. But, Antiohos et al. (2014) and S. A. Saad et al. (2015) stated the Frattini test and the SAI approach had been discovered to correspond with one other and be procedures that can be well-controlled.

Meanwhile, the Chapelle test determines the pozzolanic reactivity of the ashes in the cement mixture, followed by BS 8615-2 ("BS 8615-2",2019). This test measured the lessening of $Ca(OH)_2$ in the mix with siliceous or aluminosilicate materials. There will be

two mixtures in which calcium oxide (CaO) is present with pozzolan and without pozzolan. The mixture without pozzolan is a control mixture for the test. For the experiment on the pozzolan mixture, 1 g of pozzolan and CaO powder were mixed with 250 ml of distilled water for about 16 hours at 90℃. Then, the dissolution was cooled until it reached room temperature and filtered using 1 N of HCl solution (Katare & Madurwar, 2020; Pontes et al., 2013). At last, the amount of CaO was calculated based on the equation 2.5 as shown below.

$$\text{Mg CaO} = 2 \times ((v2-v1)/v2) \times (74/56) \times 1000 \quad (2.5)$$

Where: v1 = titration volume of the pozzolanic mixture with CaO and pozzolan

v2 = titration volume of the control mixture with CaO

On the other hand, Pontes et al. (2013) stated that the Chapelle test was preferred over the SAI test because of the low time and material usage. But, the Chapelle test only focused on CaO consumption. The Frattini test seems to be very useful in finding the reactivity of pozzolan, but this test only can be applied when the age of samples is up to 8 days. Ataie and Riding (2013) mentioned that measurement the temperature in the conductivity measurement test did not affect the measured conductivity change. The increasing electrical conductivity occurs when the dissolution of metal impurities in the ashes.

Several types of pozzolanic reaction methods determine the reactivity of ashes in the cement mortar, such as the conductivity test, SAI test, Frattini test, and Chapelle test, as recorded in Table 2.6. Overall, the SAI test seems the easiest among other methods but gives a good result on the pozzolanic reactivity (Khan et al., 2020; Yadav et al., 2020; Kalakada et al., 2022).

Table 2.6 Summary of Past Research on Finding Pozzolanic Reactivity of Waste.

Author	Material tested	Method(s) used
Hosseini and Aziz (2013)	Rice straw	Rapid evaluation test
Pontes et al. (2013)	Metakaolins, clay, rice husk, biomass ashes, fly ash eucalyptus bark ashes	Chapelle test Frattini test SAI test
Van et al. (2013)	Silica fume, rice husk	SAI test
Antiohos et al. (2014)	Rice husk	Frattini test
S. A. Saad et al. (2015)	Rice husk	SAI test
Ataie and Riding (2016)	Rice straw, wheat straw	Chapelle test
Kusbiantoro et al., (2017)	Sugarcane bagasse	Chapelle test
Roselló et al. (2017)	Rice Straw	Frattini test
Q. Xu et al. (2018)	Sugarcane bagasse	SAI test
Xu et al. (2018)	Rice husk	Rapid evaluation test
Kramar and Ducman,(2018)	Fly ash, coal	SAI test Frattini test
Kasaniya et al. (2019)	Fly ash, slag	SAI test
Yadav et al. (2020)	Sugarcane bagasse	SAI test
Khan et al. (2020)	Rice husk	SAI test
Kalakada et al. (2022)	Glass powder	SAI test

2.11 INTERFACIAL TRANSITIONAL ZONE (ITZ) ANALYSIS

The interfacial transitional zone (ITZ) is a layer located in between the aggregate and the cement paste. Cement paste consists of a double layer of calcium hydroxide crystals ($Ca(OH)_2$) aligned to the aggregate and calcium silicate hydrated (C-S-H) gel which is located beside the paste with a thickness of approximately 1 μm (Vargas et al., 2017). The ITZ is the weakest link in ordinary Portland cement (OPC) concrete, where the micro-cracks usually form when applied load. Investigation of ITZ is critical because it is

considered to have distinct microstructures than the bulk of the hardened cement paste (B. Singh et al., 2015). The significance of ITZ is the primary measurement of the mechanical properties and durability of concrete (Qudoos et al., 2019).

According to Vargas et al. (2017), cement particles cannot penetrate this zone due to the large size of aggregates. Thus, this zone consists of a high porosity structure, which affects the properties of aggregates and cement matrices. However, Golewski (2018) mentioned that the weakness of the ITZ area is due to the differences in the modulus elasticity and the shrinkage of the aggregates and cement matrix, which cause crack and high-stress concentrations in the ITZ area. The scanning electron microscopy analysis (SEM) of ITZ for the concrete with the conventional aggregate was conducted by Vargas et al. (2017), as shown in Figure 2.20 (a), (b), and (c). The SEM image shows a lot of porosity formation in the ITZ. There is also a continuous gap between phases, with mostly $Ca(OH)_2$, ettringite crystalline, and a trace of C-S-H.

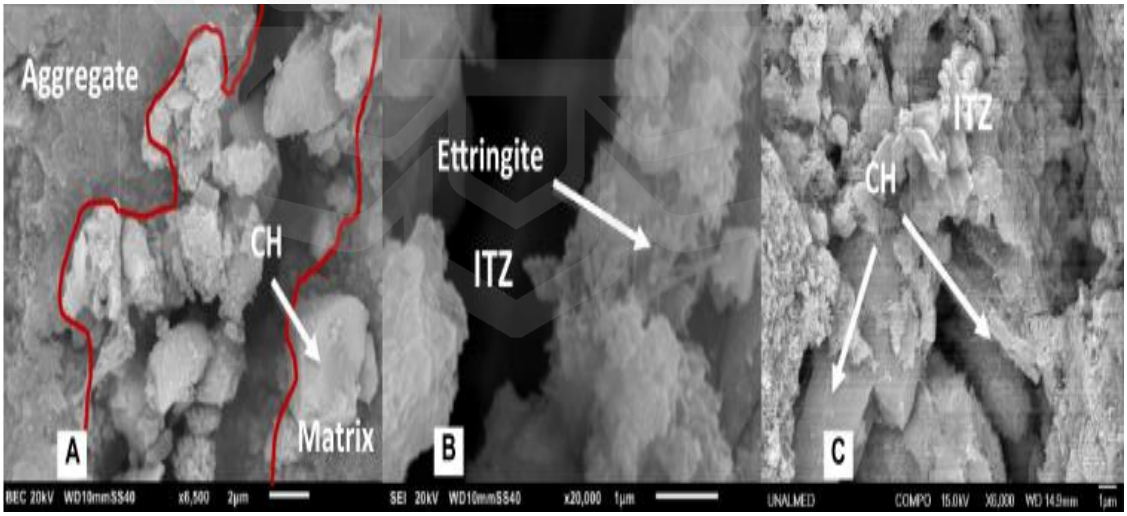

Figure 2.20 (a), (b), (c) SEM Image of Conventional Concrete (Vargas et al., 2017).

However, Qudoos et al. (2019) compared the ITZ of the conventional concrete (100% OPC) with the concrete that used wheat straw ash (10% WSA,90% OPC), as shown in Figure 2.21 (a) and Figure 2.21 (b). The conventional concrete has more pores than the specimens incorporated with WSA particles from both figures. As a result, this is proved

that the pozzolanic material presented reduces the pores and dense the microstructure of cement paste through its filler and pozzolanic effects. The pozzolan fills the voids, and the latter absorbs the $Ca(OH)_2$, creating additional hydration materials to improve the microstructure. The densification of the microstructure of the WSA samples is significant to observe in the ITZ area.

Agwa et al. (2020) mentioned that the increasing establishment of C-S-H in the concrete reduced the porosity and improved the microstructure at the ITZ part. Thus, the compressive strength of cement matrices increases. Furthermore, the C-S-H in concrete is formed when the high percentage of silicon dioxide (SiO_2) in the RSA reacts with the $Ca(OH)_2$, as shown in Figure 2.22. The percentage of SiO_2 presented in RSA is 76.8%. Lastly, the physical and chemical characteristics, including the crystallinity and morphological properties of cement paste and the aggregates, involve to the ITZ density by reducing porosity and increasing the hydrated phases. In addition, the physical characteristics, i.e., the porous structure, contributed to the accumulation of cement particles, minimizing the gap of ITZ formation, and developing C-S-H hydrated phases from the surface.

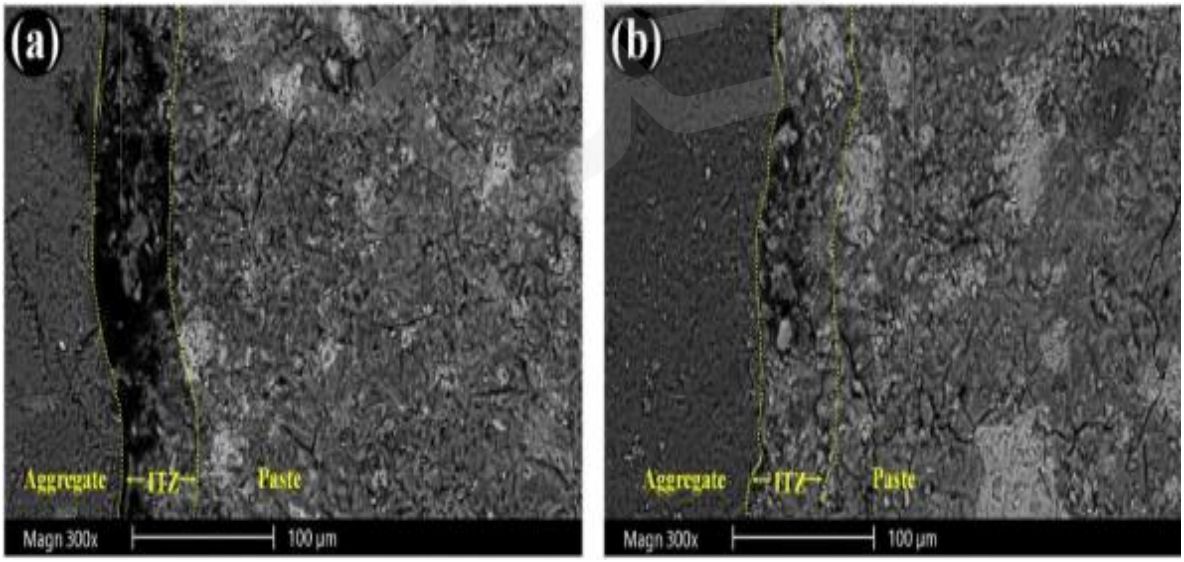

Figure 2.21 The ITZ Formation at 28 Days of Curing Process (a) Conventional Concrete (b) Cement with Wheat Straw Ash (Qudoos et al., 2019).

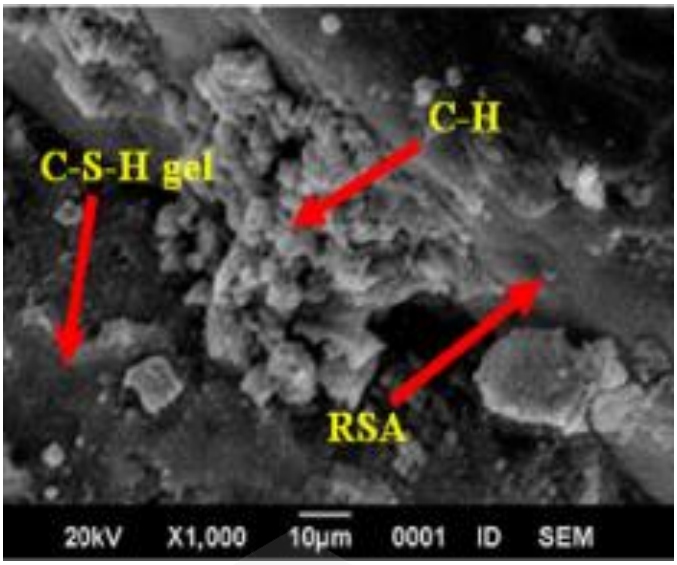

Figure 2.22 FESEM Result of RSA Incorporated in Concrete (Agwa et al., 2020).

2.12 DESIGN OF EXPERIMENT (DOE) BY USING RESPONSE SURFACE METHODOLOGY (RSM)

Response surface methodology (RSM) is an efficient instrument for various scientific applications, including chemical, industrial, and biological processes. RSM seems to be a statistical appliance for the experiment design, empirical model construction, and factor effect evaluation (Reji & Kumar, 2022). The RSM decreases the number of samples involved in the experimentation required to analyze the various parameters with wide ranges and correlations (Ahmed et al., 2020). Thakur et al. (2020) stated that G. E. P. Box and K. B. Wilson developed RSM in 1951, defining the design of the sequence of the experiments to obtain the optimal response.

In RSM, the determination of independent or dependent variables, and responses involved in the optimization analysis must be selected properly to ensure the quality of optimization result. After completing gather all important data in the RSM, a mathematical statistics analysis must be fit to examine the characteristics of responses based on the interaction with the factors. The fitted model was verified through multiple regression

analysis and analysis of variance (ANOVA), which illustrated in the contour plots and graphs. Then, the optimization analysis was continued when the model is fit and generated the optimum value of the design (Reji & Kumar, 2022).

According to Zolgharnein et al. (2013), RSM defined finding the optimum response in experimental work as the crucial step of the optimization process. Therefore, the implementation of RSM was developed in the industry. Several types of RSM can be used for the optimization process. However, two famous methods are found, i.e., central composite design (CCD) and Box-Behnken design (BBD). Both ways are usually used in the final optimization of the experiment and can analyze the responses with the independent variables on different ranges, but each technique has various features.

Generally, the CCD is involved factorial design points, the axial point, and the centre point, as illustrated in Figure 2.23. In CCD, there include two levels of the factorial design as 2^K, whereby the k is known as the number of factors involved in the design. Then, the capability of curvature can be described through the star design with 2k. The replication of the centre point is frequently used as a measurement when reproducibility and lack of model fit. Figure 2.23 also shows that α is denoted as the interval of the star point from the centre point. $N=2^K + 2K + C_0$ is used to determine the total number of design points needed (N) in the analysis, where C_0 is the replication number of centre points and K is the number of factors.

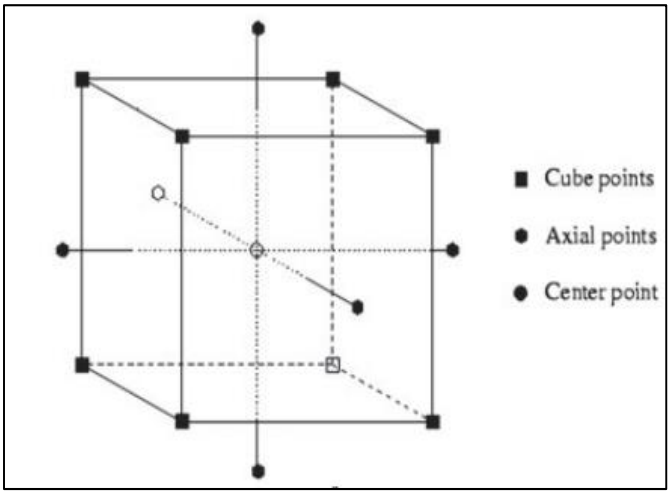

Figure 2.23 Central Composite Design (CCD) in the Cube View (Zolgharnein et al., 2013).

Furthermore, BBD is known as a rotatable or nearly rotatable second-order design. It is based on the three-level incomplete factorial design, which involves the centre points of the edges of the cube and centre points, as shown in Figure 2.24. There is three interlocking 2^2 factorial design along with the centre point. The cube view is spherical and includes the cube's vertices. Thus, it should be avoided as these points are extrapolated based on the prediction. Mathematically, the formula of $N=2k\ (k-1) +C_0$ has been used to determine the number of points involved in the experiment (N), where k is the number of variables and C_0 is the number of centre points.

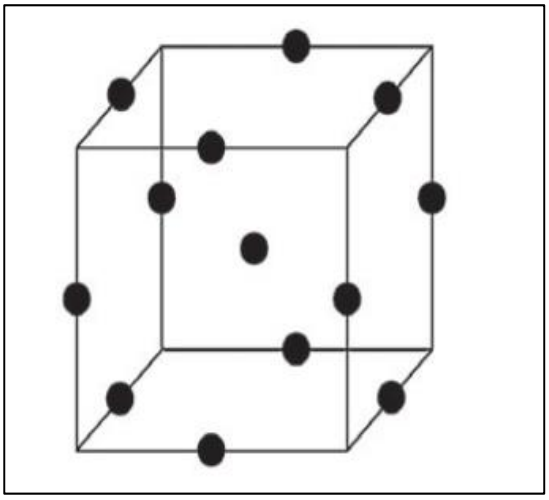

Figure 2.24 Box-Behnken Design in the Cube View (Zolgharnein et al., 2013).

Over the last few years, the RSM has significantly determined the optimal mix proportions of various concrete mixtures. It allows for interaction impact analysis in applying multiple response optimization (Zolgharnein et al., 2013; Amibo et al., 2022). As Bazargan et al. (2015) reported, RSM is an efficient and famous tool used widely across the field. It was utilized to achieve the best results with a limited number of experimental runs in RSM using Design Expert software to analyze the silica extraction in the rice husk ash (RHA) through the alkali pretreatment for energy production.

However, Thakur et al. (2020) also used CCD in RSM to optimize the formation of cellulose nanocrystals (CNC) in rice straw as a binding agent within the manufacturing of nanocomposites for various applications. As a result, Thakur et al. (2020) agreed that the RSM is useful in specifying the main variables throughout the treatment process to prepare CNC in their experiment. Based on RSM seems to be a valuable tool for designing experiments based on all past research, Zolgharnein et al. (2013), Izevbekhai et al. (2021) and, Reji and Kumar (2022).concluded that the CCD is the most preferable method for optimization analysis since the CCD predictability of CCD is more compatible than BBD. The result demonstrates that CCD outperforms the other designs in terms of prediction (Indriani & Wardhani, 2022).

2.13 GAP RESEARCH AND SUMMARY

This research aimed to identify gaps in the current literature on rice straw as a cement substitute. Since there is limited available research on using the RSA as potential pozzolan, thus, this research focused on using rice straw ash (RSA) as pozzolan in mortar production. Many past researchers preferred to use the rice husk ash (RHA) as pozzolan compared to RSA and proved that the RHA has been successfully utilized in many building materials (Munshi & Sharma, 2018; Vieira 2020). While the study seeks the efficacy of the pretreatment of RSA to improve the pozzolanic reactivity of cement mortar, a high concentration of acid used in the pretreatment is not preferable. The high concentration of acid does not significantly enhance the reactivity of the pozzolan in a mortar (Vayghan et al., 2013; Librea et al., 2019).

There is a gap in establishing the impact of pretreatment using a low hydrochloric acid (HCl) concentration. However, the finding of using a low concentration of acid for the pretreatment process is limited since most past researchers used a high concentration of acid (Qudoos et al., 2018; Wong et al., 2019; Hu et al., 2020; Rajan et al., 2020; Uda et al., 2020). At the same time, some of past researchers only focused on the incineration process to produce the ashes (Munshi & Sharma, 2018; Agwa et al., 2020; Dizaji et al., 2022). Still, the pretreatment and grinding processes are essential to forming valuable ashes in concrete production. Therefore, this research intended to find the effect of low concentration acid used for the pretreatment process to improve the reactivity of RSA in mortar. Then, continue the controlled incineration and grinding techniques to produce the highly treated RSA. Hence, the utilization of RSA as cementitious material can be identified.

CHAPTER THREE

RESEARCH METHODOLOGY

3.1 INTRODUCTION

This chapter explains the methodology of the experimental work. Figure 3.1 illustrates the schematic diagram for overall processes conducted throughout this research activity. However, the details of the process flowchart of the methods involved in this study are shown in Figure 3.2 to Figure 3.4. The flowchart of study was divided into four phases. The materials used in this research were selected according to the specific standard related to the objectives of this research. The non-standardized material was obtained through the design procedure. The experimental work focused on producing treated rice straw ash (TRSA) using low hydrochloric acid (HCl) concentration (phase 1), continuing with the incineration process at controlled high temperatures, and grinding the TRSA using a planetary ball mill machine (phase 2). The response surface methodology (RSM) through the Design Expert software was used to determine the number of samples involved in the pretreatment and incineration processes since both methods had a few factors with an extensive range. Then, finding the characterization properties of TRSA and non-TRSA (NTRSA) sample in cement mortar (phase 3), the mechanical properties of the hardened specimen, interfacial transitional zone characteristics, and pozzolanic reactivity (phase 4).

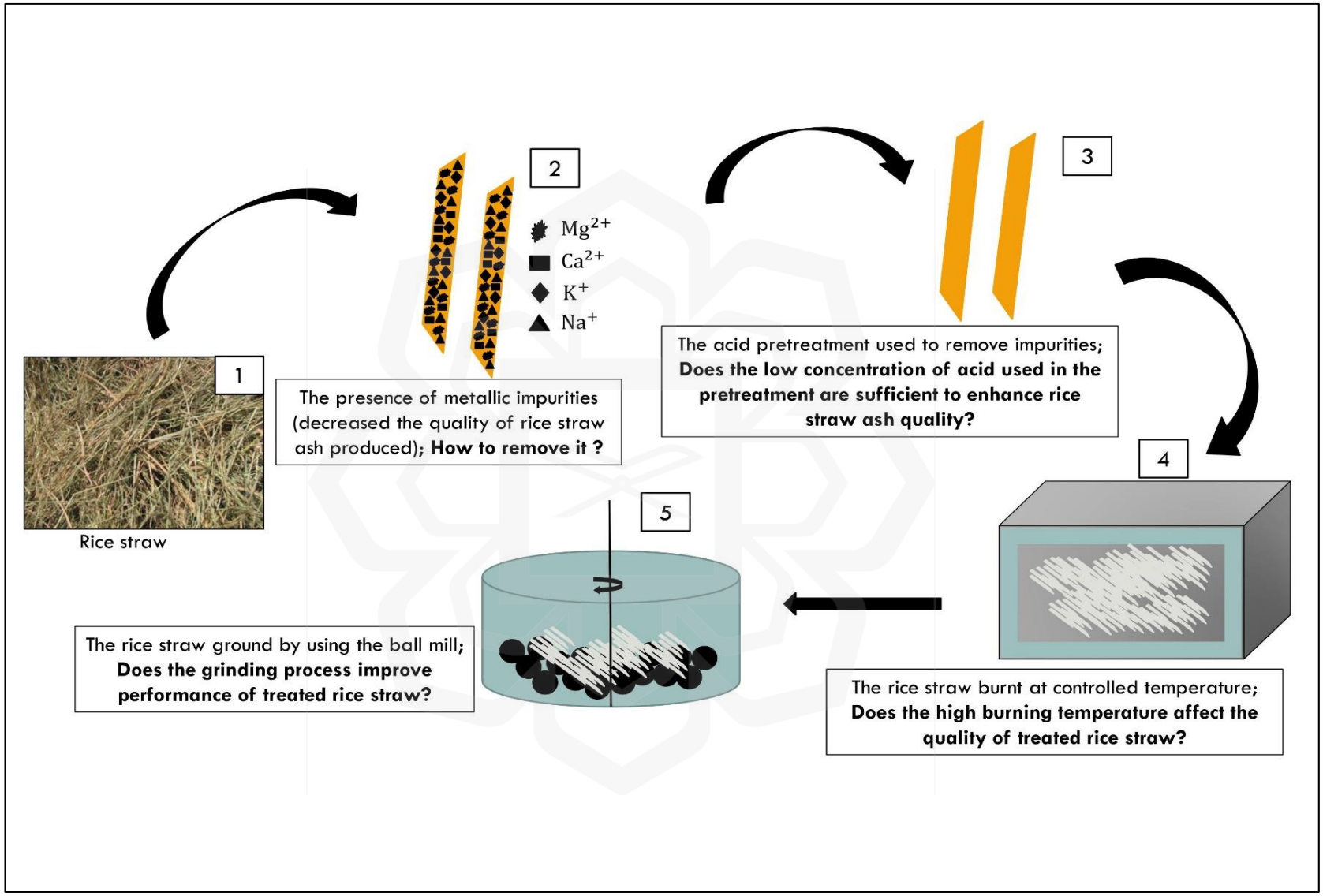

Figure 3.1 Schematic Diagram for Overall Processes in this Research.

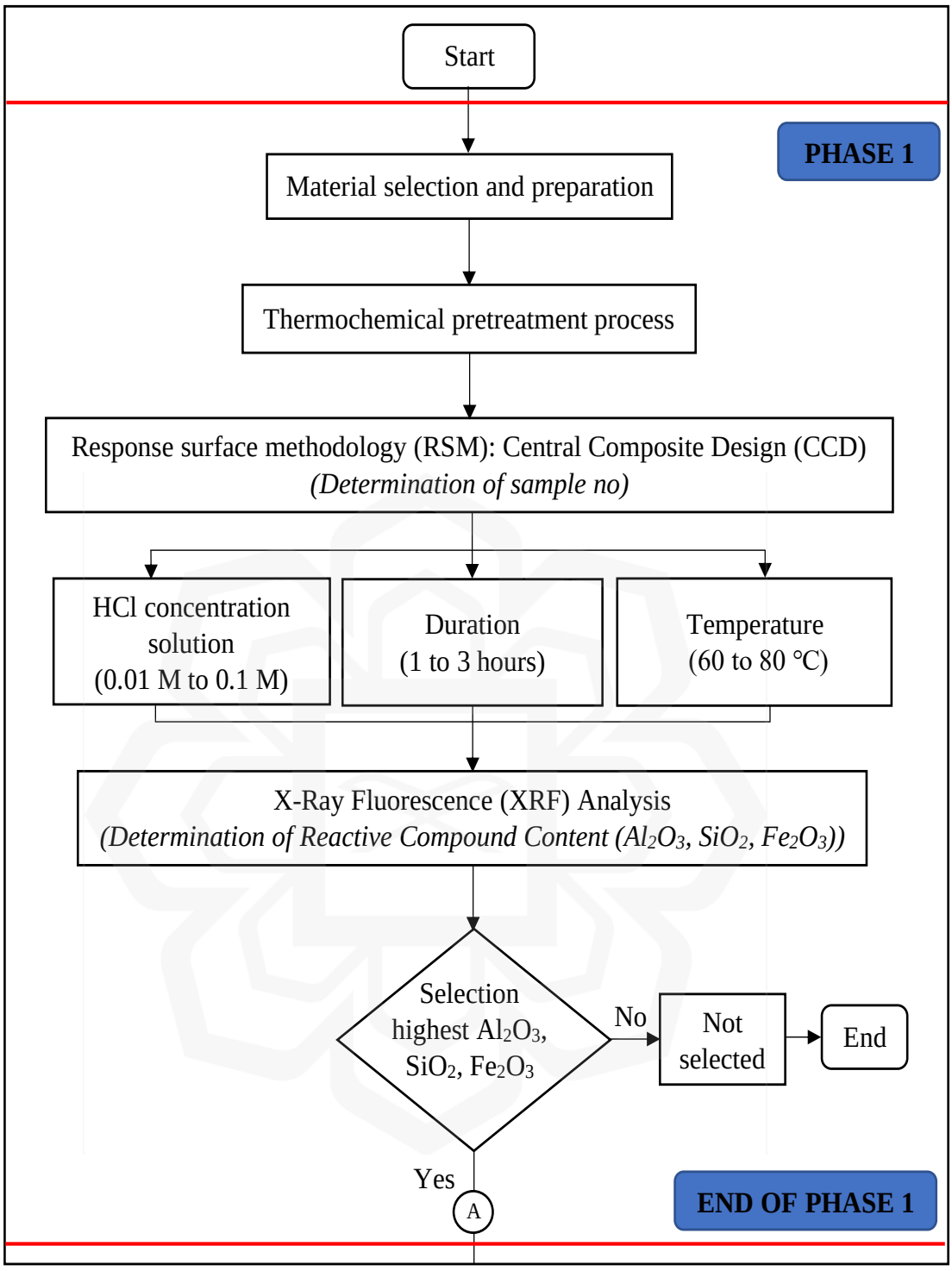

Figure 3.2: The Flowchart of Study.

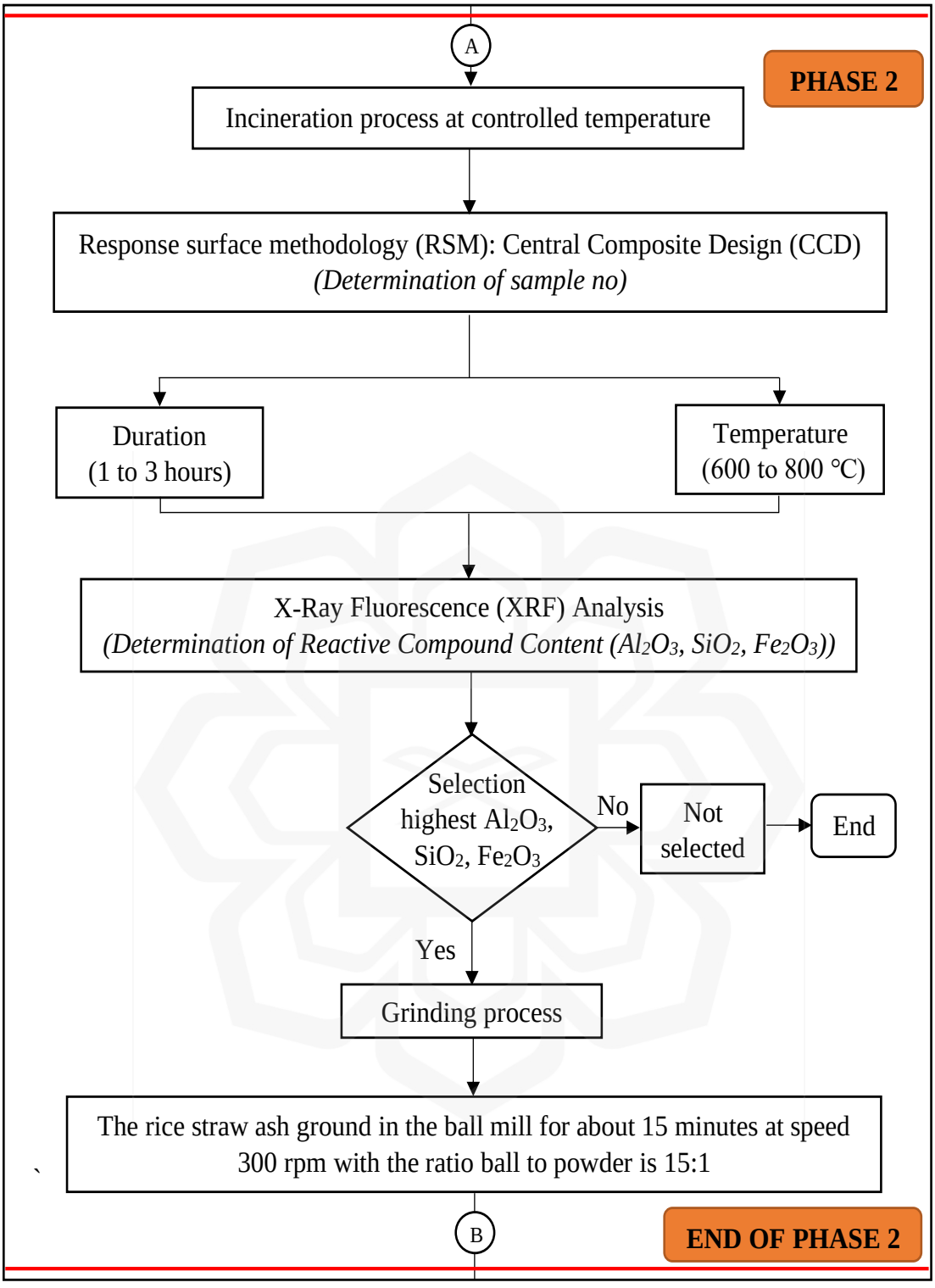

Figure 3.3: The Flowchart of Study (Con't).

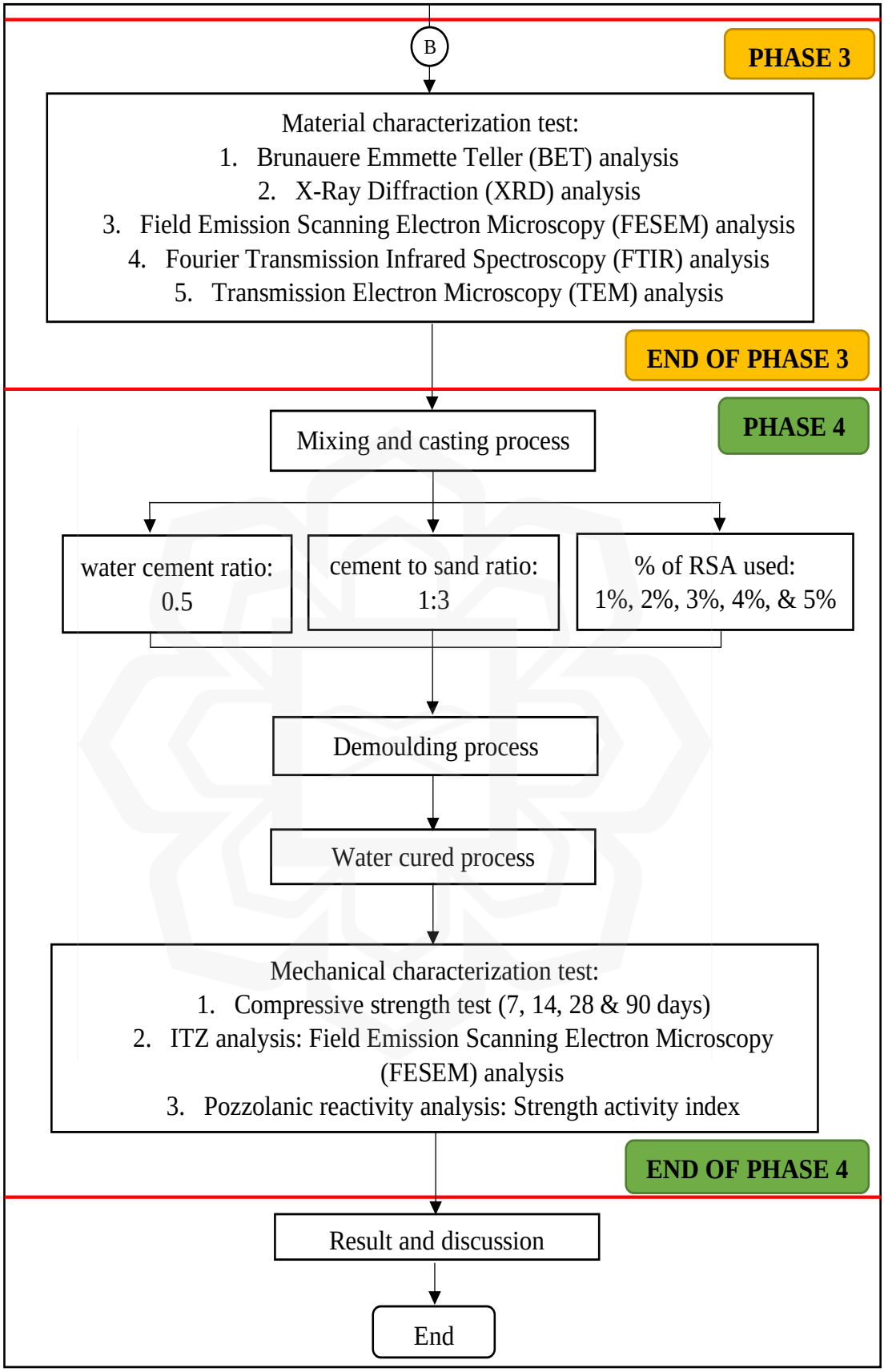

Figure 3.4 The Flowchart of Study (Con't).

3.2 PREPARATION OF A HIGHLY REACTIVE TREATED RICE STRAW ASH (TRSA) AS CEMENT REPLACEMENT MATERIAL (PHASE 1 & PHASE 2)

The rice straw ash (RSA) used to partially substitute cement in the mortar production is an efficient method to save the environment and contribute simultaneously to the conservation of natural resources. The RSA is a residue material from the incineration process of rice straw. Commonly, RSA contains a high amount of silica. The research uses the RSA to replace cement in mortar production partially. The percentage replacement of treated RSA (TRSA) as a binder in the mortar mixing is about 1%, 2%, 3%, 4%, and 5% for five mixing proportions. Thus, this research focuses on developing TRSA as a good reactive toward concrete production. The processes involved were the thermochemical pretreatment process, the incineration process at a controlled temperature, and the grinding process.

3.2.1 Thermochemical Pretreatment Process Optimization Procedure to Produce Treated Rise Straw Ash (TRSA) (Phase 1)

Firstly, the raw rice straw (RS) was collected from the paddy field area in Kodiang, Kedah. The RS was washed using the tap water several times and continued with the oven-dried process using the laboratory drying oven for about 24 hours at 80℃, as illustrated in Figure 3.5 (a) and Figure 3.5 (b). The RS was cut in 3 cm length to ensure that the RS was fully dense in the acid solution during the pretreatment process. Table 3.1 shows the range for each factor involved in the thermochemical pretreatment process. The dilute hydrochloric acid (HCl) was used to treat the RS by soaking in the HCl solution at a specific duration and temperature.

Table 3.1 Range for Each of the Factors Involved in the Process.

Types of factors involved in the pretreatment process	**Range**
HCl concentration	0.01 Molar to 0.1 Molar
Soaking duration	1 hour to 3 hours
Soaking temperature	60℃ to 80℃

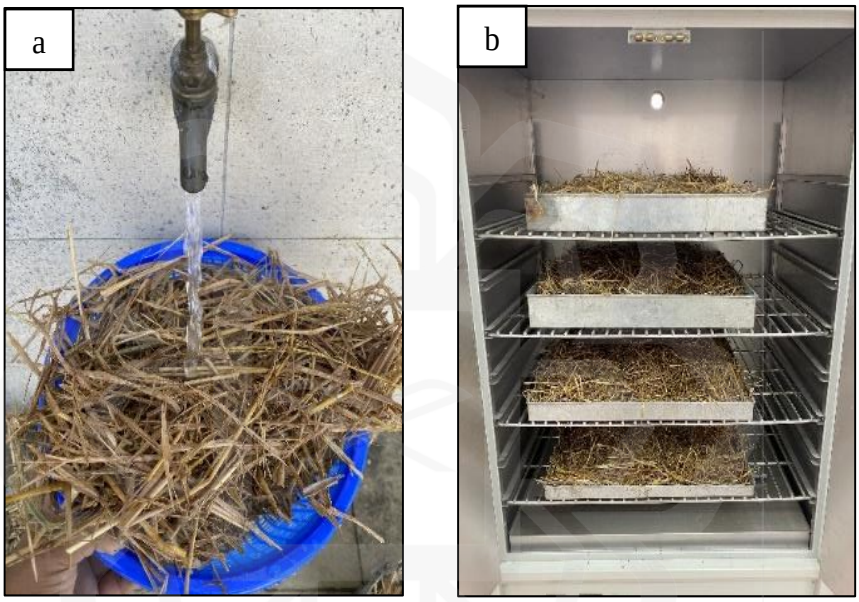

Figure 3.5 (a) Washed Rice Straw Using Tap Water, (b) Oven-Dried Rice Straw Using a Drying Oven.

Then, the design of the experiment (DOE) used the Design Expert Software to determine the number of samples involved in the pretreatment process and to minimize the time consumption since each factor had an extensive range. As stated by most past researchers, the central composite design (CCD) of the response surface methodology (RSM) was the chosen method to define the optimum sample (Zolgharnein et al., 2013; Muhammad et al., 2020; Thakur et al., 2020). Thus, this research used a CCD design to interpret the interaction between the factors and the responses involved in the pretreatment

process. The elements are soaking duration (A), soaking temperature (B), and hydrochloric acid (HCl) concentration (C). However, the response is the percentage of the reactive compound. Figure 3.6 and Figure 3.7 show three factors and a response included in the DOE.

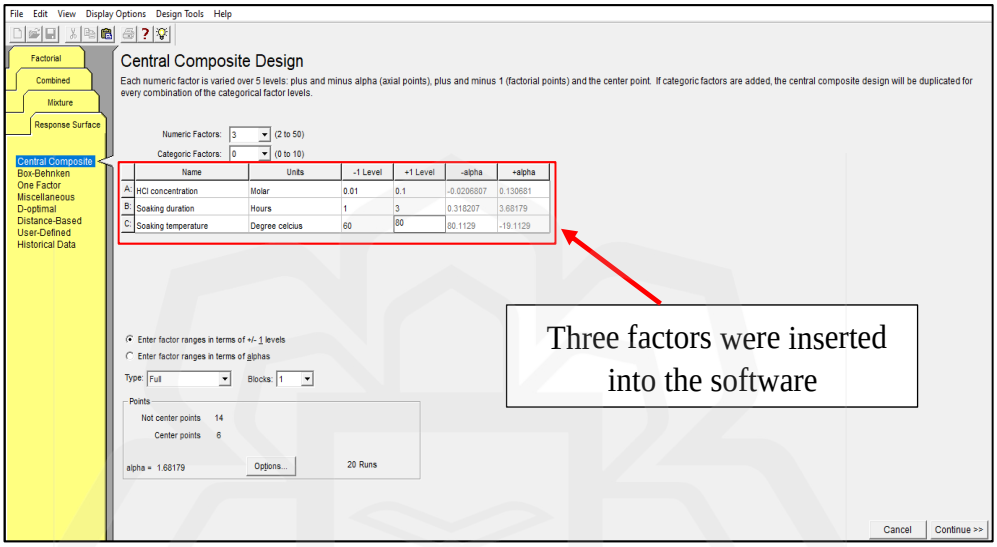

Figure 3.6 The Three Factors Involved in the Pretreatment Process.

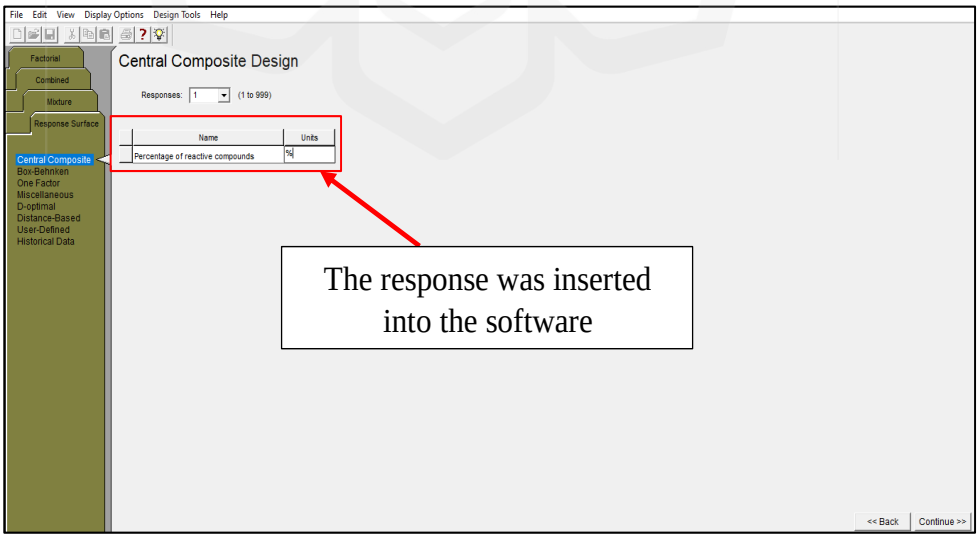

Figure 3.7 The Response Involved in the Pretreatment Process.

Table 3.2 shows 20 samples involved in this process with different HCl concentrations, soaking durations, and soaking temperatures determined by using the DOE method since the range for all factors is large. After the raw RS was washed with tap water and continued with oven-dried using the laboratory drying oven for a day at 80°C as shown in Figure 3.5 (a) and Figure 3.5 (b), the RS was used in this thermochemical pretreatment process. The dilute acid solution used in the thermochemical pretreatment process enhances the amorphous silica, reduces impurities, and improves the pozzolanic reactivity and strength of concrete. This process was conducted inside the fume chamber since HCl is a strong acid, as shown in Figure 3.8.

Figure 3.8 The Fume Chamber.

The ratio of RS and the dilute HCl solution used for this pretreatment process is 0.5 g: 40 ml. Based on that ratio, 50 g of RS: 4000 ml of dilute HCl solution. So, there was 327.30 ml of 1 M of HCl and 3672.70 ml of distilled water in the 4000 ml of dilute HCl

solution since 1 M of HCl equals 81.8 ml of HCl in 1000 ml of distilled water. Thus, the amount of HCl needed for specific concentrations and the amount of distilled water used in each pretreatment process was differ, followed by Table 3.2. The procedure for this pretreatment illustrates in Figure 3.9.

Table 3.2 Samples Involved in the Pretreatment Process Defined by DOE.

No. of run	Factor 1: HCl concentration (Molar)	Factor 2: Soaking duration (Hours)	Factor 3: Soaking temperature (℃)	Response 1: Percentage of reactive compound content (%)
1	0.01	1.00	60.00	
2	0.10	1.00	60.00	
3	0.13	2.00	70.00	
4	0.10	1.00	80.00	
5	0.10	3.00	60.00	
6	0.06	2.00	70.00	
7	0.06	0.32	70.00	
8	0.06	2.00	70.00	
9	0.06	2.00	70.00	
10	0.06	3.68	70.00	
11	0.02	2.00	70.00	
12	0.06	2.00	53.18	
13	0.06	2.00	86.82	
14	0.06	2.00	70.00	
15	0.01	3.00	60.00	
16	0.10	3.00	80.00	
17	0.01	1.00	80.00	
18	0.06	2.00	70.00	
19	0.01	3.00	80.00	
20	0.06	2.00	70.00	

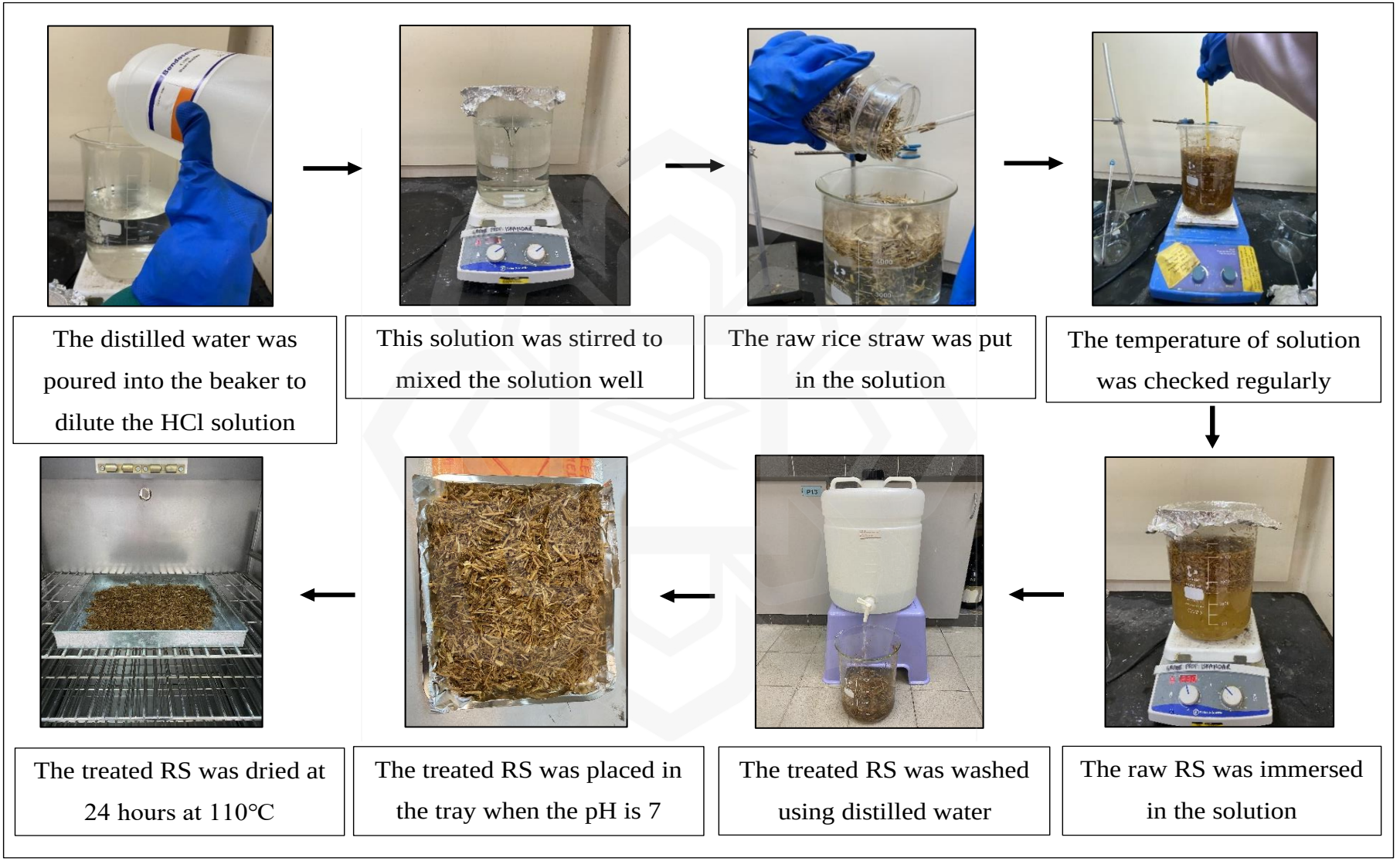

Figure 3.9 Thermochemical Pretreatment Process.

To complete this process, the percentage of reactive compounds (silicon dioxide (SiO_2), aluminium oxide (Al_2O_3), and iron (III) oxide (Fe_2O_3)) present in the ash was recorded through the x-ray fluorescence (XRF) analysis. The XRF result is the data for the response in the DOE. The chemical composition of rice straw ash (RSA) was determined through XRF analysis (Pandey and Kumar, 2019b). Silica was found as the significant component presenting the ash from XRF analysis. Based on ASTM C618, the combination of the chemical composition of SiO_2, Al_2O_3, and Fe_2O_3 is more than 70% to be used as pozzolanic material ("ASTM C618" 2014).

Thus, the chemical composition of the ground ashes was recorded through the XRF analysis. This procedure for this analysis was conducted according to ISO 12677 ("ISO 12677", 2015). The powder sample of RSA was placed into a specific container for testing. Finally, the result was displayed using the installed software. Figure 3.10 shows that the analysis was conducted using the Bruker S1 Turbo SDR Portable XRF Spectrometer X-ray Fluorescence SDD.

Figure 3.10 Bruker S1 Turbo SDR Portable XRF Spectrometer X-ray Fluorescence SDD.

Therefore**,** the interaction of experimental factors with response was determined to identify the optimum sample. The mathematical equation, a regression model between the factors (HCl concentration, soaking duration, and soaking temperature) and the response (percentage of reactive compounds content), was defined through RSM. Then, the significance of the selected model in the model regression analysis was determined to distinguish the correlation between factors and responses involved in this experiment. Usually, the quadratic model was chosen by the Design Expert software for optimization analysis.

Additionally, the ANOVA analysis in the RSM examined the quadratic model. The significance of the model also depends on the p-value, which must be less than 0.05. Nevertheless, the p-value for the lack of fit test of the model must be more than 0.05. At the same time, the RSM observed the errors and, thus, defined the correlation between the predicted and actual values. The prediction and optimization values were kept in the three dimensions (3D) surface formation. Finally, the model without any lack of fit was the selected data (Muhammad et al., 2020).

As a continuation in producing treated RSA (TRSA), the treated RS with the highest amount of reactive compound suggested by RSM was selected. Then, the incinerating and grinding processes were performed to produce the reactive TRSA. The details of those processes were explained in the following sub-section 3.2.2 as follows.

3.2.2 Incineration Process at the Controlled Temperature Optimization Procedure and Grinding Process to Produce Treated Rise Straw Ash (TRSA) (Phase 2)

After completing the thermochemical pretreatment process, the treated rice straw (TRS) was washed using purified water until pH 7. Next, oven-dried it at 110℃ for about 24 hours, as illustrated in Figure 3.9 in the previous sub-section. Thus, the dried TRS was used at a controlled temperature during the incineration process. Proper incineration at a

controlled temperature was required to obtain a good quality of reactive treated rice straw ash (TRSA). The rice straw is not preferred to be burnt under uncontrolled temperatures because the fibrous materials are not fully diminished and created carbon (Miller et al., 2019). This process was conducted using the furnace's Linn High Therm LM 312.6 model, as shown in Figure 3.11.

Figure 3.11 Furnace.

For the incineration process, the burning duration and burning temperature were varied. Since the factors had an extensive range, the design of the experiment (DOE) in the response surface methodology (RSM) of the Design Expert software was used to define the number of samples involved in this process and minimize time usage. This research used a Central Composite Design (CCD) in RSM to interpret the interaction between the factors and the responses involved in the incineration process. The elements are burning duration (A) and burning temperature (B), shown in Table 3.3 with its range. However, the response is the percentage of the reactive compound (silicon dioxide (SiO_2), aluminium oxide (Al_2O_3), and iron (III) oxide (Fe_2O_3)). Both elements and a response involved in the burning process were filled in the software to determine the sample number, as illustrated in Figure 3.12 and Figure 3.13.

Table 3.3 Types of Factors Involved in the Burning Process and Its Range.

Types of factors involved in the burning process	**Range**
Burning duration	1 hour to 3 hours
Burning temperature	600℃ to 800℃

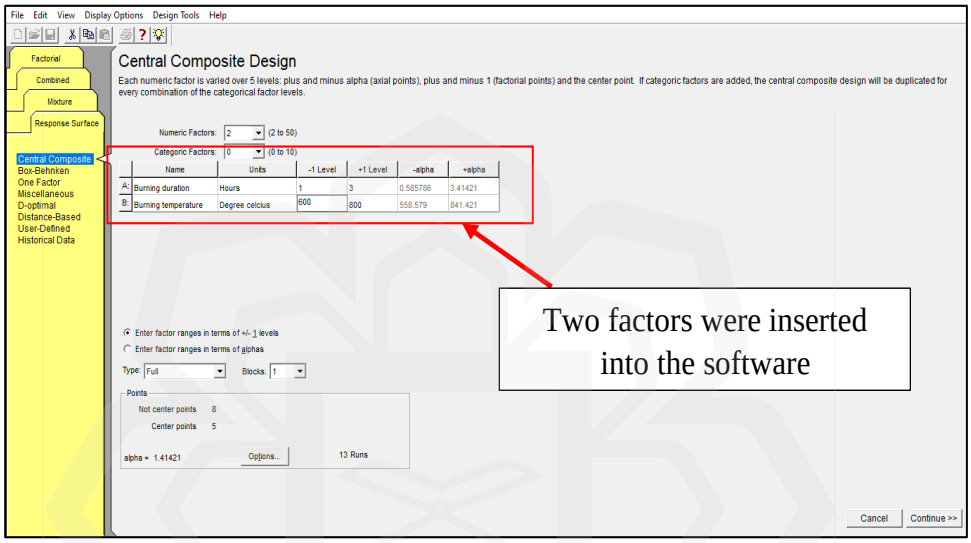

Figure 3.12 The Two Factors Involved in the Incineration Process.

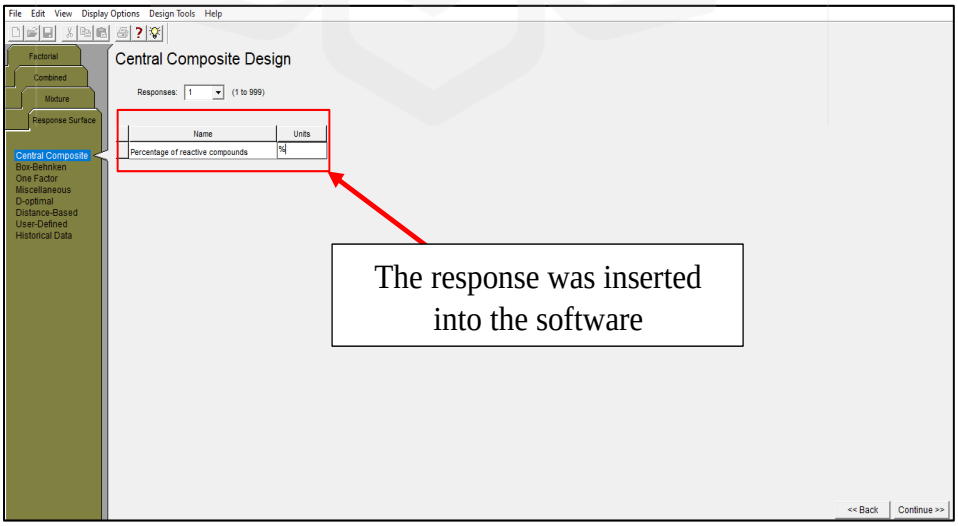

Figure 3.13 The Response Involved in the Incineration Process.

The CCD defines 13 samples in the DOE with different burning temperatures and burning durations, as illustrated in Table 3.4. The TRS was placed in the crucible and then burnt in the furnace at varied burning temperatures and duration, as shown in Figure 3.14 (a) and Figure 3.14 (b). The process was ended by determining the percentage of the reactive compound through the x-ray Fluorescence (XRF) analysis. The XRF result is the data for the response in the DOE. Based on ASTM C618, the combination of the SiO_2, Al_2O_3, and Fe_2O_3 must be more than 70% to be used as pozzolanic material ("ASTM C618" 2014). This procedure for XRF analysis was conducted according to ISO 12677 ("ISO 12677", 2015).

Table 3.4 Samples Involved in the Incineration Process Defined by DOE.

No. of Run	Factor 1: Burning duration (Hours)	Factor 2: Burning temperature (°C)	Response 1: Percentage of reactive compound content (%)
1	1.00	800.00	
2	2.00	841.42	
3	3.00	600.00	
4	2.00	700.00	
5	3.41	700.00	
6	2.00	700.00	
7	2.00	700.00	
8	3.00	800.00	
9	2.00	558.58	
10	0.59	700.00	
11	2.00	700.00	
12	1.00	600.00	
13	2.00	700.00	

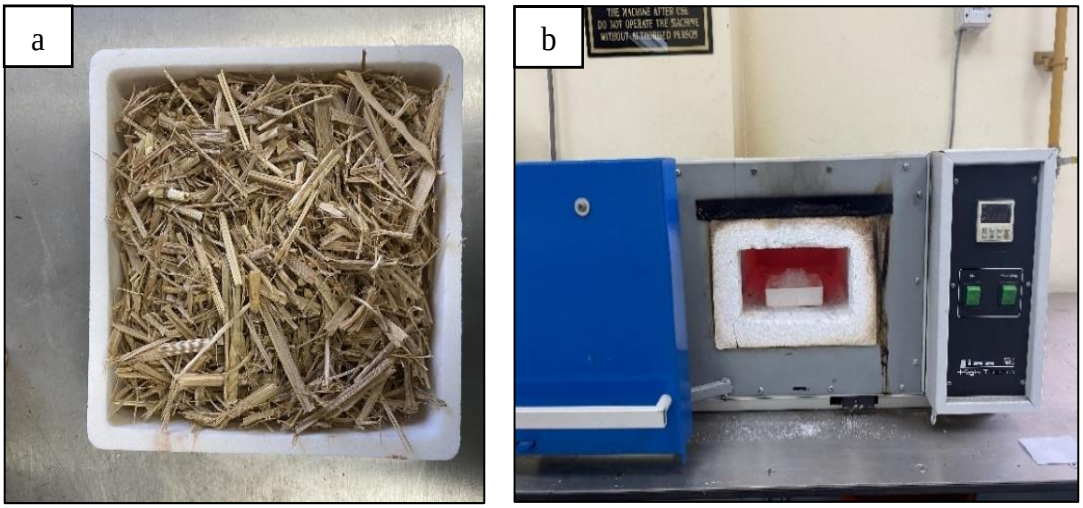

Figure 3.14 (a) The Dried TRS in the Crucible for the Incineration Process, (b) The Incineration Process Using the Furnace.

Therefore, the interaction of experimental factors with response was determined to identify the optimum sample. The mathematical equation was obtained through RSM. A regression model was selected for analyzing the interaction between factors (burning duration and burning temperature) and the response (percentage of reactive compounds content). In the RSM, the significance of the selected model, i.e., quadratic model, was determined to establish the interaction between factors and responses in this experiment.

Additionally, the ANOVA analysis in the RSM examined the quadratic model. The significance of the model also depended on the p value, which must be less than 0.05. However, the F test value for the lack of fit test of the model must be more than 0.05. At the same time, the RSM observed the errors and, thus, defined the correlation between the predicted and actual values. The prediction and optimization values were kept in the three dimensions (3D) surface formation. Finally, the fit model was the selected data (Muhammad et al., 2020).

At last, the burnt ash was ground using the planetary ball mill for grinding, as shown in Figure 3.15. The grinding process produced the finest ash with a high amount of

amorphous silica. The essential parameters, namely ball-to-powder ratio, grinding speed (revolution per minute), and grinding duration, are fixed in this process. The treated RSA (TRSA) was crushed in the ball mill for about 15 minutes at a speed of 300 rpm with a ball-to-powder ratio of 15:1 (Saad et al., 2016). The TRSA was used to replace cement in mortar production partially. The TRSA was also involved in the characterization test in sub-section 3.3. The detail of the mixing process was explained in the following sub-section, 3.4.

Figure 3.15 Planetary Ball Mill.

3.3 MORTAR TESTING AND ANALYSIS FOR CHARACTERIZATION PROPERTIES OF NON-TREATED RICE STRAW ASH (NTRSA) AND TREATED RICE STRAW ASH (TRSA) (PHASE 3)

This subsection explains on the characterization properties for both non-treated rice straw ash (NTRSA) and treated rice straw ash (TRSA) samples.

3.3.1 X-Ray Diffraction (XRD) Analysis

The materials presented mineralogical phases through X-Ray Diffraction (XRD) analysis. Munshi and Sharma (2018) used X-Ray Diffractometer Ultima IV Rigaku to identify the minerals in the NTRSA and TRSA samples. According to BS EN 13925-1, XRD analysis was used to identify the qualitative and quantitative crystalline materials in powder form ("BS EN 13925-1", 2003). Figure 3.16 illustrates that the Bruker D2 Phaser XRD analyzer was used to perform this analysis. First, a small quantity of NTRSA and TRSA powders were tested using XRD in a specific container, as shown in Figure 3.17. After that, the data obtained from this analysis was shown using the installed software. Lastly, the result was described the effect of NTRSA and TRSA incorporation in cement mortar.

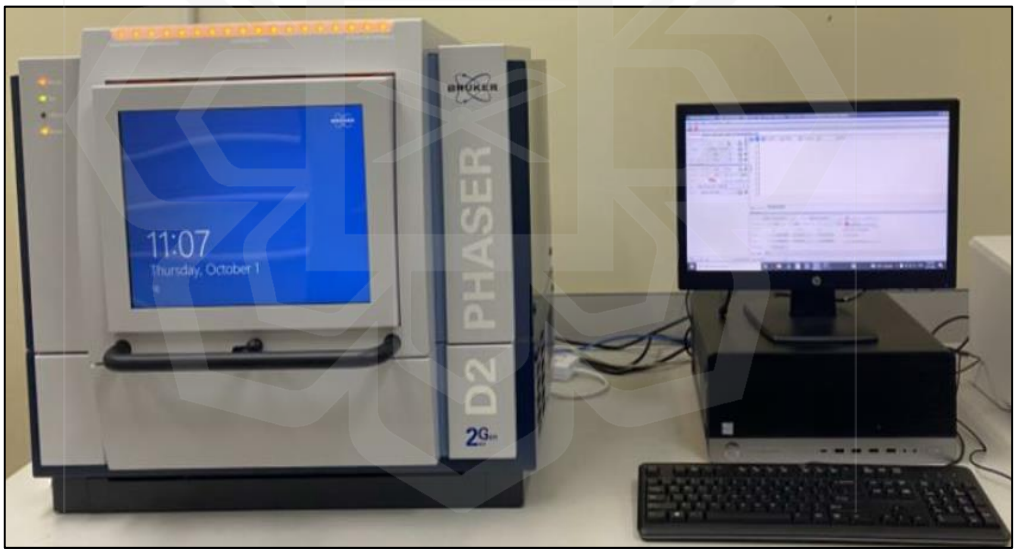

Figure 3.16 Bruker D2 Phaser XRD Analyzer.

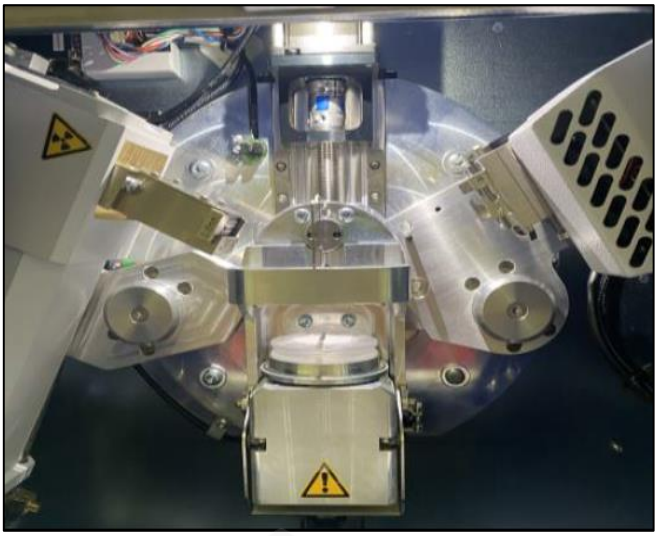

Figure 3.17 The Sample inside the XRD Machine.

3.3.2 Fourier Transforms Infrared Spectroscopy (FTIR) Analysis

For this research, the mortar pastes were prepared to undergo Fourier transforms infrared spectroscopy (FTIR) analysis (Heikal et al., 2013; Munshi & Sharma, 2018; Villca et al., 2021). The FTIR analysis was done when the age of mortar pastes reached 90 days using a Nicolet iS50 spectrometer, as shown in Figure 3.18. FTIR also characterizes the NTRSA and TRSA samples. According to ASTM E168, FTIR is an analytical technique that used infrared light to scan the samples and observed the chemical characteristic in a paste ("ASTM E168", 2016). FTIR analysis is a unique and excellent tool for scanning chemical composition. The FTIR analysis was performed to understand better the mortar's functional groups and atomic arrangements.

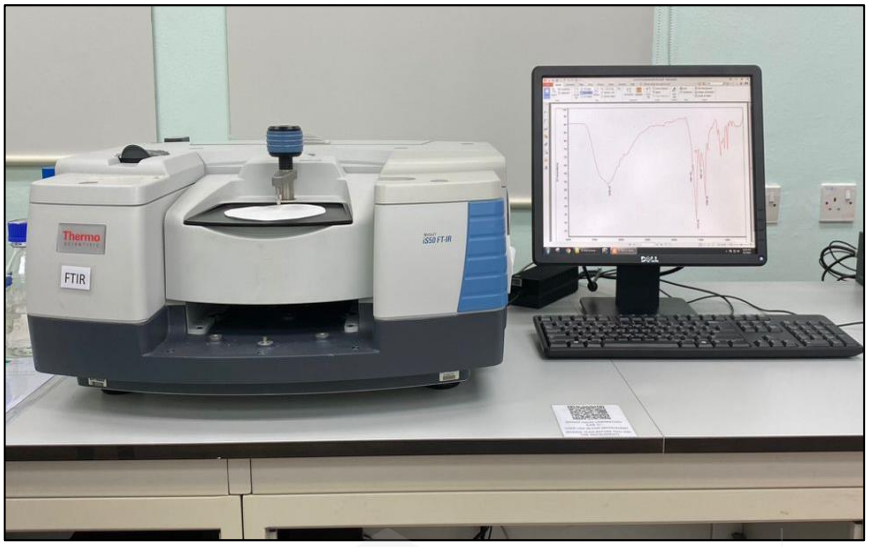

Figure 3.18 Nicolet iS50 Spectrometer.

3.3.3 Brunauer-Emmet-Teller (BET) Analysis

The surface area (SSA) of the NTRSA and TRSA samples in powder form were determined using the Brunauer-Emmet-Teller (BET) analysis through nitrogen absorption followed the standard ISO 9277 (“ISO 9277”, 2022). This analysis was conducted using the surface area and porosity analyzer model of Micromeritics TriStar II 3020, as illustrated in Figure 3.19. This analysis aims to analyze the grinding process's effect on the TRSA and differentiate it from the NTRSA sample.

Figure 3.19 Surface Area and Porosity Analyzer Model of Micromeritics TriStar II 3020.

3.3.4 Field Emission Scanning Electron Microscopy (FESEM) Analysis

The microstructure properties of the TRSA and NTRSA was determined through the field emission scanning electron microscope (FESEM) analysis. The FESEM study is a process that analyzed a sample with an electron beam to produce magnified images. It was performed at high magnifications to generate resolution images and measure tiny objects. According to ASTM C1723-10 (“ASTM C1723”, 2010), the morphologies of the NTRSA and TRSA images were shown through this analysis.

This study tested 5 g of TRSA and NTRSA powders. Firstly, both powders were coated with a small amount of gold in the FESEM machine. Next, the sputter coater machine in Figure 3.20 covered both powders to obtain a high-quality FESEM image. After the coating process, the coated sample was placed in the FESEM machine. In the FESEM machine, as illustrated in Figure 3.21, an electron gun shot a high-energy electron beam and hit the sample. Then, a secondary electron was bounced off towards the sample. At the same time, the electron gun continued to shoot the electrons at the precise location in the conversion by the amplifier and displayed the result of 3D images.

Figure 3.20 Sputter Coating Machine.

Figure 3.21 FESEM Analysis.

3.3.5 Transmission Electron Microscopy (TEM) Analysis

The material's particle size and morphology were determined through transmission electron microscopy (TEM) analysis (Farirai et al., 2020) based on ISO 25498 (“ISO 25498”, 2018).

Thus, in this research, TEM analysis was used to find the morphology and the particle size of the NTRSA and TRSA samples. 5 mg of powder sample was dissolved into 30 sonications of 100 ml of water. Then, 2 ml of sample suspension was dropped on the carbon-coated TEM grids. Lastly, the data obtained from this analysis was shown using the installed software.

3.4 MECHANICAL PROPERTIES OF TREATED RICE STRAW ASH (TRSA) INCORPORATING CEMENT MORTAR (PHASE 4)

This subchapter explains the final phase, which is the phase 4 of the study. Figure 3.22 shows the flowchart of the sample preparation of the specimens for this research. The sampling preparation was appropriately conducted to obtain the result for further analysis.

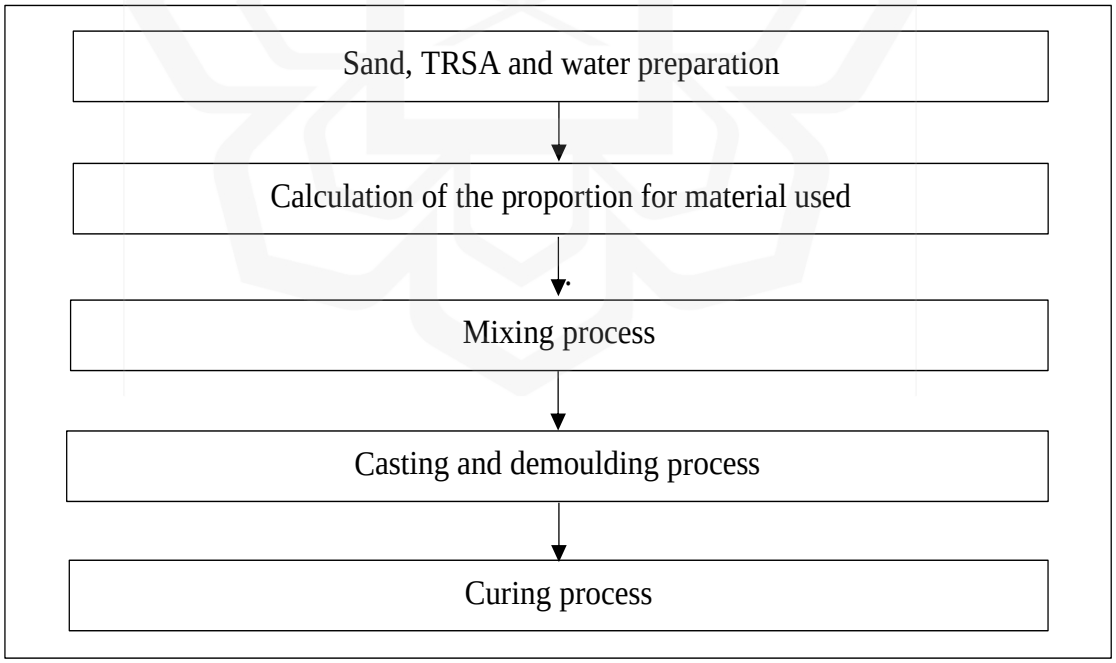

Figure 3.22 The Flowchart of the Sample Preparation.

3.4.1 Preparation of material

Materials used in this research were selected according to the specific standard related to objectives of this research. The non-standardized material was obtained through the design procedure. The low normality of hydrochloric acid (HCl) used in the pretreatment enhances silica content and removes impurities. The low normality of HCl used for the immersion process of rice straw is more effective in extracting the content of silicon dioxide (SiO_2) in the rice straw than sulphuric acid (H_2SO_4) and nitric acid (HNO_3) (Nazopatul et al., 2018).

However, the Ordinary Portland cement (OPC) type 1 is used in this research, which complies with Malaysian Standard, BS EN 197-1:2000 (Raheem & Kareem, 2017a). It is in grey coloured powder. The rate of hardening for cement is medium. The hydration process occurred when OPC created bonds between materials when mixed with water into a compact mixture. So, the mortar mixtures become hardened and stiffed and developed their strength. The rice straw ash (RSA) used as cement replacement material is an efficient method to reduce air pollution and contribute simultaneously to the conservation of natural resources. The RSA is a residue material from the burning process of rice straw. Commonly, RSA contains a high amount of silica. In the research. The RSA was used to partially replace the cement in the mortar production. The percentage replacement of RSA as a binder in the mortar mixing is about 1, 2, 3, 4, and 5% for five mixing proportions.

Furthermore, the sieve analysis was conducted to produce a grading curve for fine aggregates according to ASTM C 136 (“ASTM C136”,2019). The sieving analysis for sand used in this study was done one day before mixing. A mechanical sieve is a device that separates wanted elements from unwanted material. The grading curve is plotted in the graph of per cent passing (%) versus sieve size (mm) for fine aggregates, as shown in Figure 3.23. Typically, the grading of fine aggregates is the proportions of the size of particles must be less than 5 mm. The sieve analysis result of fine aggregates for this research is shown in Table 3.5. The fineness modulus value of fine aggregates was 2.211.

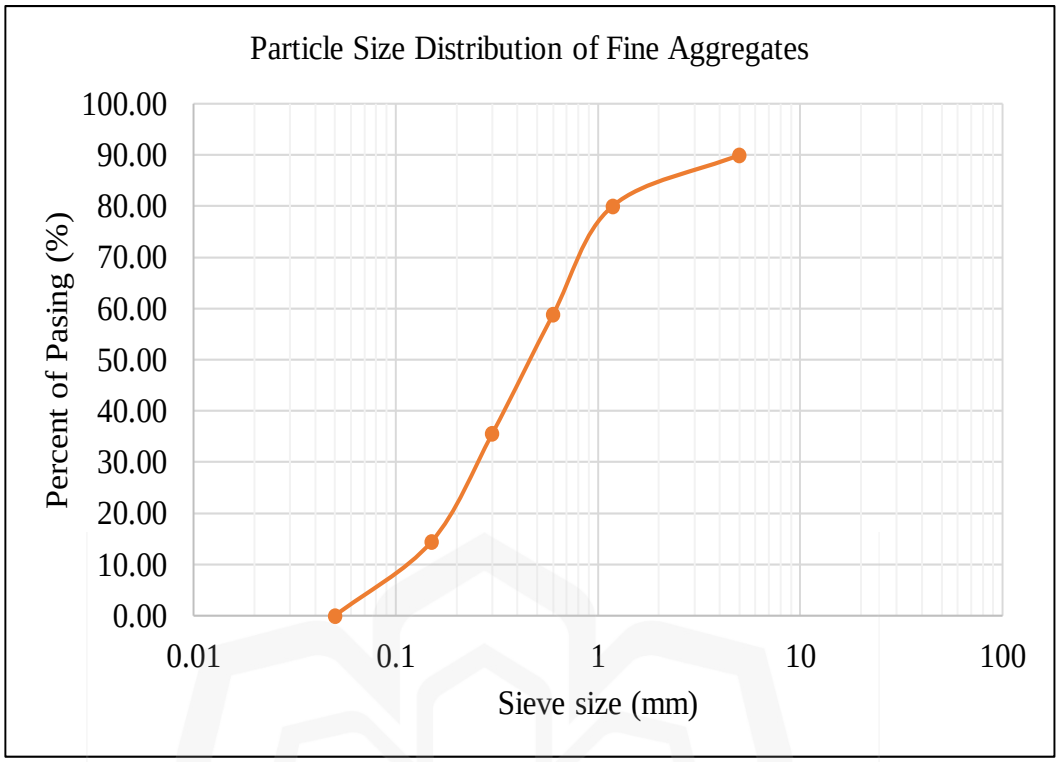

Figure 3.23 Particle Size Distribution of Fine Aggregates.

Table 3.5 Sieve Analysis of Fine Aggregates.

Sieve (mm)	Weight of sieve (kg)	Weight of sieve + sample (kg)	Weight of sample (kg)	Cumulative weight sample (kg)	Cumulative %	% Passing
5.00	0.00	0.00	0.00	0.00	0.00	100.00
2.36	1.00	1.90	0.90	0.90	10.00 *	90.00
1.18	0.80	1.70	0.90	1.80	20.00*	80.00
0.60	0.90	2.80	1.90	3.70	41.11*	58.89
0.30	0.85	3.00	2.10	5.80	64.44*	35.56
0.15	0.80	2.70	1.90	7.70	85.56*	14.44
pan	0.75	2.05	1.30	9.00	100.00	0.00

*Fineness modulus: (10.00+20.00+41.11+64.44+85.56)/100 = 2.211.

3.4.2 Mix Design Using Treated Rice Straw Ash (TRSA) as Partial Replacement of Cement in Mortar Production

There are 78 samples of mortars produced in this research. However, the ratio of binder to sand is 1:3 according to BS 5628-1, and the water-cement ratio is 0.5. Therefore, both ratios were applied to all samples. The aim is to observe the effect of TRSA partially replacing the cement content in the mortar on the mechanical properties. Table 3.6 shows the mixture proportion of the mortar incorporated with TRSA. As reported in Table 3.6, all mortars were mixed with the same amount of sand and water.

Table 3.6 The Mixture Proportion of Mortar (kg/m^3).

Mix code	TRSA	Cement	Sand	Water
Control mix	0	300	825	150
TRSA-1	3	297	825	150
TRSA-2	6	294	825	150
TRSA-3	9	291	825	150
TRSA-4	12	288	825	150
TRSA-5	15	285	825	150

The mixing process of mortar followed ASTM C451 (“ASTM C451”,2021). The mixing process was conducted using a mortar mixer, as shown in Figure 3.24. Based on that standard, cement, sand, and TRSA were mixed at a low speed to ensure homogeneity of those dry materials before putting the water inside the mixer in the first thirty seconds of the mixing process. Then, water was mixed with dry materials for another thirty seconds. Lastly, the speed of the mixer changed to high speed for one minute.

The fresh mortar was cast into 50 mm of steel cubes. The number of specimens for each of the mixed codes was 13 cubes. So, there were 78 cubes of samples in this study. The specimens were de-moulded after a day and immersed in tap water until the testing days. Curing is one of the vital processes for mortar hardening. This curing method was conducted according to BS 1881(“BS 1881”, 2011). The curing used in this research is the water curing method. The mortar specimens were placed in a water tank until the testing days. The type of water used for curing the mortar was tap water. All steps were repeated in producing cement mortar incorporating NTRSA. Lastly, the hardened specimens were tested to determine the mechanical properties TRSA mortar and compared with NTRSA mortar in the following sub-sections, 3.4.3 to 3.4.5.

Figure 3.24 Mortar Mixer.

3.4.3 Method Testing and Analysis for Pozzolanic Reactivity of Treated Rice Straw Ash (TRSA) in Cement Mortar

The pozzolanic reaction of the NTRSA and TRSA samples were determined through a strength activity index (SAI) test (S. A. Saad et al., 2015; Qudoos et al., 2018; Khan et al., 2020) . The mixture proportion for SAI test was tabulated in Table 3.7.

Table 3.7 Mixture Proportion for SAI Test.

Materials	Control sample	TRSA/NTRSA mortar
OPC (g)	450	360
Sand (g)	1350	1350
TRSA/NTRSA (g)	0	90
Water (ml)	225	225

ASTM C311 is the standard procedure for measuring good pozzolanic reactivity through the SAI test of a mortar ("ASTM C311", 2005). The SAI result was based on the compressive strength for both mortar (control mortar and mortar incorporated with 20% pozzolan) at 7 and 28 days. Good pozzolanic reactivity was defined when the average SAI result increase by about 75% after the age of the mortar reaches 28 days. The SAI result was determined using the equation 3.1.

$$SAI = (A/B) \times 100\% \quad (3.1)$$

Where: A = mean compressive strength of mortar with pozzolan

B = mean compressive strength of control mortar

3.4.4 Method Testing and Analysis for Compressive Strength of Treated Rice Straw Ash (TRSA) in Cement Mortar

The compression test was conducted to evaluate the development of the compressive strength of the hardened mortar. This test analyzed the impact of treated rice straw ash (TRSA) as a partial replacement in cement mortar. After the age of the 50 mm x 50 mm x 50 mm cubes achieved 7, 14, 28, and 90 days, the compressive strength of each mortar was measured according to ASTM C109/C109M ("ASTM C109/C109M", 2021). The strength development of TRSA incorporating cement mortar will be compared with the NTRSA mortar strength. The test was conducted using the digital compressive testing machine with a 3000 kN compression capacity, as illustrated in Figure 3.25.

Figure 3.25 Compression Testing Machine.

3.4.5 Method Testing and Analysis for Interfacial Transitional Zone Analysis

The interfacial transitional zone (ITZ) aims to identify the correlation between the microstructure properties of the NTRSA and TRSA. The observation on ITZ of mortar incorporated with TRSA was made on the 3 to 4 mm thin slice of mortar and compared with the reference sample (control mix) and NTRSA mortar sample. The field scanning electron microscopy (FESEM) analysis was conducted again for this analysis. The test was done when the mortar age reached 90 days. First, the thin slice of mortar sample was coated with gold coating using the sputter coating machine. Then, The FESEM analysis was performed once the sample was coated.

3.5 CHAPTER SUMMARY

As conclusion, the x-ray Fluorescence (XRF) analysis was involved in phase 1 and phase 2. The characterization of ashes in phase 3 was determined through X-Ray Diffraction (XRD) analysis, Fourier transforms infrared spectroscopy (FTIR) analysis, Brunauer-Emmet-Teller (BET) analysis, transmission electron microscopy (TEM) analysis and field emission scanning electron microscope (FESEM) analysis. For the final phase, the strength activity index (SAI) test, compression test and FESEM analysis were included to identify the mechanical properties of ashes in cement mortar.

Lastly, this section summarizes the methodology of experimental work for this research, as shown in Table 3.8.

Table 3.8 Summary of the Methodology of Experimental Work.

Analysis	Test	Sample condition	Standard/ Reference
Chemical composition	XRF Analysis	5 g of TRSA and NTRSA powder sample	BS EN ISO 12677:2011
Mineralogical analysis	XRD Analysis	5 g of TRSA and NTRSA powder sample	BS EN 13925-1:2003
Structural elucidation analysis	FTIR Analysis	5 g of TRSA and NTRSA powder sample	ASTM E168:2016
Specific surface area	BET Analysis	5 g of TRSA and NTRSA powder sample	ISO 9277:2010
Microstructural analysis	FESEM Analysis	5 g of TRSA and NTRSA powder sample	ASTM C1723:2010
Morphology	TEM Analysis	5 g of TRSA and NTRSA powder sample	ISO 25498:2018
Pozzolanic Reactivity	SAI Test	50 mm x 50 mm x 50 mm of mortar cube	ASTM C311:2005
Compressive strength	Compression Test	50 mm x 50 mm x 50 mm of mortar cube	ASTM C109/C109M:2021
ITZ Analysis	FESEM Analysis	3-4 mm of the concrete piece of mortar cube	ASTM C1723:2010

CHAPTER FOUR

RESULT AND DISCUSSION

4.1 OVERVIEW

The fourth chapter discusses the result obtained from several tests conducted, as mentioned in chapter three. In addition, it includes an explanation of the optimization analysis for the thermochemical pretreatment and incineration processes to produce treated rice straw ash (TRSA) since both methods involve an extensive range of factors. Then, there is the elaboration and discussion on the characterization properties of non-TRSA (NTRSA) and TRSA. Furthermore, discussions on the mechanical properties of cement mortar incorporating TRSA include compressive strength development, pozzolanic reactivity, and interfacial transitional zone (ITZ) analysis.

4.2 THERMOCHEMICAL PRETREATMENT PROCESS OPTIMIZATION (PHASE 1)

First, the complete process for optimization by using Design Expert software is the thermochemical pretreatment process and the incineration process. The central composite design (CCD) in the response surface methodology (RSM) analysis in the Design Expert was selected for this analysis. The thermochemical pretreatment process used the RSM to define the sample number since the factors involved had an extensive range as well as to minimize time consumption.

From RSM, 20 samples with different HCl concentrations, soaking duration, and soaking temperature were engaged in the thermochemical pretreatment process. The independent variables with its range as illustrated in Table 4.1. After conducting this pretreatment process, each sample's percentage of reactive compound content was determined through X-Ray Fluorescence (XRF) analysis. Then, the result of XRF analysis for response one was filled in the RSM array for further analysis in the DOE, as shown in Table 4.2. The analysis of flow for phase 1 is multiple regression analysis, analysis of variance (ANOVA), validation of the significance of the model through several graphs generated by CCD in RSM (normal probability graph, externally studentized residuals against run number graph, and predicted against actual values graph), three dimensions (3D) contour plot, and optimization analysis.

Table 4.1 Variables and Limit Level for Independent Variables for the Thermochemical Pretreatment Process.

Variables	Unit	Symbols	Levels	
			-1	+1
HCl concentration	Molar	A	0.01	0.1
Soaking duration	Hours	B	1	3
Soaking temperature	Degree Celsius	C	60	80

Based on the result of response 1 in Table 4.2, the percentage of reactive compound content for each experiment involved in the pretreatment process is more than 70%, as mentioned by ASTM C618. The eighth experimental run has the highest percentage of reactive compound content, 99.6%, while the least is 87.21% for the eighteenth experimental run. Therefore, the TRSA was used as cement replacement material (CRM) since it met the standard ASTM C618.

Table 4.2 RSM Array from Design Expert for Thermochemical Pretreatment Process.

Run	Factor 1 A: HCl concnetration (Molar)	Factor 2 B: Soaking duration (Hours)	Factor 3 C: Soaking temperature (Degree celsius)	Response 1 Percentage of reactive compounds (%)
1.	0.06	2.00	70.00	97.28
2.	0.06	2.00	70.00	97.89
3.	0.10	1.00	60.00	94.56
4.	0.10	3.00	60.00	89.07
5.	0.06	2.00	70.00	98.63
6.	0.06	2.00	80.00	96.52
7.	0.06	2.00	70.00	98.12
8.	0.06	2.00	70.00	99.60
9.	0.10	3.00	80.00	94.33
10.	0.10	2.00	70.00	96.89
11.	0.01	1.00	80.00	91.62
12.	0.01	3.00	80.00	95.64
13.	0.10	1.00	80.00	92.15
14.	0.06	3.00	70.00	93.60
15.	0.06	1.00	70.00	95.81
16.	0.01	1.00	60.00	89.43
17.	0.01	2.00	70.00	95.12
18.	0.01	3.00	60.00	87.21
19.	0.06	2.00	70.00	98.63
20.	0.06	2.00	70.00	98.21

The first analysis in the RSM for this phase is the multiple regression analysis, which is included a summary of the sequential model sum of squares, lack of fit tests, and model summary statistics for response 1. The fit summary of multiple regression analysis for response 1 is recorded in Table 4.3. Table 4.3 is the initial summary before the model is modified and any interaction terms are eliminated. The Design Expert software selected the model in the CCD of the RSM. The Design Expert highlighted the criteria for the model selection, in which the p-value of the sequential model sum of squares is less than 0.05. It selected the highest order polynomial where all terms are significant and the model. Based on the result of the sequential model sum of the squares for response 1, the quadratic is the highest order polynomial where the additional terms are significant, and the model is not aliased.

Then, the lack of fit test determines the selected insignificant model with lack of fit, where the p-value is more than 0.05. As illustrated in Table 4.3, the suggested model for this model is also quadratic. For the model summary statistics in the multiple regression analysis, the model maximizing the adjusted R-squared and predicted R-squared values were selected, and the quadratic model was chosen. The quadratic is the highest-order polynomial where the additional terms are significant. The model is not aliased for all analyses in the fit summary and is used in the analysis of variance (ANOVA).

Table 4.3 Fit Summary of Multiple Regression Analysis for Response 1.

The sequential model sum of the squares						
Source	**Sum of squares**	**Degrees of freedom**	**Mean squares**	**F-value**	**p-value**	**Comment**
Mean	1.806E+005	1	1.806E+005			
Linear	35.78	3	11.93	0.95	0.4408	
2FI	35.22	3	11.74	0.92	0.4589	
Quadratic	158.57	3	52.86	70.36	<0.0001	Suggested
Cubic	5.13	5	1.03	2.15	0.2098	
Residual	2.38	5	0.48			
Total	1.808E+005	20	9039.80			
Lack of fit tests						
Source	**Sum of squares**	**Degrees of freedom**	**Mean squares**	**F-value**	**p-value**	**Comment**
Linear	198.92	11	18.08	37.96	0.0004	
2FI	163.70	8	20.46	42.96	0.0003	
Quadratic	5.13	5	1.03	2.15	0.2098	Suggested
Cubic	0.000	0				
Pure Error	2.38	5	0.48			
Model Summary Statistics						
Source	**Std. Dev.**	**R-Squared**	**Adj R-Squared**	**Pred R-Squared**	**PRESS**	**Comment**
Linear	3.55	0.1509	-0.0083	-0.5916	377.33	
2FI	3.57	0.2995	-0.0238	-4.2598	1247.02	
Quadratic	0.87	0.9683	0.9398	0.8265	41.13	Suggested
Cubic	0.69	0.9900	0.9618			

Furthermore, the second analysis involved in the RSM is the ANOVA, which was conducted to analyze the statistical significance of the model coefficients (Amibo et al., 2022). Table 4.4 illustrates the result of the ANOVA analysis for response 1. The F-value of 33.96 implies the model is significant, so there is only a 0.01% chance that an F-value this large could occur due to noise. The p-value for this response is less than 0.05. Thus, the model is significant. In this case, A, C, AC, A^2, B^2, and C^2 are significant model terms. The model becomes significant when the p-value is small (Indriani & Wardhani, 2022).

In addition, the insignificant of the lack of fit F-value was considered by the Design Expert for ANOVA analysis. The lack of fit F-value for this analysis is 2.15, implying the lack of fit is insignificant and it meets the requirement made by the Design Expert. The pred R-squared of 0.8265 is in reasonable agreement with the adj R-squared of 0.9398. The value of the R-Squared is 0.9683, which is close to 1. When the R-Squared was close to 1, the actual and predicted values had a good agreement and were highly accepted (Amibo et al., 2022). At the same time, the adequate precision value for the response is also essential because it measures the signal to the noise ratio. The adequate precision measures the signal-to-noise ratio where the desired value is 4 (Bazargan et al., 2015; Muhammad et al., 2020). The ratio of adequate precision is 18.289, which indicated an adequate signal. Thus, this model uses to navigate the design space.

Table 4.4 ANOVA Analysis for Response 1.

Source		Sum of squares	Degrees of freedom	Mean squares	F-value	p-value	Comment
Model		229.57	9	25.51	33.96	<0.0001	Significant
A-HCl concentration		6.08	1	6.08	8.09	0.0174	
B-Soaking duration		1.28	1	1.28	1.70	0.2216	
C-Soaking temperature		20.34	1	20.34	27.07	0.0004	
AB		3.47	1	3.47	4.62	0.0572	
AC		7.77	1	7.77	10.34	0.0092	
BC		24.19	1	24.19	32.20	0.0002	
A^2		5.25	1	5.25	6.99	0.0245	
B^2		19.38	1	19.38	25.79	0.0005	
C^2		7.11	1	7.11	9.47	0.0117	
Residual		7.51	10	0.75			
	Lack of Fit	5.13	5	1.03	2.15	0.2098	Insignificant
	Pure Error	2.38	5	0.48			
Cor Total		237.08	19				
Std. Dev.	**Mean**	**C.V.%**	**PRESS**	**R-Squared**	**Adj R-Squared**	**Pred R-Squared**	**Adeq Precision**
0.87	95.02	0.91	41.13	0.9683	0.9398	0.8265	18.289

Before moving on to the optimization analysis, three graphs are essential to analyze for validation of the model, whether significant or not. The graphs are the normal probability graph, the residuals against the expected response graph, and the data predicted by the RSM graph are essential to ensure that the fitted models are adequate to prevent inaccurate outcomes. In Figure 4.1, the normal probability graph is linear. The linear pattern of the graph indicates that the model is validate. If the graph is non-linear, the model is wrong. In addition, the graph of externally studentized residuals against the predicted response value seems distributed randomly, and the predicted and actual values correspond well in Figure 4.2 and Figure 4.3, respectively. Therefore, the model is found significant to be used in the design space based on all graphs. Similar results were discussed and concerned by previous researchers (Bazargan et al., 2015; Muhammad et al., 2020; Thakur et al., 2020; Gun et al., 2022).

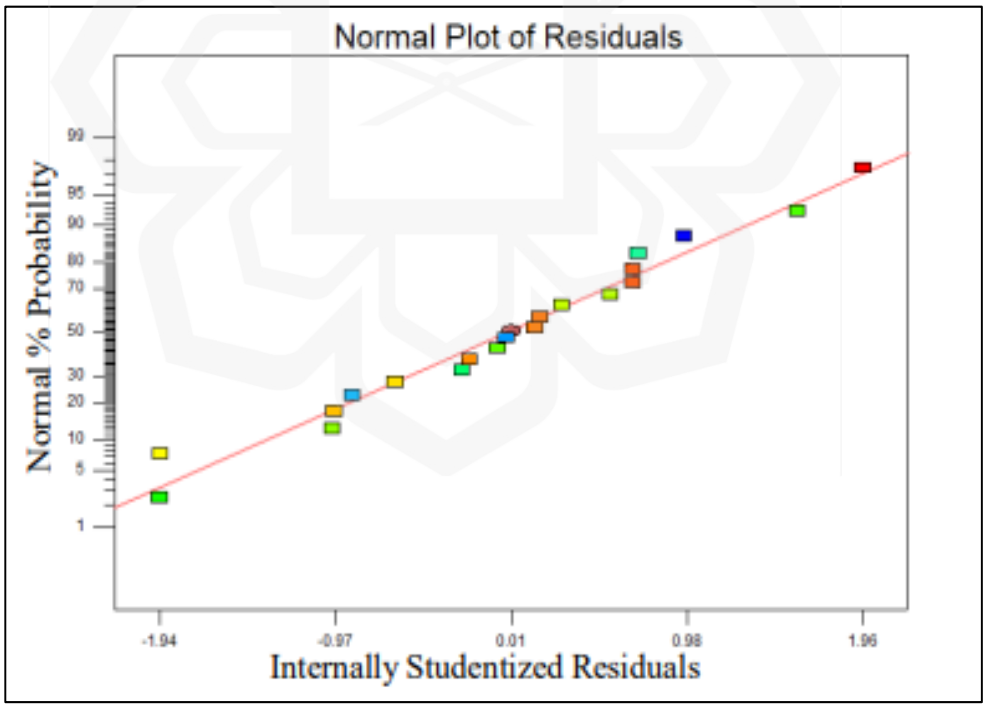

Figure 4.1 Normal Probability Graph for Run No 1 – 20.

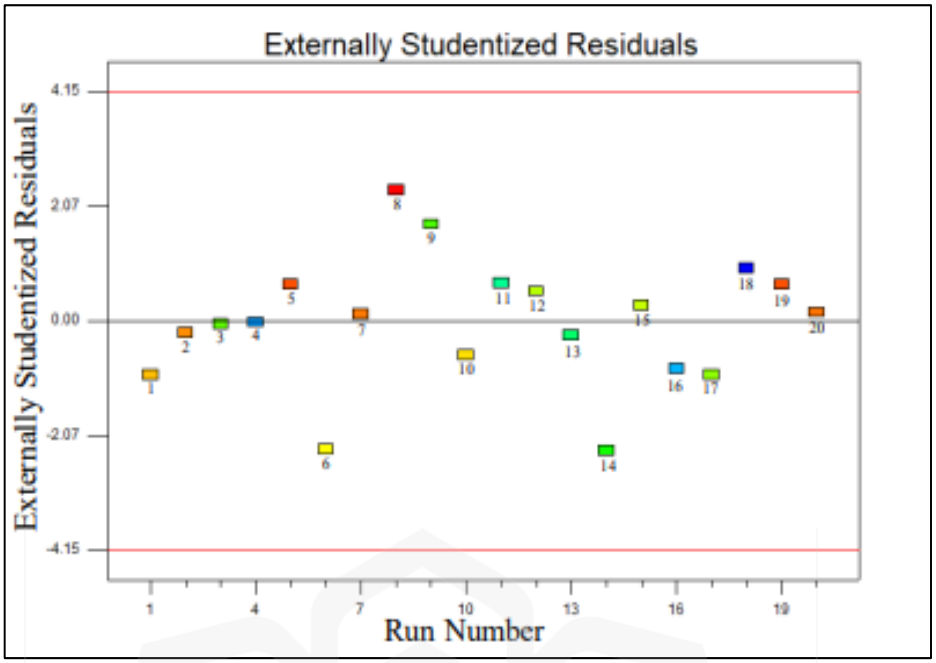

Figure 4.2 The Externally Studentized Residuals vs. Predicted Response Graph for Run 1 – 20.

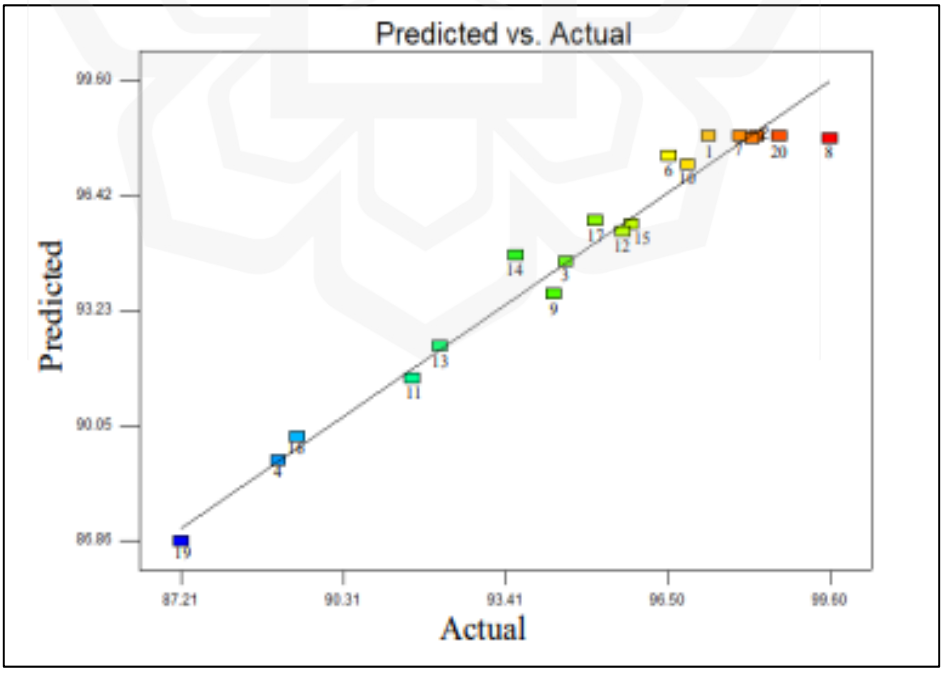

Figure 4.3 Model Precision Diagnostic Graph for Run 1 – 20.

The fourth analysis is the interaction of factors involved in this analysis is explained in the three-dimensional (3D) response surface plot shown in Figure 4.4 (a)–(c). A 3D contour plot is a planar presentation of the reaction surface in two dimensions. The analysis also used a contour plot to predict the results (Thakur et al., 2020). The percentage of reactive compound content does not necessarily increase when all factors, namely hydrochloric acid (HCl) concentration, soaking duration, and soaking temperature, increase. As a result, combining high HCl concentration with the long soaking duration and the high soaking temperature is not lead to the highest percentage of reactive compound content. It is also proved that the low HCl concentration, less than 0.1 M, helps increase the amount of silica present in the ash (more than 70%).

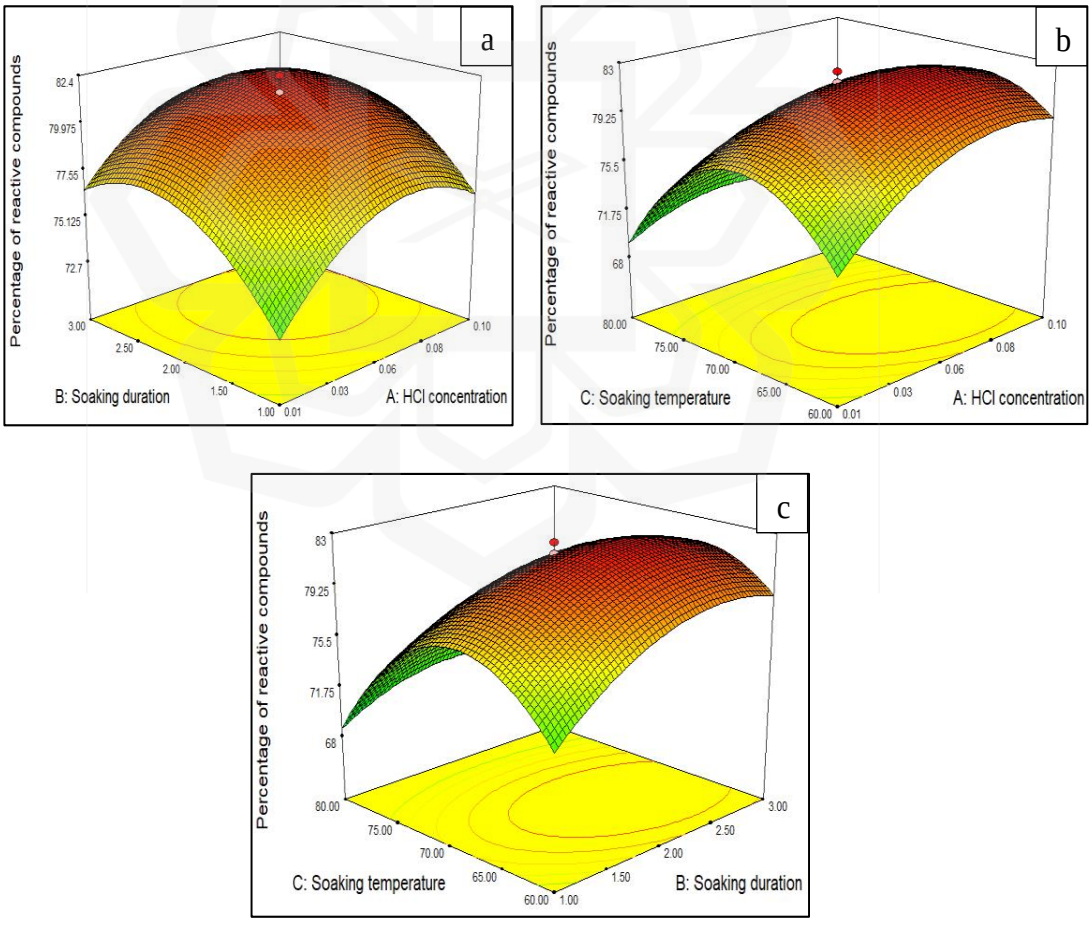

Figure 4.4 (a)-(c) 3D Contour Plot for Interaction between All Factors.

After that, optimization is the process of raising the efficiency of a system to maximize its advantages. For the optimization analysis result, as shown in Figure 4.5, one solution is suggested by the Design Expert out of the 20 runs with a desirability function of 89.8%. By comparing the combination parameters suggested with the experimental run, the HCl concentration chosen is 0.06 M, the soaking duration is 2 hours, and the soaking temperature is 70℃. However, three experiments using the suggested parameter combination value underwent optimization analysis. Therefore, those three experiments are repeated to reduce errors and ensure that the selected optimum parameter combination is significant.

Name	Goal	Lower Limit	Upper Limit	Lower Weight	Upper Weight	Importance
HCl concentration	is in range	0.01	0.1	1	1	3
Soaking duration	is in range	1	3	1	1	3
Soaking temperature	is in range	60	80	1	1	3
Percentage of reactive compound content	maximize	87.21	99.6	1	1	3

Solutions

Number	HCl concentration	Soaking duration	Soaking temperature	Percentage of reactive compound content	Desirability	
1	0.06	2.04	73.74	98.3402	0.898	Selected

1 Solutions found

Figure 4.5 Table of Solution Results for this Analysis in RSM.

Before confirming the solution as the best combination parameters for the pretreatment process, the result of the XRF analysis (response 1) is compared to the estimated value from the model to see if the suggested model is adequately predicted since it is selected randomly from the design space. Both values of response 1 for predicted and actual are expected to fall within the prediction index (PI) to indicate that the model is significant. From Figure 4.6, the prediction value of the percentage of reactive compound content in RSM is 98.34%, while the XRF analysis results for each model with the same value of each factor (HCl concentration = 0.06 M, soaking duration = 2 hours, and soaking temperature = 70℃) is above 97.00%. So, the range of XRF analysis results for actual reaction fall between 95% PI low and 95% PI high. The values of 95% PI low and 95% PI

high are shown in Figure 4.6. Therefore, the model is validated since the actual experimental result is within the expected range for any involved factor.

Factor	Name	Level	Low Level	High Level	Std. Dev.	Coding
A	HCl concentration	0.061	1.00E-02	0.100	0.000	Actual
B	Soaking duration	2.04	1	3.00	0.000	Actual
C	Soaking temperature	73.74	60.00	80.00	0.000	Actual

Response	Prediction	SE Mean	95% CI low	95% CI high	SE Pred	95% CI low	95% CI high
Percentage of reactive compound content	98.3402	0.31	97.66	99.02	0.92	96.29	100.39

Figure 4.6 Table of Prediction Result for this Analysis in RSM.

In conclusion, the satisfaction of using a thermochemical pretreatment process to produce an amorphous silica rice straw is proved in this study. Overall, the percentage of reactive compound content in the ashes for each experimental run is more than 87%. Thus, the ash is used in concrete production because the reactive compound content (SiO_2, Al_2O_3, and Fe_2O_3) is more than 70%, as mentioned in ASTM C618 (Kasaniya et al., 2019). And then, RSM with a CCD is discovered as a helpful method for finding the optimum value of variables. As a result, the optimum experimental condition (HCl concentration = 0.06 M, soaking duration = 2 hours, and soaking temperature = 70°C) to obtain a high-quality of CRM.

4.2.1 Summary (Phase 1)

In phase 1, it proves that the thermochemical pretreatment process using dilute HCl concentration is suitable and effective in increasing the silica amount and decreasing impurities in the ash. Otherwise, unlike the previous studies, using a high acid concentration in the pretreatment process can harm the environment (Munshi & Sharma,

2018). So, in a nutshell, the pretreatment process at 70℃ using 0.06 M of hydrochloric acid (HCl) for about 2 hours is selected to be further assessed in the next phase.

4.3 INCINERATION PROCESS AT CONTROLLED TEMPERATURE OPTIMIZATION AND GRINDING PROCESS (PHASE 2)

In phase 1, the discussion focused on finding the effectiveness of the thermochemical pretreatment process in the production of treated rice straw (TRS). The X-Ray Fluorescence (XRF) analysis stated that the optimum TRS was formed when the hydrochloric acid (HCl) concentration is 0.06 M, the soaking duration is 2 hours, and the soaking temperature is 70 ℃. Thus, for the continuation of this analysis, the TRS is produced based on the value of the optimum parameter obtained in the thermochemical pretreatment process for the incineration process in phase 2.

Similar to the pretreatment process, the incineration process also used central composite design (CCD) of the response surface methodology (RSM) in the Design Expert to define sample numbers since the factors involved have an extensive range as well as to reduce time consumption. From RSM, there are 13 samples involved in the incineration process. In addition, there are two independents variable involved in the incineration process. The limit of the range of those variables is annotated as -1 (minimum) and +1 (maximum), which indicate low and high, respectively. Table 4.5 shows the independent variables with their range. However, the percentage of reactive compound content present in the treated rice straw ash (TRSA) is the response for this process.

Table 4.5 Variables and Limit Level for Independent Variables.

Variables	Unit	Symbols	Levels	
			-1	+1
Burning duration	Hours	A	1	3
Burning temperature	Degree Celsius	B	600	800

After the RSM defines the number of samples involved in the incineration process, each experimental work is conducted to determine the result of the response. First, the response value is ascertained through XRF analysis. Then, when the RSM array is completed, it proceeds with the analysis part. The analysis of flow for phase 2 is multiple regression analysis, analysis of variance (ANOVA), validation of the significance of the model through several graphs generated by CCD in RSM (normal probability graph, externally studentized residuals against run number graph, and predicted against actual values graph), three dimensions (3D) contour plot, and optimization analysis.

Table 4.6 shows the various experimental run combinations according to the RSM array with the response value. Based on Table 4.6, the highest result for response 1 is 98.70% in the twelfth experimental run, while 96.60% is the lowest result obtained from the first experimental run. Overall, the percentage of reactive compound content for each experiment involved in the pretreatment process is more than 70%, as mentioned by ASTM C618. Thus, TRSA is used as cement replacement material (CRM).

Table 4.6 RSM Array from Design Expert.

Run	Factor 1 A: Burning duration (Hours)	Factor 2 B: Burning temperature (Degree celsius)	Response 1 Percentage of reactive compounds (%)
1.	1.00	800.00	96.60
2.	2.00	841.42	96.87
3.	3.00	600.00	97.60
4.	2.00	700.00	96.83
5.	3.41	700.00	97.66
6.	2.00	700.00	97.04
7.	2.00	700.00	96.97
8.	3.00	800.00	97.45
9.	2.00	558.58	97.75
10.	0.59	700.00	97.70
11.	2.00	700.00	96.86
12.	1.00	600.00	98.70
13.	2.00	700.00	96.94

Next, the fit summary of the multiple regression analysis is provided in the RSM as the first analysis for this process, shown in Table 4.7, which includes the sequential model sum of squares, lack of fit test, and model summary statistics for response 1. Table 4.7 is the initial summary before the model is modified and any interaction terms are eliminated. Then, the Design Expert software selects the model with the highest-order polynomial in the CCD of the RSM. For the model selection of the sequential model sum of squares, the p-value of the sequential model sum of squares is less than 0.05. As recorded in Table 4.7, the quadratic model is selected since the p-value is less than 0.05.

However, the p-value of the lack of a fit test for this analysis is significant, and the opposite of the Design Expert needed. The p-value must be more than 0.05. Nevertheless,

the Design Expert stated that the p-value is still accepted when the value of p is more than 0.01. Thus, the Design Expert selected the quadratic model even though the p-value is less than 0.05. For the model summary statistics in the multiple regression analysis, the model maximizing the adjusted R-squared and predicted R-squared values are selected, and the quadratic model was chosen. Based on Table 4.7, the highest-order polynomial for response 1 in which the additional terms matter is quadratic, and the model is not aliased for any analyses in the fit summary. It uses in the analysis of variance (ANOVA).

Table 4.7 Fit Summary for Incineration Process at Controlled Temperature.

The sequential model sum of the squares						
Source	**Sum of squares**	**Degrees of freedom**	**Mean squares**	**F-value**	**p-value**	**Comment**
Mean	1.231E+005	1	1.231E+005			
Linear	1.54	2	0.77	3.18	0.0855	
2FI	0.95	1	0.95	5.82	0.0391	
Quadratic	1.29	2	0.65	25.61	0.0006	Suggested
Cubic	0.13	2	0.066	7.15	0.0341	
Residual	0.046	5	9.159E-003			
Total	1.231E+005	13	9468.64			
Lack of fit tests						
Source	**Sum of squares**	**Degrees of freedom**	**Mean squares**	**F-value**	**p-value**	**Comment**
Linear	2.39	6	0.40	55.62	0.0008	
2FI	1.44	5	0.29	4023	0.0016	
Quadratic	0.15	3	0.049	6.89	0.0466	Suggested
Cubic	0.017	1	0.017	2.39	0.1973	

Pure Error	0.029	4	7.170E-003			
Model Summary Statistics						
Source	**Std. Dev.**	**R-Squared**	**Adj R-Squared**	**Pred R-Squared**	**PRESS**	**Comment**
Linear	0.49	0.3885	0.2662	-0.1565	4.58	
2FI	0.40	0.6285	0.5047	0.0458	3.78	
Quadratic	0.16	0.9553	0.9234	0.7226	1.10	Suggested
Cubic	0.096	0.9884	0.9722	0.7121	1.14	

After that, the analysis of variance (ANOVA), as the second analysis, was conducted to examine the statistical significance of the model coefficients (Amibo et al., 2022). Table 4.8 illustrates the result of the ANOVA analysis for response 1. The F-value for lack of fit in this model is 29.95, and the p-value is less than 0.05, which implies that the model is significant. The F-value of the lack of fit is 6.89, and the p-value is 0.0466, indicating that the lack of fit is significant. In contrast, the Design Expert stated that the p-value is still accepted when the value of p is more than 0.01. In addition, for response 1, the value of the degree of freedom for lack of fit is 7, and a pure error of 3. Therefore, the test must be statistically significant, with the least number of degrees of freedom being 3, while the maximum is 4 for pure (Muhammad et al., 2020). In this analysis, B, AB, A^2, and B^2 are significant model terms. The model is significant if the p-value is small (Indriani & Wardhani, 2022).

Concurrently, the adequate precision value for the response is also essential because it identifies the signal to the noise ratio. The desirable value of adequate precision is more than 4. For this response, the value of adequate precision is 17.120. The predicted R-Squared of 0.7226 is only a 0.2008 difference from the adjusted R-Squared, which is a reasonable agreement between the predicted and adjusted R-Squared. The value of the R-Squared for this analysis is 0.9553, which is close to 1. When the R-Squared was close to

1, the actual and predicted values had a good agreement and were highly accepted (Amibo et al., 2022). Thus, this model is used to navigate the design space.

Table 4.8 ANOVA Analysis for Incineration Process at Controlled Temperature.

Source		**Sum of squares**	**Degrees of freedom**	**Mean squares**	**F-value**	**p-value**	**Comment**
Model		3.78	5	0.76	29.95	0.0001	Significant
A-Burning duration		0.012	1	0.012	0.47	0.5172	
B- Burning temperature		1.53	1	1.53	60.42	0.0001	
AB		0.95	1	0.95	37.63	0.0005	
A^2		1.11	1	1.11	43.86	0.0003	
B^2		0.32	1	0.32	12.62	0.0093	
Residual		0.18	1	0.025			
	Lack of Fit	0.15	7	0.049	6.89	0.0466	Significant
	Pure Error	0.029	3	7.170E-003			
Cor Total		3.96	12				
Std. Dev.	**Mean**	**C.V.%**	**PRESS**	**R-Squared**	**Adj R-Squared**	**Pred R-Squared**	**Adeq Precision**
0.16	97.31	0.16	1.10	0.9553	0.9234	0.7226	17.120

Before moving on to optimization analysis, it is essential to ensure that the fitted models are adequate to prevent inaccurate outcomes. Three graphs are essential to analyze for validation of the model, whether significant or not. Therefore, a normal probability plot for response one is evaluated. The externally studentized residuals' normal probability graph in Figure 4.7 is linear. The data in Figure 4.7 shows errors when normally distributed if they are not linear, and it is assumed that the model's prediction is wrong. Plotting the residuals against the expected response in Figure 4.8 demonstrates that they were randomly dispersed. Furthermore, Figure 4.9 illustrates that the experimental data and the values predicted by Design Expert correspond rather well. Thus, the model is found to be adequate. Similar results were discussed and concerned by previous researchers (Bazargan et al., 2015; Muhammad et al., 2020; Thakur et al., 2020; Gun et al., 2022).

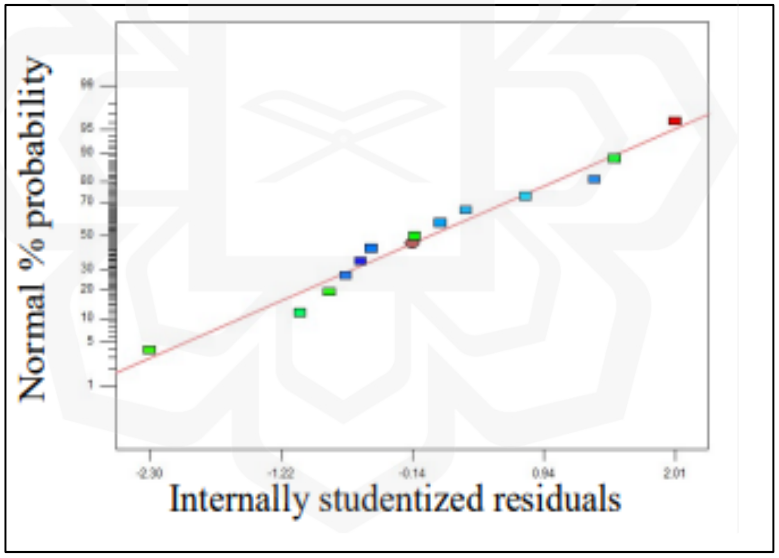

Figure 4.7 Normal Probability Graph for Run 1 – 13.

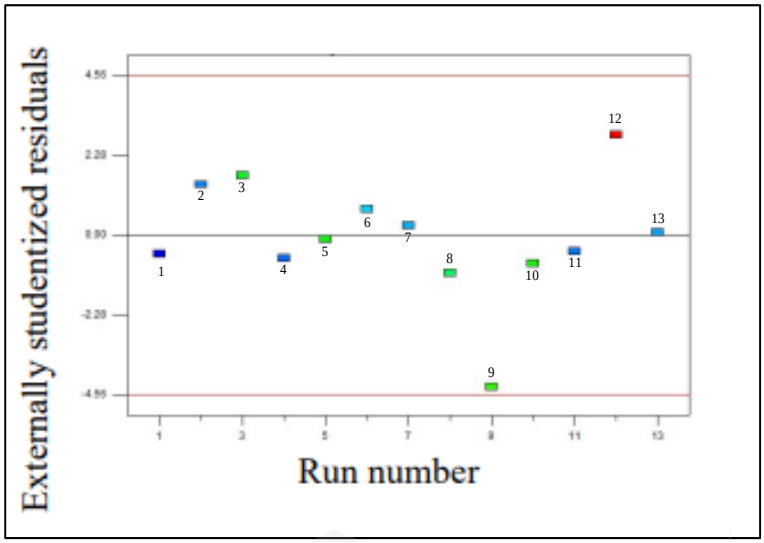

Figure 4.8 The Externally Studentized Residuals vs Predicted Response Graph for Run 1 – 13.

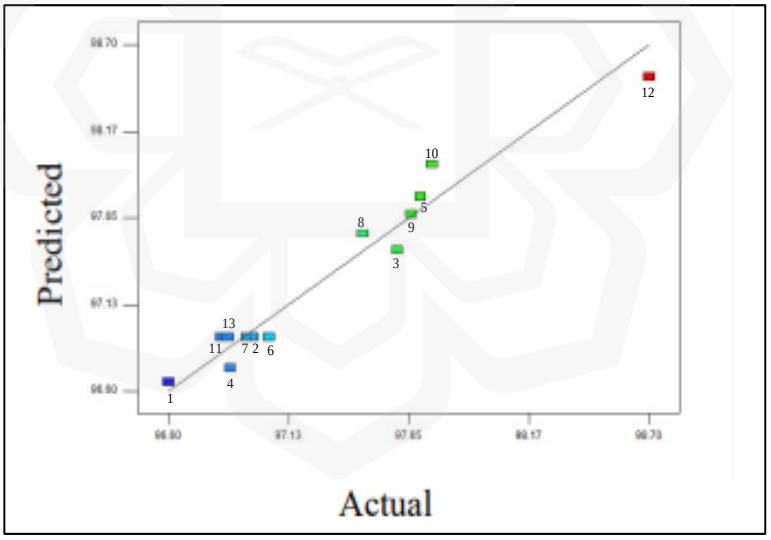

Figure 4.9 Model Precision Diagnostic Graph for Run 1 – 13.

The fourth analysis is the three-dimensional (3D) contour plot is also used in the analysis to predict the results (Thakur et al., 2020). A 3D contour plot is a planar presentation of the reaction surface in two dimensions. The 3D response surface plot in Figure 4.10 illustrates how the elements in this investigation interacted with one another.

When all factors, namely burning duration and burning temperature, are increased, the proportion of reactive chemical content does not necessarily follow. The highest percentage of reactive chemical content is not achieved when the burning duration and burning temperature are high. It is also demonstrated that ash with a short burning duration and low burning temperature produces high silica. It observes that there is no significant influence on the amount of silica in the TRSA towards the high temperature of the incineration process.

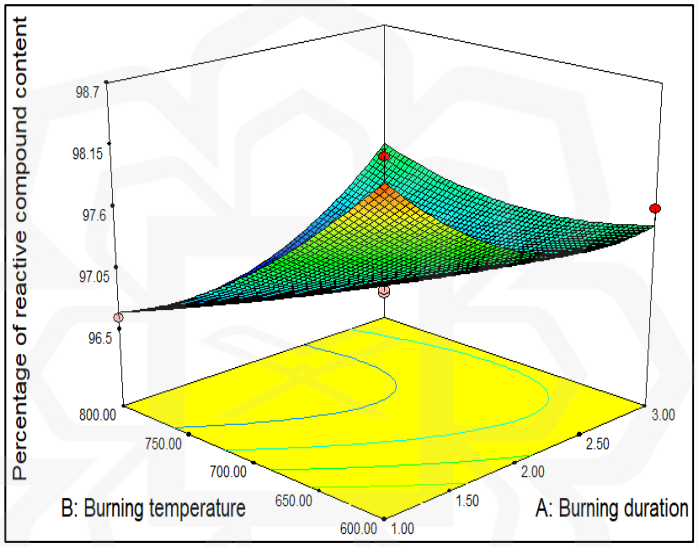

Figure 4.10 3D Contour Plot for Interaction Between Both Factors.

Then the last analysis is the optimization analysis, as shown in Figure 4.11, the Design Expert preferred 6 solutions out of the 13 runs. Optimization is increasing the efficiency of analysis to maximize its quality. However, 3 experiments from the 6 solutions provided by the Design Expert are selected for optimization analysis. Therefore, those 3 experiments are repeated to reduce errors and ensure that the selected optimum parameter combination is significant. The first solution suggested by Design Expert, as illustrated in Figure 4.11, has the highest desirability function, which is 90.7%, with a burning duration of 1 hour and a burning temperature of 600℃.

Name	Goal	Lower limit	Upper limit	Lower weight	Upper weight	Importance
Burning duration	Is in range	1	3	1	1	3
Burning temperature	Is in range	600	300	1	1	3
Percentage of reactive compound content	Maximize	96.6	98.7	1	1	3

Solutions

Number	Burning duration	Burning temperature	Percentage of reactive compound content	Desirability	
1	1.00	600.00	98.5039	0.907	Selected
2	1.00	609.54	98.3768		
3	3.00	800.00	97.5536		
4	2.08	600.00	97.5396		
5	3.00	600.00	97.4522		
6	2.85	600.00	97.4204		

6 solutions found

Figure 4.11 Table of Solution Results for this Analysis in RSM.

Before confirming the solution as the best combination parameters for the incineration process, the XRF analysis (response 1) compares to the estimated value from the model to see if the suggested model is adequately predicted since it is selected randomly from the design space. Both values of response 1 for predicted and actual are expected to fall within the prediction index (PI) to indicate that the model is significant. From Figure 4.12, the prediction value of the percentage of reactive compound content in RSM for the first solution is 98.38%, while the XRF analysis results for model with the same value of each factor (burning duration = 1 hour and burning temperature = 600°C) is above 98.70%. So, the range of XRF analysis results for actual reaction falls between 95% PI low and 95% PI high. The values of 95% PI low and 95% PI high are shown in Figure 4.12. Therefore, the model is validated since the actual experimental result is within the expected range for any involved factor for the first solution.

Factor	Name	Level	Low level	High level	Std. dev.	Coding
A	Burning duration	1.00	1.00	3.00	0.000	Actual
B	Burning temperature	609.54	600.00	800.00	0.000	Actual

Response	Prediction	SE Mean	95% CI low	95% CI high	SE Pred	95% PI low	95% PI high
Percentage of reactive compound content	98.3768	0.12	98.10	98.65	0.20	97.91	98.84

Figure 4.12 Table of Prediction Result for this Analysis in RSM.

Overall, the satisfaction of using the incineration process at a controlled temperature to produce an amorphous silica TRSA is proved in this study. Furthermore, the percentage of reactive compound content in the ashes for each experimental run is more than 96.60% which shows that the ashes can be used in concrete production. Thus, as mentioned in the standard of ASTM C618, the ashes can act as pozzolanic material and CRM when the reactive compound content (SiO_2, Al_2O_3, and Fe_2O_3) is more than 70% (Kasaniya et al., 2019). Additionally, the RSM shows that the optimum experimental condition (burning duration = 1 hour and burning temperature = 600℃) has a 90.70% desirability function to obtain a high-quality TRSA.

Therefore, the incineration process at a controlled temperature is suitable and effective in increasing the silica amount and decreasing impurities present in the ash. Lastly, the incineration process at 600℃ for about 1 hour is selected to be further assessed in the grinding process. The TRSA undergoes the grinding process using a planetary ball mill. The TRSA grind for about 15 minutes at a speed of 300 rpm with a ratio ball-to-powder is 15.1 (Saad et al., 2022). The characterization of ground TRSA compared to non-TRSA (NTRSA), and the usage of ashes are deliberated in phases 3 and 4, respectively.

4.3.1 Summary (Phase 2)

From phase 1, the rice straw is treated at 70℃ for about 2 hours using a low hydrochloric acid (HCl) concentration, 0.06 M, in the thermochemical pretreatment process. Then, for phase 2, the treated rice straw is burnt at 600℃ for about 1 hour and continued with the grinding process. Those optimum combinations of factors involved in phases 1 and 2 exhibited excellent results regarding enhancing the amount of reactive compound content and diminishing impurities that disturb the performance of TRSA to replace cement.

4.4 CHARACTERIZATION OF TREATED RICE STRAW ASH (TRSA) AND NON-TREATED RICE STRAW ASH (NTRSA) (PHASE 3)

As a continuation of the previous section, there is an explanation of the influence of the pretreatment process, incineration process and grinding process on the characterization properties of treated rice straw ash (TRSA) and non-TRSA (NTRSA) are discussed in this phase 3.

4.4.1 Mineralogical Characteristics of Treated Rice Straw Ash (TRSA) and Non-Treated Rice Straw Ash (NTRSA)

Analysis of the mineralogical characteristics for both ashes TRSA, and NTRSA are illustrated in the X-Ray diffraction (XRD) analysis and discussed in this sub-section. The XRD analysis conducts to identify further the formation of any crystalline phases formed in the ashes. Based on the XRD pattern, a broad and no-sharp peak shows amorphous silica, while a sharp spectra peak shows crystalline (Wong et al., 2019).

Figure 4.13 depicts that the crystalline degree formed in the TRSA is lower than NTRSA in Figure 4.14. The absence of sharp peaks in the XRD pattern for TRSA indicates the presence of amorphous silica. There is a broad, intense peak at $2\boldsymbol{\theta}$ value of 22° for the XRD pattern of TRSA. This observation is similar to previous researchers, where the amorphous condition formed in the XRD analysis of the pozzolanic material that undergoes an acid treatment process (Embong et al., 2016; Nazopatul et al., 2018; Wong et al., 2019; Hu et al., 2020; Rajan et al., 2020). It shows that the acid treatment effectively removes impurities in the pozzolanic material before incineration. It is supported by the finding of X-Ray Fluorescence (XRF) analysis on the chemical composition present in the TRSA, which justify that the percentage of impurities, especially potassium oxide (K_2O), is 0.0%.

When there is a low amount of metal impurities such as K_2O, the eutectic reaction can prevent from occurring (Umeda & Kondoh, 2010). Wong et al. (2019) mentioned that no crystallized silica formed in the treated ash due to the acid treatment process, which removes the crystallization catalyst known as K_2O. Furthermore, Bazargan et al. (2015) also discussed the similar fact that the metal impurities and salt react with the silica that presence in the pozzolanic material caused eutectic reaction due to the formation of sintered ash during the incineration process, even though the material burnt at high temperature of 1400℃. The eutectic reaction will be formed when the melting point for each component is below 800℃.

On the other hand, the presence of crystalline degree in the XRD pattern of NTRSA is high, as shown in Figure 4.14. There are a lot of sharp peaks illustrated for NTRSA in between $2\boldsymbol{\theta}$ value of 20° to 30° and 40° to 50°. It shows that the NTRSA is sensitive to the burning temperature, which forms the eutectic reaction and the surface melting of metallic impurities such as K_2O (Vayghan et al., 2013). This observation is in line with Wong et al. (2019), who mentioned that the crystallization of silica present in the material depends on the burning temperature, where the peak increase is formed according to the temperature. Unlike treated material using acid treatment, the amorphous silica remains the same as long as the burning temperature is lower than 900℃. Therefore, the temperature seems to affect the formation of crystalline silica towards the NTRSA.

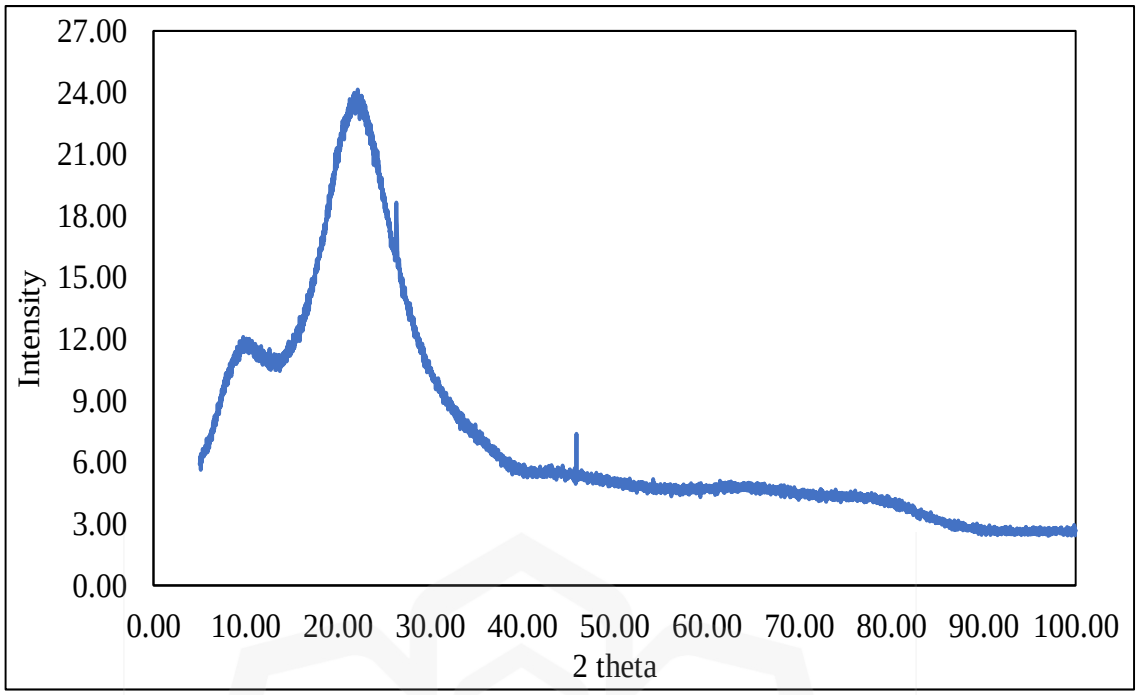

Figure 4.13 XRD Analysis of TRSA.

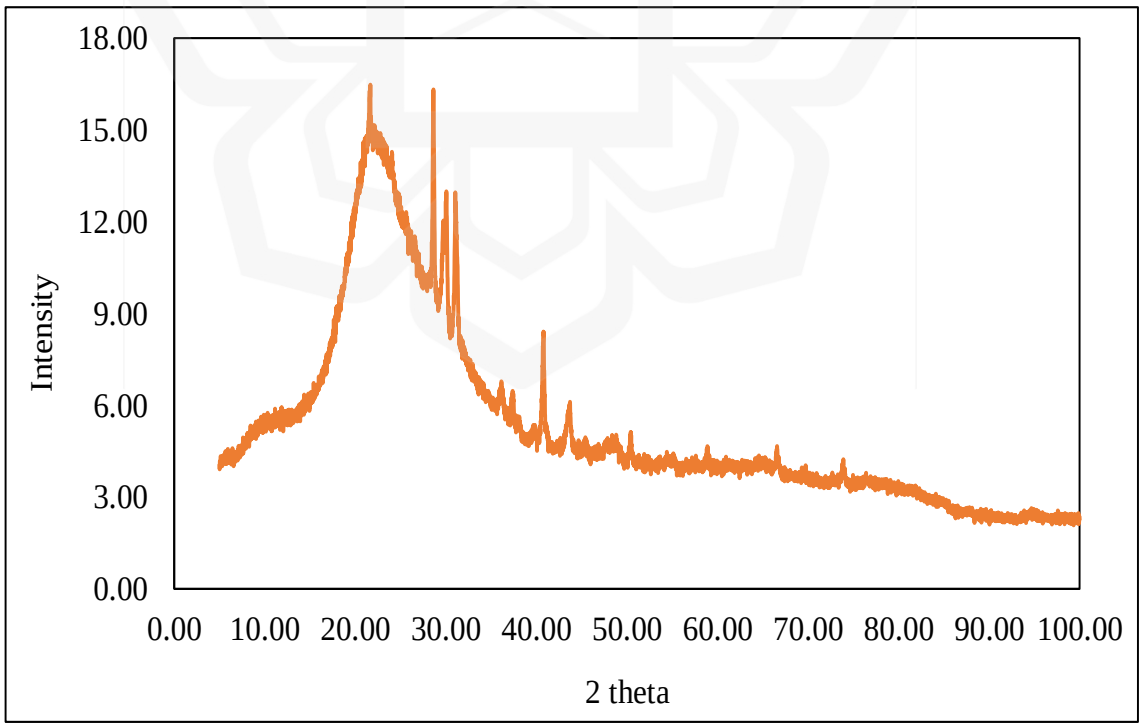

Figure 4.14 XRD Analysis of NTRSA.

4.4.2 Structural Elucidation of Treated Rice Straw Ash (TRSA) and Non-Treated Rice Straw Ash (NTRSA)

The result of the Fourier transforms infrared spectroscopy (FTIR) pattern of TRSA and NTRSA are explained and discussed in this part of the thesis. The FTIR analysis of NTRSA was compared with TRSA. The FTIR result was shown from the range of wavenumber between 650 cm^{-1} to 4000 cm^{-1}.

Based on the FTIR result of TRSA, as shown in Figure 4.15, the percentage of transmittance peak for the formation of Si-O functional group are observed at the wavenumber 800 cm^{-1} and 990 cm^{-1} known as stretching Si-O band and 1070 cm^{-1} assigns as stretching Si-O-Si/Al. Those peaks indicate silica presented in the material (W. Xu et al., 2018; Záleská et al., 2018). Munshi and Sharma (2018) also mentioned that the Si-O-Si/Al stretching band is predominant in the FTIR analysis. Furthermore, there is no peak presence at the wavenumber near 1500 cm^{-1} for TRSA, indicating that the amount of carbon was removed from the treated material. When there is no carbon bond in the material, it performs well due to fewer impurities. All important functional groups are found in the FTIR result of the TRSA. Therefore, this is a sign of the formation of amorphous silica and the reduction of impurities. Hence, it thoroughly supports the XRD result discussed in the previous section. There are also absorption bands of molecular water which are the O-H stretching band and H-O-H bending band at 1650 cm^{-1} and 3450 cm^{-1}, respectively and this same finding from the previous researcher (Munshi & Sharma, 2018).

As for the NTRSA in Figure 4.16, the peaks corresponding to Si-O bonds are formed similarly to the TRSA. The wavenumber for Si-O bonds is 800 cm^{-1}, 900 cm^{-1}, and 1060 cm^{-1}. There are also absorption bands of molecular water which are the O-H stretching band at 3450 cm^{-1} and the H-O-H bending band at 1650 cm^{-1} and this is the same finding with TRSA. Nevertheless, the formation of silanol symmetric bond vibration, Si-O-Silanol, is weaker than the TRSA. The intensity of silica in the predominant peak, stretching Si-O-Si/Al of NTRSA, is lesser than TRSA. At the same time, there is the carbonyl (C=O) bond

at the wavenumber 1400 cm^{-1} for NTRSA. A similar finding by past researchers, Xu et al. (2018) and Bhattacharyya et al. (2020), where the C=O bond existed for non-treated material due to the presence of carbon. The unburnt cellulose and lignin of the material cause the formation of the C=O bond.

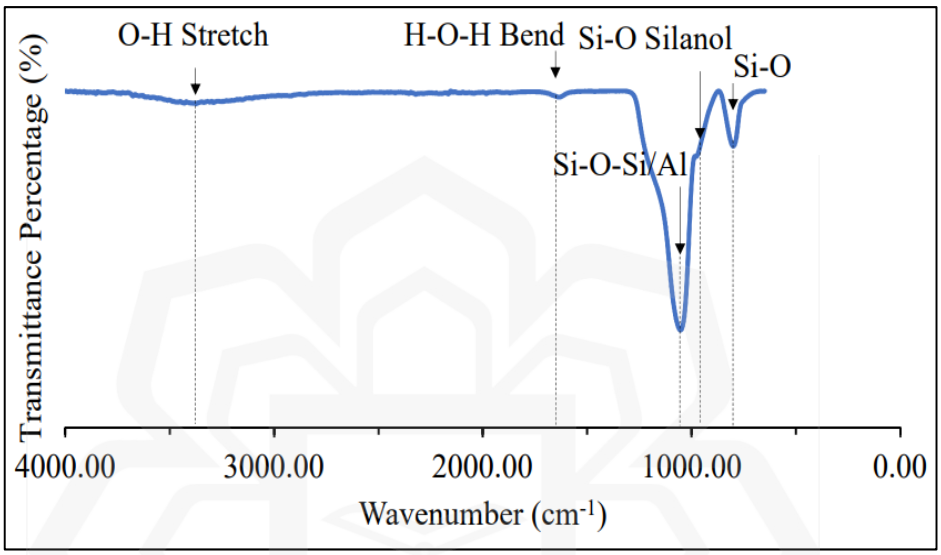

Figure 4.15 FTIR Analysis of TRSA.

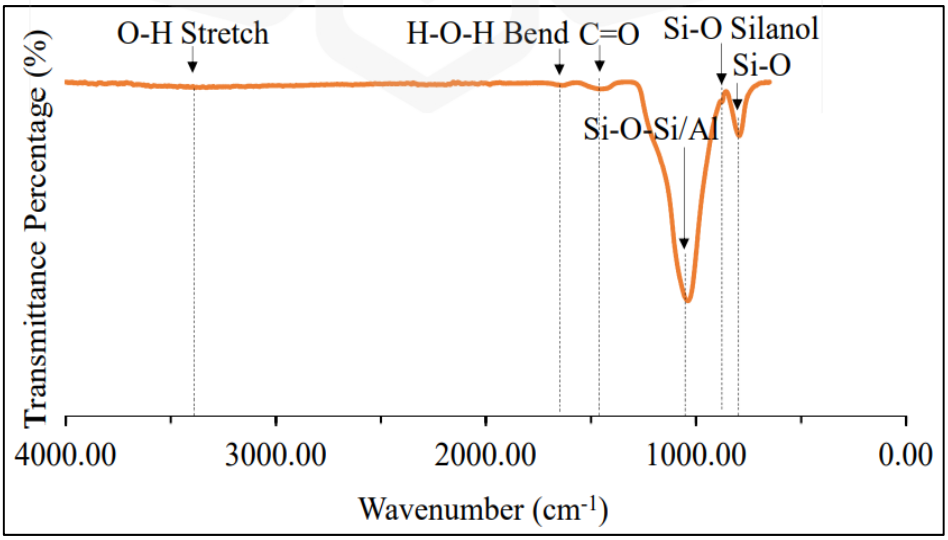

Figure 4.16 FTIR Analysis of NTRSA.

4.4.3 Physical Characteristics of Treated Rice Straw Ash (TRSA) and Non-Treated Rice Straw Ash (NTRSA)

The acid treatment, incineration process at controlled temperature, and grinding process affect the materials' physical characteristics. The reduction size of the particle produce through all processes will have a large specific surface area (SSA) and a small pore size. Therefore, it creates excellent pozzolanic reactivity and improves the material's performance as a pozzolan. In this regard, the specific surface area (SSA) and pore size of TRSA and NTRSA were determined through Brunauer-Emmet-Teller (BET) analysis and Barret-Joyner-Halenda (BJH) analysis.

Based on Table 4.9, the value of SSA for TRSA, 296.58m^2/g, is higher than NTRSA, 16.35m^2/g because the size of the TRSA particle smaller than the NTRSA particle. When the particle size is small, the SSA value is high. Therefore, the SSA value of TRSA has a huge difference from NTRSA. It shows that the particle's size contributes to the value of SSA. The low value of SSA for NTRSA is because of unburnt carbon content. The presence of unburnt carbon content was determined through the FTIR analysis in Section 4.4.2 (Refer Figure 4.16) .The unburnt carbon content increases the rigidity of the NTRSA structure, making it hard to mill (Saad et al., 2022). At the same time, the colour of NTRSA is darker than TRSA due to the existence of unburnt carbon, and the particle of TRSA is smaller than NTRSA after the incineration process at 600℃ for about 1 hour, as shown in Figure 4.17 (a) and Figure 4.17 (b).

Table 4.9 The SSA and Pore Characteristics of TRSA and NTRSA.

Sample	Specific surface area (BET-SSA) (m^2/g)	Pore characteristic (BJH)		
		Adsorption cumulative pore surface area (m^2/g)	Adsorption cumulative pore volume (cm^3/g)	Adsorption cumulative average pore diameter (nm)
TRSA	296.58	290.23	0.5227	75.8
NTRSA	16.35	10.81	0.0505	131.16

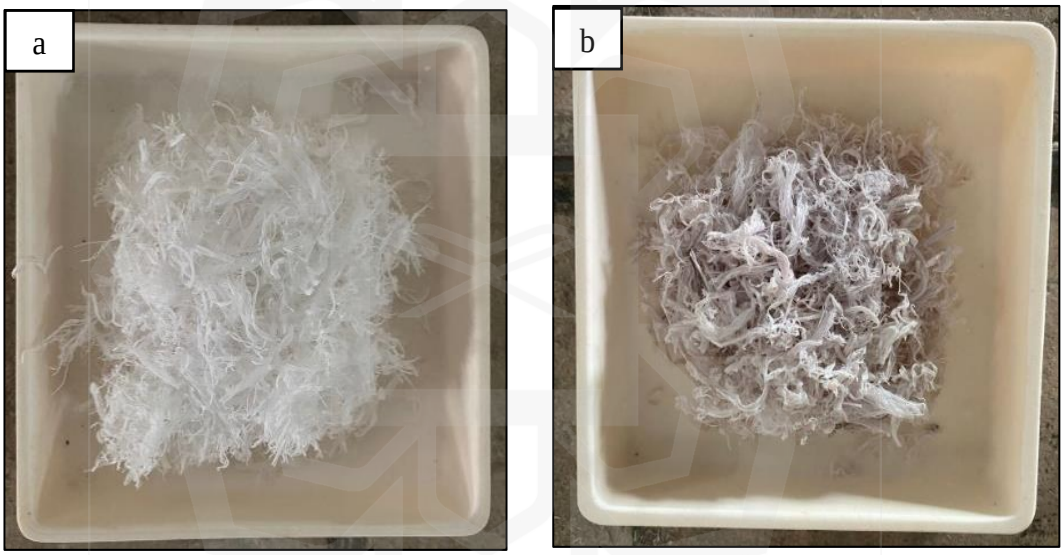

Figure 4.17 Digital Photo of Samples After Incineration Prior to Grinding Process (a) TRSA, and (b) NTRSA.

For the pore features, the adsorption cumulative pore surface area of TRSA, 290.23 m^2/g, is also higher than NTRSA, 10.81 m^2/g, because the NTRSA consists fewer amount of porous structure compared to the TRSA sample. The presence of porous structure in TRSA is more than NTRSA was proved through FESEM analysis in Section 4.4.4. Unwanted metallic impurities such as potassium and sodium that encapsulated on the surface of raw rice straw had been eliminated through acid leaching process. This

phenomenon causing porous structure formation in TRSA. Similar observation was recorded by (Khan et.al., 2020). The adsorption cumulative pore volume of the material is high when the BET-SSA and the adsorption cumulative pore surface area are high. The NTRSA has a lower adsorption cumulative pore volume, 0.0505 cm^3/g, than TRSA, 0.5227 cm^3/g. In a nutshell, the TRSA was determined to have a high value of SSA, pore surface area, pore volume, and small diameter compared to NTRSA.

Moreover, the physical adsorption-desorption isotherm known as physisorption isotherm for BET-SSA result of ground NTRSA and TRSA was plotted to identify absorbent characteristics as stated in the International Union of Pure and Applied Chemistry (IUPAC) (Alothman, 2012), as shown in Figure 4.18. The type of physisorption is the type of the adsorption caused by the amount of nitrogen gas (N_2) correspondent to the sample's surface. Based on the IUPAC, six types of physisorption isotherms are type I shows the absorbent is a microporous structure, non-porous or macroporous for type II, III, and VI, and the mesoporous structure for type V, and IV. The physisorption isotherm was illustrated the amount of absorbed N_2 depended on the relative pressure, temperature, and the morphology of the sample's surface.

Based on Figure 4.19, the physisorption isotherm graph for TRSA is type IV, which means the absorbent is a mesoporous structure. The interaction between the absorbent and the absorbate of TRSA is good since it has mesoporous structure. Meanwhile, the physisorption isotherm graph for NTRSA in Figure 4.20 is type III, showing that the absorbent is macroporous. This is because the size of the absorbent is large, and then, the interaction between the absorbent and the absorbate of NTRSA is weak. Therefore, the interaction between the absorbent and the absorbate of TRSA is better than NTRSA since the absorbent of TRSA is mesoporous. The absorbent is referred to the NTRSA or TRSA, while the adsorbate is the N_2 gases used in this analysis.

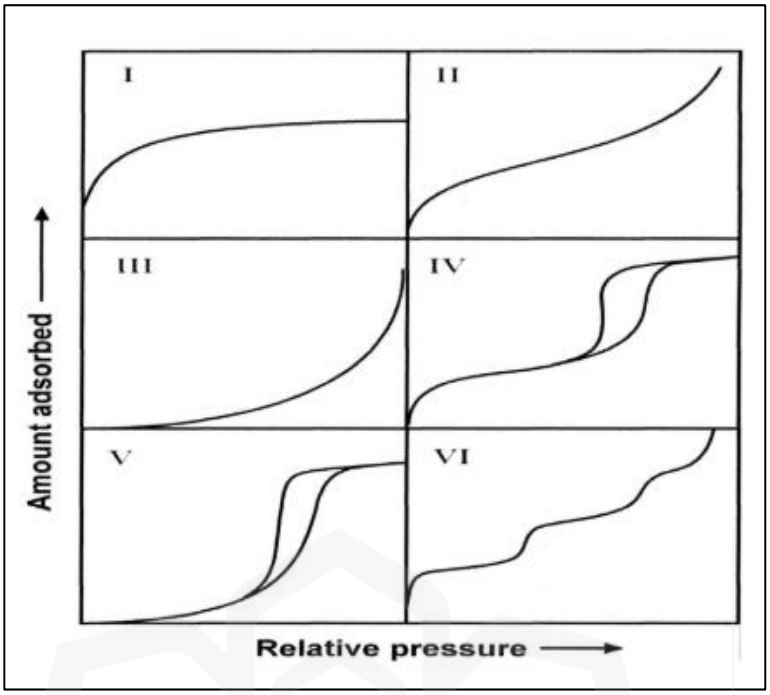

Figure 4.18 IUPAC Classification on the Absorbent Characteristics (Alothman, 2012).

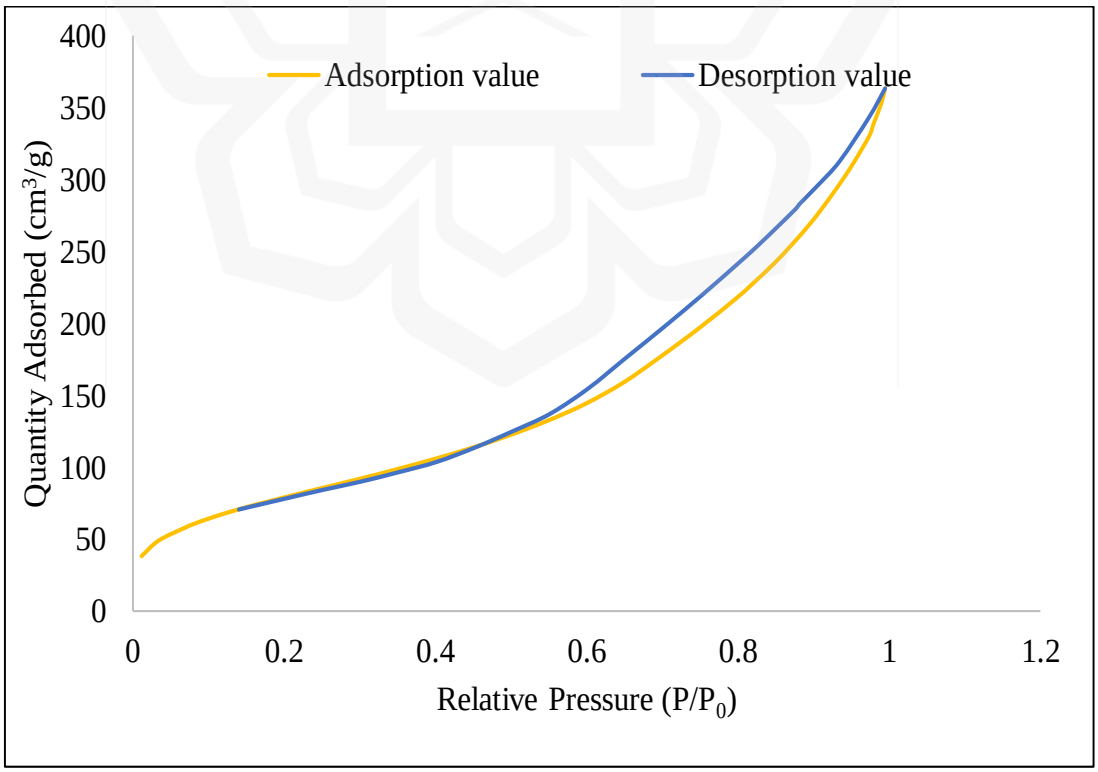

Figure 4.19 Physisorption Isotherm for BET-SSA of Ground-TRSA.

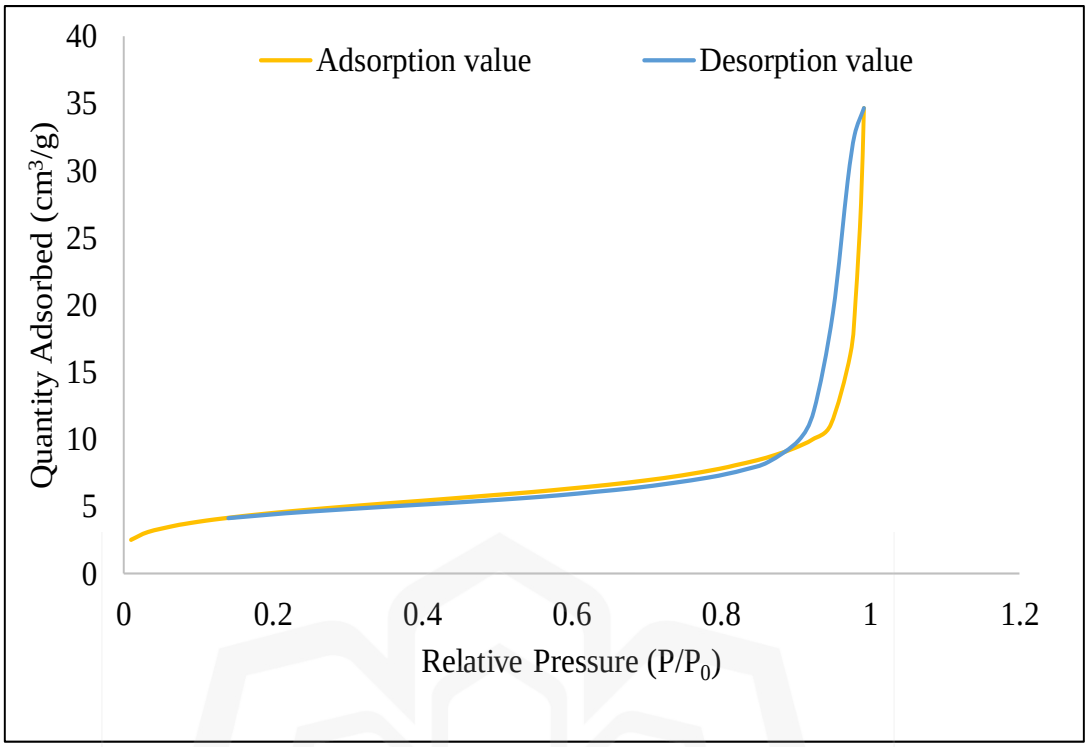

Figure 4.20 Physisorption Isotherm for BET-SSA of Ground-NTRSA.

4.4.4 Morphology of Treated Rice Straw Ash (TRSA) and Non-Treated Rice Straw Ash (NTRSA)

As for the morphological analysis of TRSA and NTRSA, the field emission scanning electron microscopy (FESEM) analysis for both ashes was conducted to identify the microstructure of the particle of ashes. There are low (500X) and high (10000X) magnifications of FESEM images to describe the morphology of both ashes. Figure 4.21 (a) and (b) and Figure 4.22 (a) and (b) illustrate the FESEM images of NTRSA and TRSA, respectively, before the grinding process. The TRSA formed through an acid treatment process using an optimum combination of parameters, treated using 0.06 M hydrochloric acids (HCl) and soaked at 70℃ for about 2 hours and continued with the incineration process at an optimum temperature of 600℃ for about 1 hour. Meanwhile, the NTRSA only undergoes an incineration process using similar parameters to TRSA.

Based on the FESEM image, as shown in Figure 4.21 (a), the NTRSA has needle-like particles with a corrugated and rough surface. The NTRSA also consists of an irregular shape and size. This finding of NTRSA was similar to the observation by previous researchers (Yao et al., 2016; Pandey & Kumar, 2019b; Bhattacharyya et al., 2020). The structure of NTRSA looks rigid compared to TRSA due to the presence of carbon. As proved in Fourier transforms infrared spectroscopy (FTIR) analysis in Section 4.4.4, there is a carbonyl (C=O) bond in the NTRSA (Refer Figure 4.16). The unburnt carbon makes the NTRSA particles rigid (Venkatanarayanan & Rangaraju, 2015). Therefore, its performance is poor when pozzolanic material with a high amount of carbon is used to replace mortar production.

However, the FESEM image of unground TRSA in Figure 4.22 (a) illustrated that there are more small particles than NTRSA. The fine size of TRSA proves that the structure of TRSA is soft, which means it is easy to break into small particles without undergoing the grinding process. The FESEM image of unground TRSA, Figure 4.22 (b), with high magnification, shows pore structures filled with agglomerated fine particles. The acid treatment is a possible reason that succeeds in breaking the rigid structure of the TRSA. The cellulose, lignin, and hemicellulose structure of TRSA are broken, and thus, the rice straw's rigid structure will be disturbed and broken. The observation is in line with the past research that has been conducted by (Gupta & Shukla, 2020).

Additionally, the FESEM image of TRSA in Figure 4.22 (a) also illustrated an irregular shape and size of the particle, which is similar to NTRSA. Furthermore, the morphology of ground NTRSA and TRSA were also observed in this sub-section. Figure 4.23 (a) and (b) and Figure 4.24 (a) and (b) show the FESEM images of ground NTRSA and TRSA, respectively. FESEM image of NTRSA proved that the NTRSA particles are bigger than TRSA even though the NTRSA undergoes a grinding process. This observation shows that the NTRSA particle is difficult to mill. In contrast, the TRSA is easy to mill and obtain fine particle.

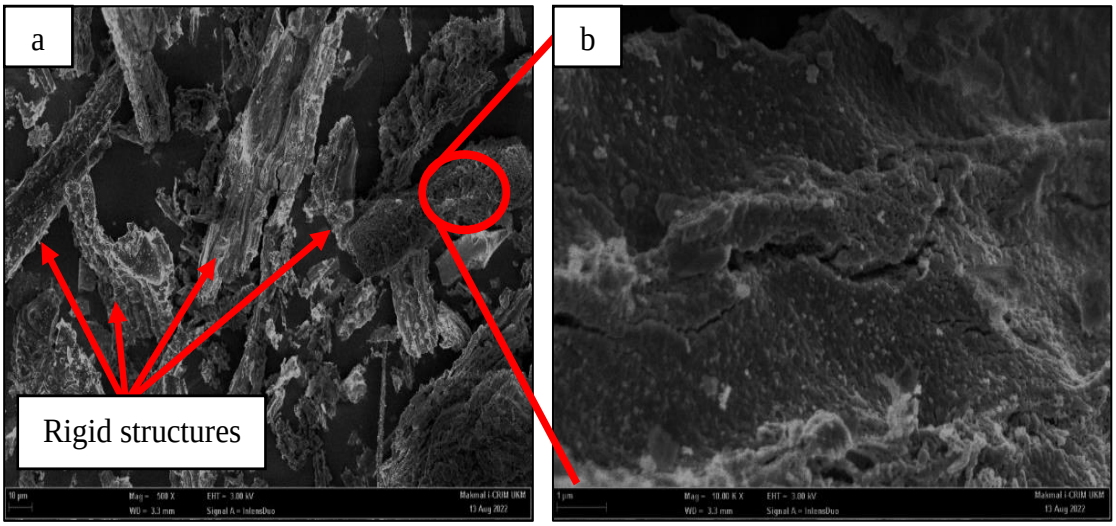

Figure 4.21 FESEM Image of Unground NTRSA at (a) 500X Magnification and (b) 10000X Magnification.

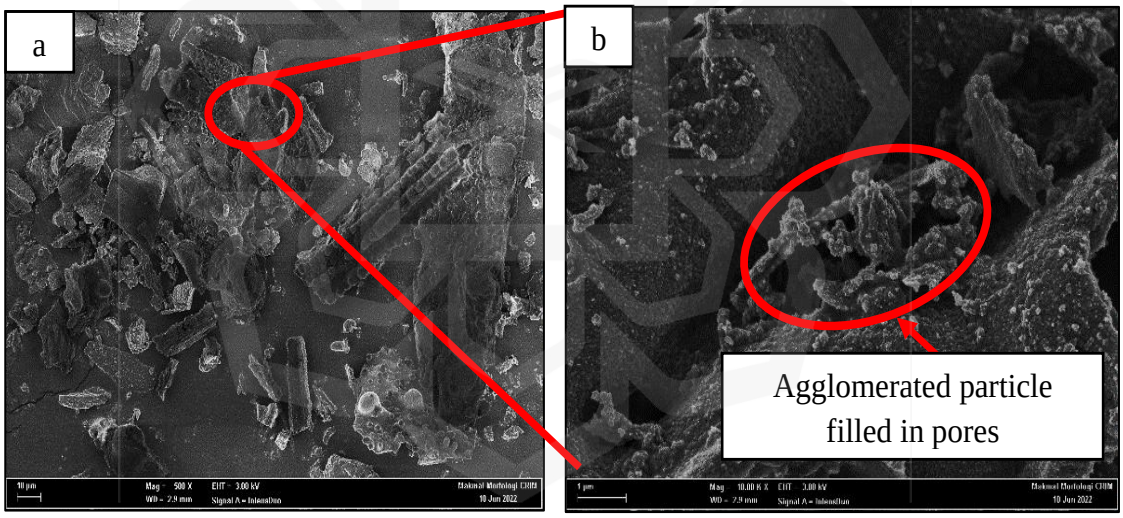

Figure 4.22 FESEM Image of Unground TRSA at (a) 500X Magnification and (b) 10000X Magnification.

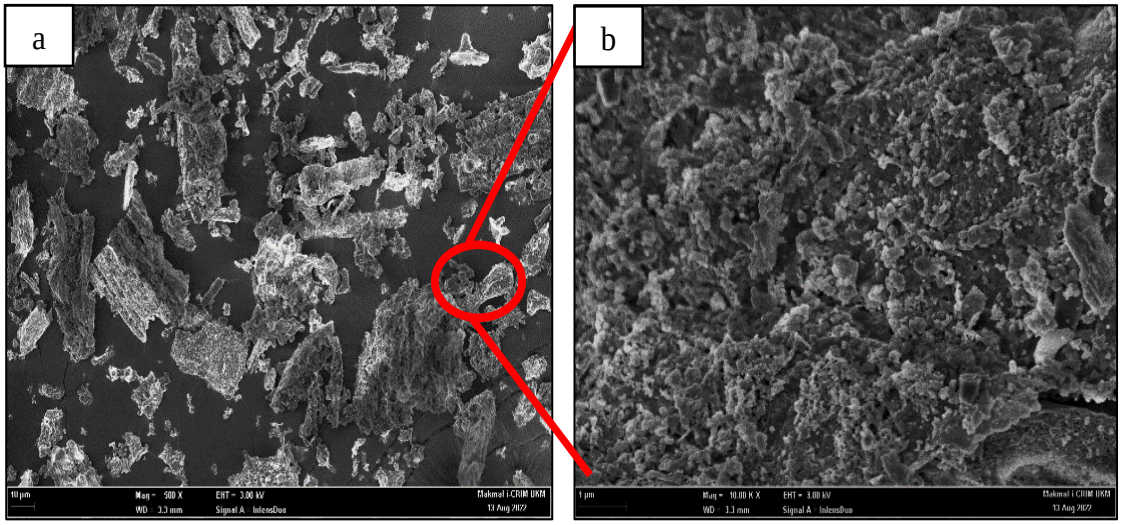

Figure 4.23 FESEM Image of Ground NTRSA at (a) 500X Magnification and (b) 10000X Magnification.

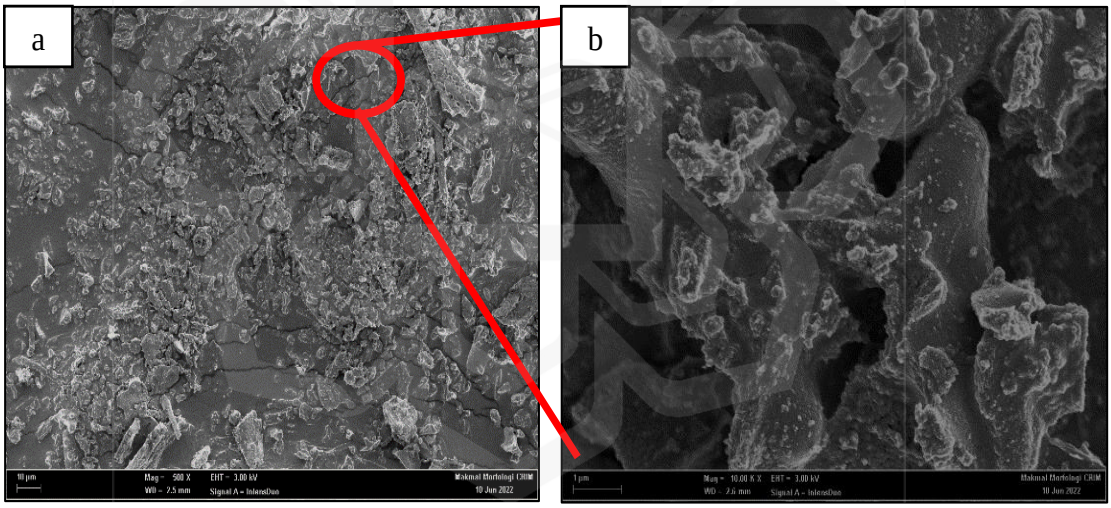

Figure 4.24 FESEM Image of Ground TRSA at (a) 500X Magnification and (b) 10000X Magnification.

In addition, the morphology of TRSA and NTRSA were further analyzed using transmission electron microscopy (TEM) analysis. The TEM analysis is significant in determining nano-sized particles of the ashes. The nano-sized ashes have filled the void formed between aggregates and cement paste, reducing the porosity of concrete. Thus, the

performance of mortar-based pozzolan material is good. TEM analysis records the TRSA with a nano-sized particle between 4.505 nm to 6.278 nm, which is smaller than the NTRSA, as shown in Figure 4.25 (a) and Figure 4.25 (b). The range size of NTRSA is from 28.09 nm to 45.63 nm.

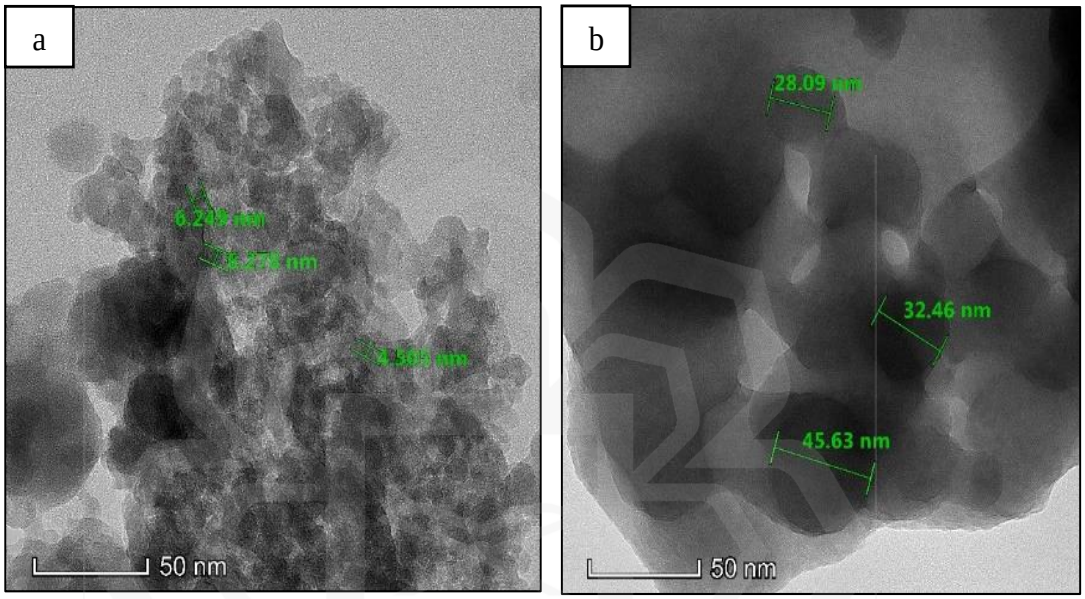

Figure 4.25 TEM Analysis on Size of Nanomaterial of (a) TRSA, and (b) NTRSA.

Referring to the TEM image of Figure 4.26 (a1), the TRSA has an agglomeration particle, while the NTRSA has an aggregation particle, as shown in the TEM image of Figure 4.26 (b1). The agglomeration particles formed when the aggregate (silica) in the ash formed a cluster structure (Farirai et al., 2020). The particles of silica are widely scattered and collide, forming an agglomeration (Amibo et al., 2022). Rahmi et al. (2021) mentioned that agglomeration usually happens because of the loss of interaction between nanoparticles and surfaces.

In contrast, the aggregation forms in the NTRSA proved that there is a metal impurity, especially potassium oxide, K_2O. Those impurities melted on the silica particles,

and the aggregation formed and enhanced the ash's crystallinity (Chen et al., 2013). Based on the x-ray fluorescence (XRF) analysis conducted for this research, the NTRSA has 9.40% of K_2O while 0.0% is in TRSA. Thus, the acid treatment effectively removes those impurities (Munshi & Sharma, 2018; Nazopatul et al., 2018). This observation proved that the acid treatment is significant for producing a good TRSA without metal impurities that caused the aggregation.

However, the identification of amorphous silica can be detected through the absence of the lattice fringes formation in the TEM image (Sankar et al., 2016). Based on the high magnification of TEM images, Figure 4.26 (a2) detected no formation of lattice fringes in the TRSA, while the TEM image of NTRSA in Figure 4.26 (b2) was shown there is the presence of lattice fringes. This observation indicates that the TRSA has amorphous silica due to the absence of lattice fringes instead of NTRSA. For further verification on the presence of amorphous silica in the ash, the TEM image of the selected area electron diffraction (SAED) pattern was prepared for both TRSA and NTRSA samples. The TEM analysis also assisted the SAED pattern, which is a significant result for nanomaterial whether the ashes consist of amorphous silica (Uda et al., 2021).

Referring to the SAED pattern of NTRSA in the TEM image, as shown in Figure 4.26 (b3), the crystalline structure was captured, as seen in the formation of a white dot. Nevertheless, the white dots are absent in the SAED pattern of TRSA in the TEM image, as shown in Figure 4.26 (a3). Thus, it is confirmed that the TRSA contained amorphous silica. Nayak and Datta (2021) mentioned that the absence of the crystalline structure in the SAED pattern is a strong indication of the amorphous condition of ash. This finding was supported by the XRD analysis of TRSA, which illustrated the formation of a broad, intense peak in the XRD pattern, which is an amorphous nature in TRSA.

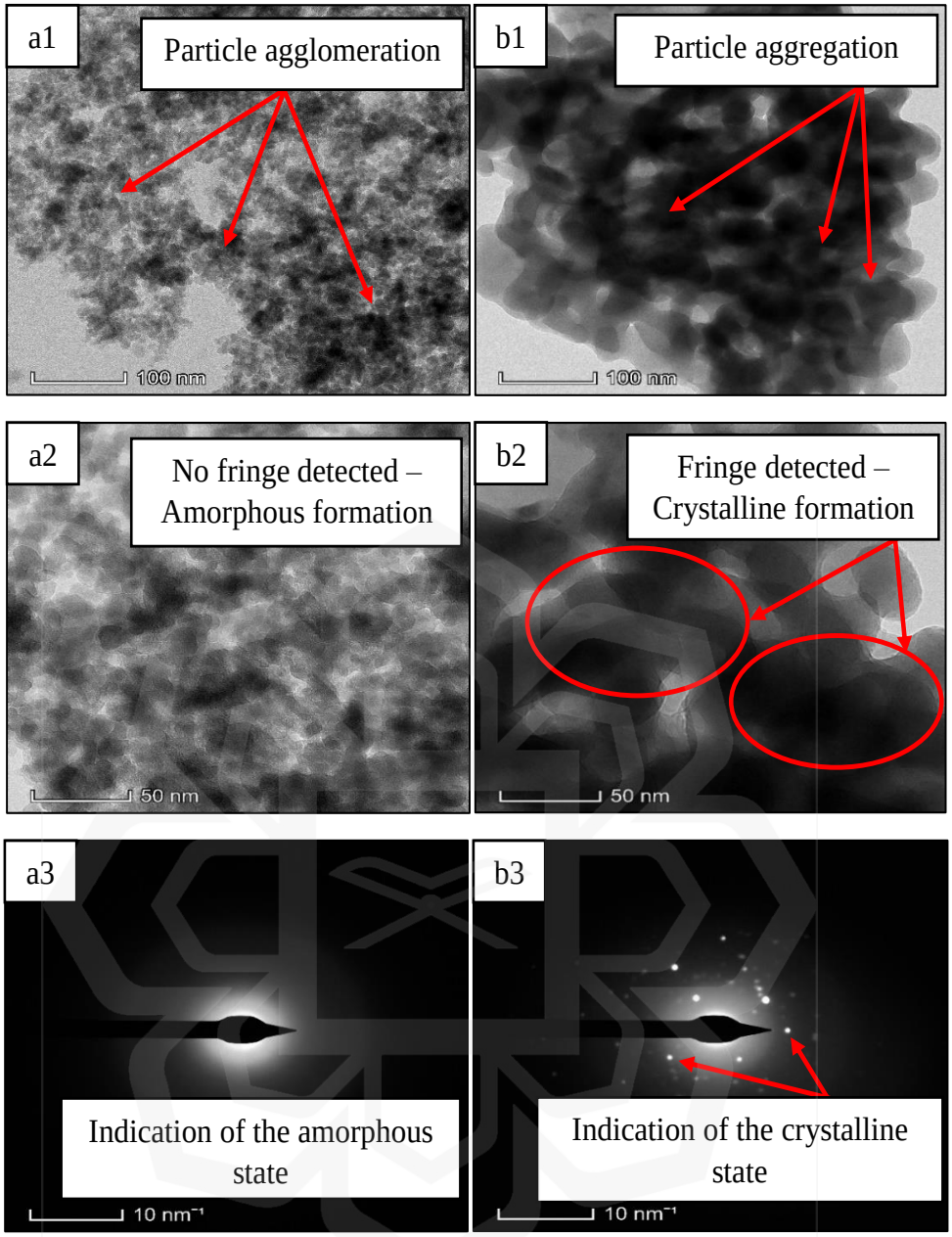

Figure 4.26 High Magnificant of TEM Analysis of (a1)-(a3) TRSA, and (b1)-(b3) NTRSA.

4.4.5 Summary (Phase 3)

As for the characterization properties of treated rice straw ash (TRSA) in this phase 3, the XRD analysis was illustrated that the TRSA is in the amorphous state, while the non-TRSA (NTRSA) was in the crystalline state. Then, the FTIR analysis also proved the presence of all important functional group (Si-O, Si-O-Si/Al) that shown the formation of amorphous silica. In addition, the TRSA had a higher value of pore surface area, pore volume, and smaller diameter than NTRSA through BET and BJH analysis. As for the morphology properties of TRSA, FESEM analysis was illustrated that the particle TRSA was fine compared to NTRSA, even without undergoing grinding process. At last, TEM analysis was recorded that the TRSA was a nano-sized particles between 4.505 nm to 6.278 nm. TEM analysis also recorded TRSA was in an amorphous state since the absence of white dot in the TEM image of SAED pattern.

Overall, the TRSA is in the amorphous state with the silica, not the impurities. The high amorphous silica produces a good pozzolanic material, which will cause an excellent pozzolanic reaction in developing the concrete strength.

4.5 MECHANICAL PROPERTIES OF CEMENT MORTAR INCORPORATING TREATED RICE STRAW ASH (TRSA) (PHASE 4)

This part of this research highlights the result related to the mechanical properties of mortar-based treated rice straw ash (TRSA) and non-treated rice straw ash (NTRSA), including the identification of pozzolanic reactivity, development of mortar strength at 7, 14, 28, and 90 days, and interfacial transitional zone (ITZ) analysis. Furthermore, an excellent pozzolanic reactivity of mortar incorporating pozzolan material with high amorphous silica contributes to the excellent development of mortar strength. In addition, it improves the pozzolanic reactivity and reduces the ITZ gap in the mortar.

4.5.1 Pozzolanic Reactivity Analysis: Strength Activity Index (SAI) Test

To further identify the reactivity of TRSA and NTRSA incorporating cement mortar, the strength activity index (SAI) test was conducted by replacing about 20% of cement with pozzolanic material and the percentage of SAI value is more than 75% after the age of mortar reaches 28 days following the standard of ASTM C311 (Venkatanarayanan & Rangaraju, 2013; Abdulmatin et al., 2018; Athira et al., 2019; Khan et al., 2020).

Based on Table 4.10, the mortar strength of the control mixture sample was 13.24 MPa at 7 days, and 26.41 MPa at 28 days and the highest strength activity index (SAI) value was obtained for the TRSA sample, 127.63% and 136.74% at 7, and 28 days, respectively. The highest SAI value indicates that the TRSA has good pozzolanic material, creating excellent pozzolanic reactivity. When a good pozzolanic material is present in the mortar mixture, the primary reaction (hydration process) occurs and continues with the secondary reaction (pozzolanic reaction) for further development of mortar strength. At the same time, the porosity and permeability of mortar reduce when the SAI value increases.

However, both SAI results of the TRSA and NTRSA samples fulfil the requirement stated in standard ASTM C311, whereby the percentage of SAI values at 7 and 28 days is more than 75%. This condition shows that the TRSA and NTRSA have pozzolanic characteristics similar to cement. Nevertheless, the composition of TRSA has a difference of 37.83% of SAI values with NTRSA. A possible reason for this situation is that the acid treatment and incineration process using an optimum combination parameter effectively produce the pozzolan with a good pozzolanic characteristic. The beneficial and crucial of an additional calcium-silicate-hydrate (C-S-H) formed through pozzolanic reaction due to the high amorphous silica of TRSA (Athira et al., 2019).

Table 4.10 Strength Activity Index (SAI) Result.

Sample	Compressive strength at 7 days (MPa)	Compressive strength at 28 days (MPa)	SAI value at 7 days (%)	SAI value at 28 days (%)
Control mix	13.24	26.41	-	-
NTRSA	12.32	25.26	93.05	95.66
TRSA	16.89	36.11	127.63	136.74

4.5.2 Compressive Strength Development of Cement Mortar Incorporating Treated Rice Straw Ash (TRSA) and Non-Treated Rice Straw Ash (NTRSA)

The mortar strength for both hardened specimens incorporating TRSA and NTRSA is analyzed for 90 days. The mortar strength value is recorded for both specimens to identify the presence of the additional calcium-silicate-hydrate (C-S-H) formed through pozzolanic reaction and developed mortar strength. In addition, this research compared the compressive strength values for TRSA with the control mortar and NTRSA specimens. Figure 4.27 and Figure 4.28 illustrate the compressive strength development of 90 days for TRSA and NTRSA specimens, respectively.

Generally, the compressive strength value for cement mortar incorporating pozzolanic material (TRSA and NTRSA) exhibited significant improvement at age 7 to 28 days. However, the compressive strength values more or less with no significant differences when the mortar age exceeds 28 days to 90 days. The increment of early strength development for both specimens was induced by the presence of TRSA and NTRSA as pozzolanic material in the cement mortar. Early strength development is referred to as the hydration reaction in the cement mortar (Vieira et al., 2020). Nevertheless, the TRSA compositions has higher compressive strength values than NTRSA compositions throughout 28 days. This is because the TRSA has a less pore diameter and more densified porous structure formed from the formation of calcium-silicate-hydrate (C-S-H) phase than

NTRSA. The less porous structure cause more water to be involved in the hydration process of mortar (Vieira et al., 2020).

Based on Figure 4.27, the mortar strength of the control mixture sample and TRSA (1% to 4%) samples increases from the age of mortar from 7 days until 90 days. While the mortar strength of 5% of TRSA composition shows an increasing pattern throughout 28 days, the strength decreases when the mortar age goes beyond 28 days until 90 days. For the 7 and 14 days of mortar age, 5% of TRSA composition has the highest compressive value, 18.68 MPa and 24.44 MPa, respectively. However, the composition of 4% of TRSA shows the highest compressive strength value, which is 41.76 MPa at 28 days and 54.21 MPa at 90 days. Therefore, for the strength development of TRSA mortar, 4% is sufficient to replace cement for further development of mortar strength. It also improves by about 60.27% of the compressive strength compared to the control mixture sample.

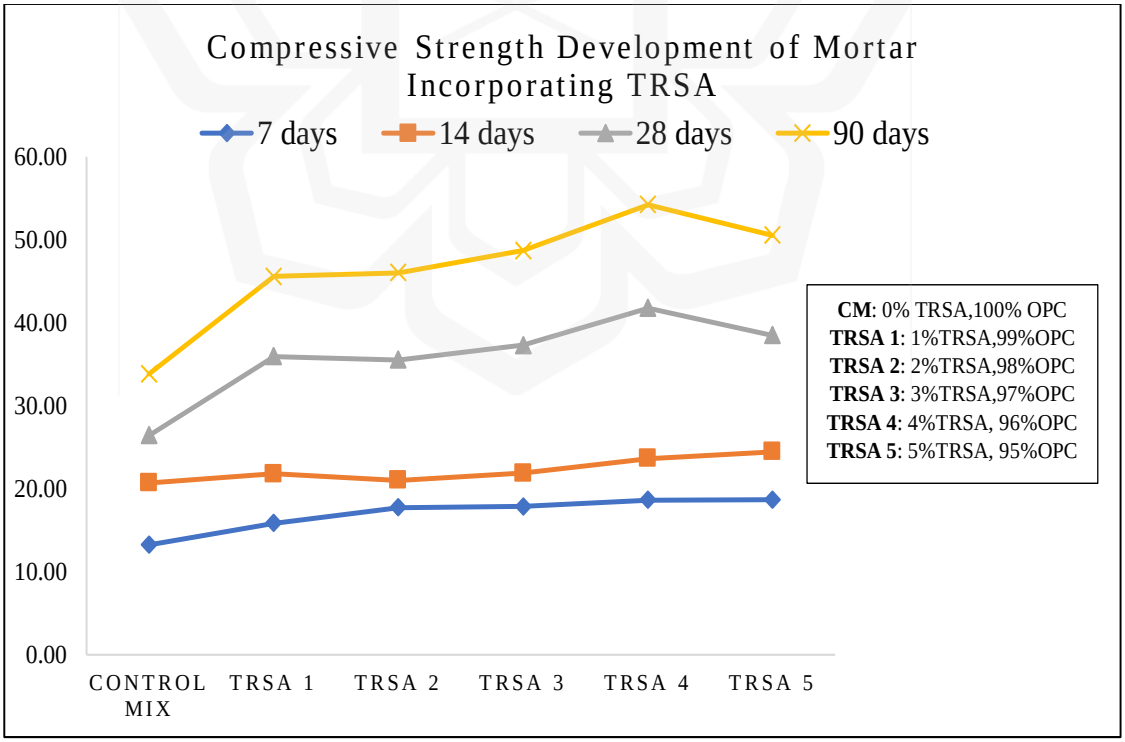

Figure 4.27 Compressive Strength Values for Mortar Incorporating TRSA.

On the other hand, for the NTRSA mortar, as illustrated in Figure 4.28, the mortar strength of the 1% to 5% of NTRSA samples is lower than the control mixture sample at 7 days to 90 days. For the 7, 14, 28 and 90 days of mortar age, the control mixture composition has the highest compressive value, 13.24 MPa, 20.70 MPa, 26.41 MPa and 33.82 MPa, respectively. Thus, the strength development of the NTRSA mortar is lower than the control mixture and TRSA sample. In addition, the performance of NTRSA incorporating cement mortar was disturbed by impurities, especially potassium oxides (K_2O), as stated in the XRF analysis. Vayghan et al. (2013), Xu et al. (2018), and Librea et al. (2019) mentioned that metal impurities such as calcium oxide (CaO), magnesium oxide (MgO), and K_2O were interrupted the performance of ashes as a pozzolan in the concrete production. At the same time, by supporting the result of FTIR analysis, a carbonyl bond (C=O) formed through unburnt carbon also disturbs the performance of NTRSA mortar. The presence of carbon in the ash required a high amount of water which can caused the decreasing strength of the concrete (Venkatanarayanan & Rangaraju, 2015).

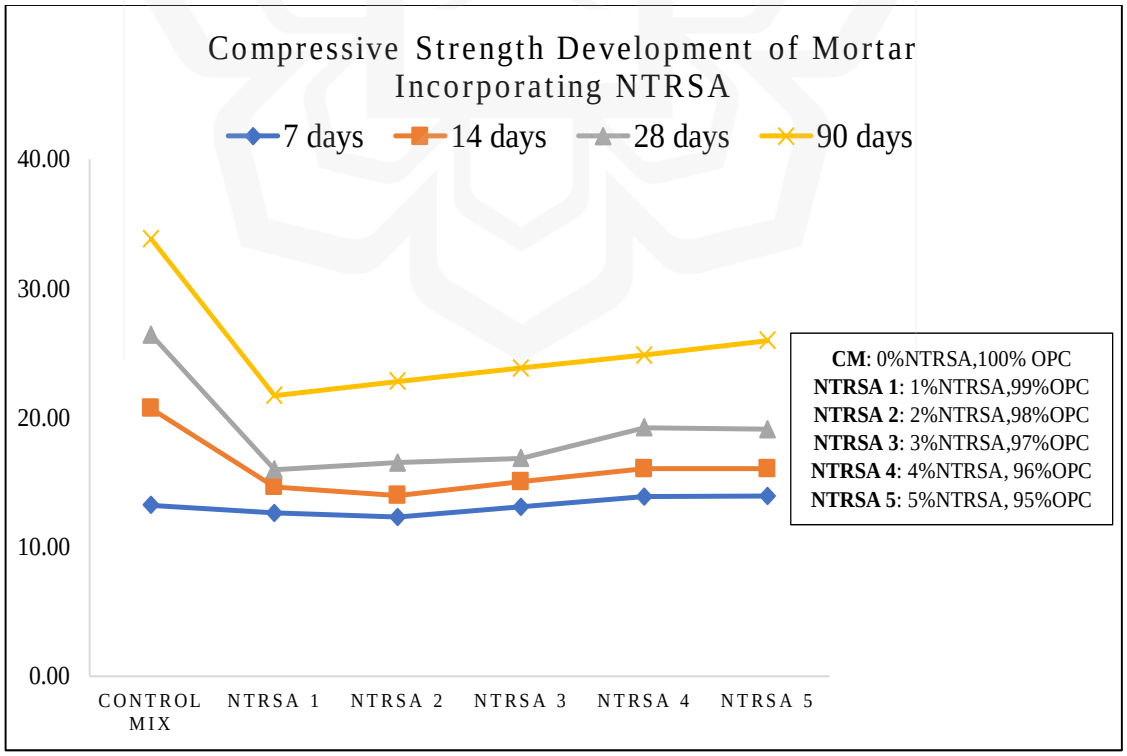

Figure 4.28 Compressive Strength Values for Mortar Incorporating NTRSA.

Overall, an optimum combination of involved factors in the thermochemical pretreatment and incineration process at the controlled temperature and continued with the grinding process efficiently produced a highly reactive TRSA. In addition, the cement mortar incorporating TRSA with amorphous silica has higher compressive strength throughout 90 days than NTRSA mortar. In conclusion, a small amount of 4% of TRSA is enough to boost the performance of the mortar. Based on previous researchers, 10% of RSA cement replacement exhibited good cement strength development without acid pretreatment process. (Vargas 2017, Munshi & Sharma 2019, Dabai & Muhammad 2017, Munshi 2013).

Therefore, acid pretreatment was removed the unwanted metallic impurities presence in the ash and improved the performance of TRSA based mortar. For this research, amount of silica produced in the TRSA at 4% was optimum to enhance the strength. Unlike other researchers, they needed 10% of RSA to replace cement in mortar in order to have a good development strength.

4.5.3 Interfacial Transitional Zone Analysis (ITZ) of Cement Mortar Incorporating Treated Rice Straw Ash (TRSA) and Non-Treated Rice Straw Ash (NTRSA)

The interfacial transitional zone (ITZ) is a gap between the cement paste and aggregates at which the microcrack usually occurs at first when the load is applied toward the mortar production (B. Singh et al., 2015). ITZ analysis is vital to support the mechanical properties of cement mortar incorporating TRSA and NTRSA. First, the small ITZ gap shows a strong bond between the aggregates and cement matrix paste formed in the mortar production. Then, it creates a high compression value. Table 4.11 tabulated the ITZ gap measured for the control mixture sample, NTRSA sample at 90 days, and TRSA sample at 90 days. Based on Table 4.11, the TRSA has the smallest ITZ gap with a value of 832 nm, while the ITZ gap of the control sample is the biggest, which is 2.544 µm. Therefore, it observes that the TRSA improves the gap of ITZ in cement mortar compared to NTRSA.

Table 4.11 Average ITZ Gap Measured for All Samples.

Sample	Average ITZ gap measured (μm)
Control mixture	2.544
TRSA	0.832
NTRSA	1.340

Furthermore, field emission scanning electron microscopy (FESEM) images, as shown in Figure 4.29 to Figure 4.31 illustrate the formation of the ITZ gap in the control mixture sample, TRSA and NTRSA, respectively. FESEM images illustrate a better illustration of the difference in the size of the gap for the control, TRSA, and NTRSA samples. The formation of pores at the ITZ gap of the control mixture sample and NTRSA sample cause weak ITZ, and in turn, the strength for both samples is lower than TRSA.

According to Xu et al. 2018, the minor ITZ gap causes to increase in the compression strength due to the formation of a strong bond between the aggregates and cement paste in the mortar. The dense ITZ formed in the mortar due to the fine particles of TRSA and its high pozzolanic reactivity. Supporting the finding on BET-SSA analysis, the TRSA has a smaller pore diameter than NTRSA. The pore diameter of TRSA is 75.8 nm, while NTRSA is 131.16 nm. Additionally, the high pozzolanic reactivity of TRSA in cement mortar was proved through the strength activity index (SAI) test, as analyzed in the previous section, where the pozzolanic reactivity of TRSA is higher than NTRSA and control mixture sample. The microstructure of the TRSA sample in Figure 4.30 is dense compared to the control mixture sample and NTRSA sample in Figure 4.31.

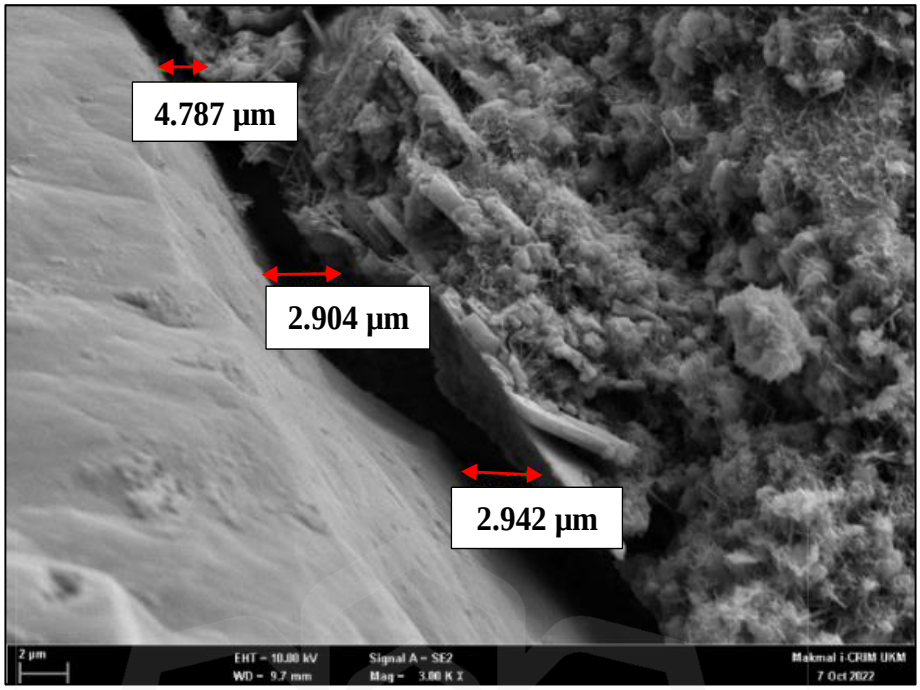

Figure 4.29 FESEM Image for ITZ Gap Measured of Control Mortar.

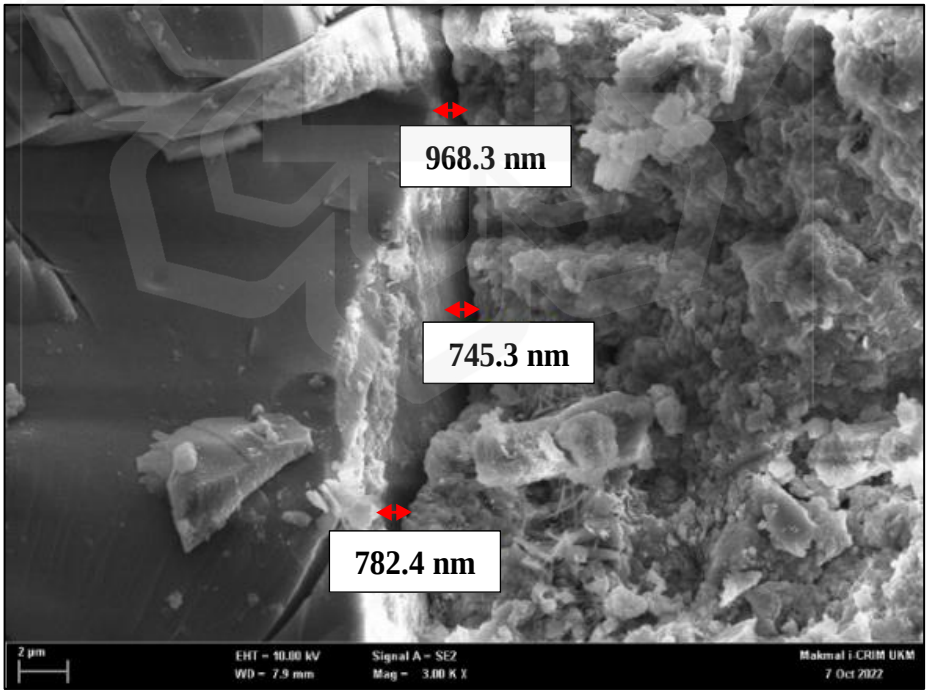

Figure 4.30 FESEM Image for ITZ Gap Measured of TRSA Mortar.

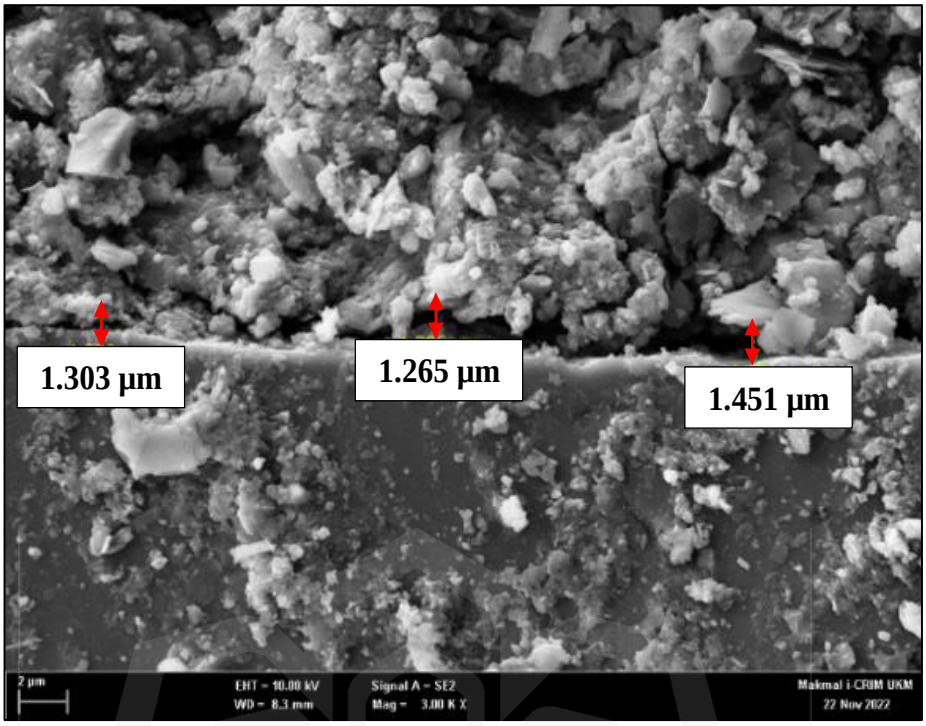

Figure 4.31 FESEM Image for ITZ Gap Measured of NTRSA Mortar.

4.5.4 Summary (Phase 4)

This subchapter presented detailed results on the pozzolanic reactivity analysis using the SAI method together with the performance of cement mortar incorporating TRSA and NTRSA as well as interfacial transitional zone (ITZ) analysis.

In conclusion, for the SAI test, all samples successfully fulfil the requirement of the standard of ASTM C311, which needs a minimum strength value of 75% for both SAI values at 7 and 28 days. The highest SAI value was obtained for the TRSA sample, 127.63% and 136.74% at 7 and 28 days, respectively. For the compressive strength of TRSA throughout 90 days, 5% of TRSA composition had the highest compressive value, 18.68 MPa at 7 days and 24.44 MPa at 14 days. However, the composition of 4% of TRSA showed the highest compressive strength value, which is 41.76 MPa at 28 days and 54.21 MPa at 90 days. On the other hand, all NTRSA samples showed poor performance of

compressive strength development throughout 90 days compared to the control mixture samples and TRSA samples. Lastly, for the ITZ analysis, the average ITZ gap measured for TRSA was the smallest, with a value of 832 nm.

CHAPTER FIVE

CONCLUSION AND RECOMMENDATIONS

5.1 CONCLUSION

This research focuses on producing a highly treated rice straw ash (TRSA) to partially replace cement in mortar through thermochemical pretreatment (phase 1), the incineration process at a controlled temperature, and the grinding process (phase 2). In phases 1 and 2, the percentage of reactive compound content in the TRSA was recorded to validate that the TRSA can be used as cement replacement material (CRM) based on ASTM C618, which required more than 70%. The reactive compound contents are silicon dioxide (SiO_2), aluminium oxide (Al_2O_3), and iron (III) oxide (Fe_2O_3). First, the optimization was analyzed for phases 1 and 2 to select the best combination of parameters involved in the thermochemical pretreatment and incineration processes. Then, the TRSA continued the grinding process using the planetary ball mill. Finally, the TRSA was prepared using those parameters in phases 1 and 2 for analysis of characterization and mechanical properties of TRSA in phase 3 and phase 4, respectively. Based on results obtained from phases 3 and 4, the following paragraphs in this part are explained according to the research objectives.

The first objective of this research was to establish the effect of the pretreatment and incineration process using a low concentration of acid on reactive compound content in TRSA. This objective was achieved through phases 1 and 2. As described in the previous chapter, a highly reactive TRSA was successfully produced using a low concentration of hydrochloric acid (HCl) in the thermochemical pretreatment and incineration process at a controlled temperature. The thermochemical pretreatment process was conducted based on the optimum values of involved factors, which are 0.06 M of HCl concentration, 2 hours of soaking duration and 70°C soaking temperature. Like the pretreatment process, the

incineration process was performed using optimum values of involved factors, 600°C burning temperature and 1 hour burning duration. As a result, the total percentage of reactive compound content was effectively enhanced in the rice straw. It was recorded at 99.60% for the thermochemical pretreatment process and 98.70% for the incineration process. The TRSA produced in this research met the requirement specified by the standard ASTM C618, which is more than 70% to be used as CRM in mortar production.

Moreover, the second objective of this research was to determine the characteristics of TRSA and non-TRSA (NTRSA). The second objective was achieved in phase 3. As discussed in chapter 4, TRSA was proved to be in the amorphous state as illustrated in x-ray diffraction (XRD) analysis and becomes a good pozzolanic material and creates an excellent pozzolanic reaction in developing the mortar strength. The Fourier transforms infrared spectroscopy (FTIR) analysis also proved the presence of essential function groups contributing to the amorphous state in the TRSA. At the same time, the NTRSA's carbonyl bond formed through unburnt carbon also disturbed the performance of NTRSA mortar. The high amorphous silica produced in TRSA had confirmed through transmission electron microscopy (TEM) analysis, whereby there was amorphous silica instead of crystalline. When there was no crystalline formation, it showed the indication of amorphous silica. The crystalline formation has been recorded in the TEM analysis of NTRSA. TEM analysis also recorded that the size of TRSA particles is more petite than NTRSA. The size of TRSA was between 4.505 nm to 6.278 nm. Thus, the TRSA had a high specific surface area (SSA), 296.58m^2/g, compared to NTRSA, 16.35m^2/g, as analyzed through BET-SSA analysis. When the particle size is small, the SSA value is high. The nano-sized ashes have filled the void formed in a mortar and reduced the porosity of the mortar. Thus, the performance of concrete-based pozzolan material is excellent. The FESEM image of TRSA (Figure 4.22) illustrated that it had smaller particles than NTRSA, even though there was no grinding aid. The structure of TRSA particles looked softer than NTRSA because of the effective acid treatment.

Furthermore, the third objective of this research was to evaluate the mechanical properties of cement mortar incorporating TRSA. The third objective was achieved in phase 4. For the mechanical properties of TRSA-based mortar, all samples achieved the requirement of the standard of ASTM C311, which has a minimum strength needs a value of 75% for both SAI values at 7 and 28 days. The highest SAI value was obtained for the TRSA sample, 127.63% and 136.74% at 7 and 28 days, respectively. For the compression test, the cement mortar incorporating 4% of TRSA showed an excellent performance in developing the mortar strength throughout 90 days and improved by 60.27% strength compared to the control and NTRSA samples. Lastly, the TRSA also improved the ITZ gap, as the size of the ITZ gap is nano-sized and recorded as the smallest gap.

In conclusion, all objectives in this research were achieved. A highly reactive TRSA has been produced through a thermochemical pretreatment process, followed by an incineration process at a controlled temperature and continued with the grinding process. The TRSA is an excellent pozzolanic material with high amorphous silica and produces a high pozzolanic reaction, as examined through the SAI test. The percentage of SAI values for TRSA successfully fulfills the requirement in the standard of ASTM C311, which needs 75% of SAI value at the 7 and 28 days of mortar age. Then, the 4% of TRSA is sufficient to replace cement in mortar production that improved by 60.27% of compressive strength throughout 90 days. A small amount of TRSA gives a mighty improvement in mortar production.

5.2 RECOMMENDATION AND FUTURE WORKS

Although all objectives were achieved in this research, there are still many gaps to identify for future work. The treated rice straw ash (TRSA) is recommended for further study as a sole binder in cementless mortar (geopolymer) production since it has high amorphous silica and similar pozzolanic properties to cement. For the optimization analysis of the thermochemical pretreatment process and the incineration process, the impurities that

disturb the performance of TRSA as pozzolan must be established through the atomic absorption spectrophotometer (AAS) test. In addition, the compressive strength development of TRSA-based mortar is suggested to be recorded over a year to identify its durability and sustainability. Lastly, conducting the flexural and tensile tests is also recommended to obtain the effect of TRSA in the cement mortar after applying those tests.

REFERENCES

Abdel-Shafy, H. I., & Mansour, M. S. M. (2018). Solid waste issue: sources, composition, disposal, recycling, and valorization. *Egyptian Journal of Petroleum*, *27*(4), 12751290.

Abdulmatin, A., Tangchirapat, W., & Jaturapitakkul, C. (2018). An investigation of bottom ash as a pozzolanic material. *Construction and Building Materials*, *186*, 155–162.

Agwa, I. S., Omar, O. M., Tayeh, B. A., & Abdelsalam, B. A. (2020). Effects of using rice straw and cotton stalk ashes on the properties of lightweight self-compacting concrete. *Construction and Building Materials*, *235*, 117541.

Ahmed, I. I., Adebisi, J. A., Agunsoye, J. O., Bello, S. A., Ramakokovhu, M. M., Daramola, M. O., & Hassan, S. B. (2020). Optimisation of acid pre-treatment parameters in silica extraction process from cassava periderm. *Materials Today: Proceedings*, *38*, 749–755.

Alothman, Z. A. (2012). A review: fundamental aspects of silicate mesoporous materials. *Materials*, *5*(12), 2874–2902.

Amibo, T. A., Beyan, S. M., & Damite, T. M. (2022). Production and optimization of bio-based silica nanoparticle from teff straw (eragrostis tef) using RSM-based modeling, characterization aspects, and adsorption efficacy of methyl orange dye. *Journal of Chemistry*, *2022*.

Antiohos, S. K., Papadakis, V. G., & Tsimas, S. (2014). Rice husk ash (RHA) effectiveness in cement and concrete as a function of reactive silica and fineness. *Cement and Concrete Research*, *61–62*, 20–27.

ASTM C109/C109M. (2021). Standard Test Method for Compressive Strength of Hydraulic Cement Mortars (Using 2-in. or [50 mm] Cube Specimens). American Society for Testing and Materials

ASTM C136/C136M. (2023). Standard Test Method for Sieve Analysis of Fine and Coarse Aggregates. American Society for Testing and Materials

ASTM C150. (2010). ASTM C 150/ C150M-15 Standard Specification for Portland Cement. American Society for Testing and Materials

ASTM C1732. (2010). StandardGuide for Examination of Hardened Concrete Using Scanning Electron Microscopy Specification. American Society for Testing and Materials

ASTM C311. (2005). Standard Test Methods for Sampling and Testing Fly Ash or Natural Pozzolans for Use in Portland Cement Concrete. American Society for Testing and Materials

ASTM C451. (2023).Standard Test for Early Stiffening of Hydraulic Cement (Paste Method). American Society for Testing and Materials

ASTM C618. (2014). Standard Specification for Coal Fly Ash and Raw or Calcined Natural Pozzolan for Use in Concrete. American Society for Testing and Materials

ASTM E168. (2016). Standard Practices For General Techniques of Infrared Quantitative Analysis. American Society for Testing and Materials

Ataie, F. F., & Riding, K. A. (2013). Thermochemical pretreatments for agricultural residue ash production for concrete. *Journal of Materials in Civil Engineering*, *25*(11), 1703–1711.

Ataie, F. F., & Riding, K. A. (2016). Influence of agricultural residue ash on early cement hydration and chemical admixtures adsorption. *Construction and Building Materials*, *106*, 274–281.

Athira, G., Bahurudeen, A., & Appari, S. (2019). Sustainable alternatives to carbon intensive paddy field burning in India: a framework for cleaner production in agriculture, energy, and construction industries. *Journal of Cleaner Production*, *236*, 117598.

Bazargan, A., Bazargan, M., & McKay, G. (2015). Optimization of rice husk pretreatment for energy production. *Renewable Energy*, *77*, 512–520.

Beidaghy Dizaji, H., Zeng, T., Hartmann, I., Enke, D., Schliermann, T., Lenz, V., & Bidabadi, M. (2019). Generation of high quality biogenic silica by combustion of rice husk and rice straw combined with pre- and post-treatment strategies-a review. *Applied Sciences*, *9*(6), 1083.

Benhelal, E., Shamsaei, E., & Rashid, M. I. (2021). Challenges against CO2 abatement strategies in cement industry: a review. *Journal of Environmental Sciences (China)*, *104*, 84–101.

Bhattacharyya, P., Bhaduri, D., Adak, T., Munda, S., Satapathy, B. S., Dash, P. K., Padhy, S. R., Pattanayak, A., Routray, S., Chakraborti, M., Baig, M. J., Mukherjee, A. K., Nayak, A. K., & Pathak, H. (2020). Characterization of rice straw from major cultivars for best alternative industrial uses to cutoff the menace of straw burning. *Industrial Crops and Products*, *143*, 111919.

Bibi, T., Ali, A., Zhang, J., Naseer, A., & Islam, S. U. (2020). Microscopic analysis of the deleterious effects of ammonium nitrate fertilizer on concrete. *Construction and Building Materials*, *249*, 118716.

Bie, R. S., Song, X. F., Liu, Q. Q., Ji, X. Y., & Chen, P. (2015). Studies on effects of burning conditions and rice husk ash (RHA) blending amount on the mechanical behavior of cement. *Cement and Concrete Composites*, *55*, 162–168.

BS EN 196-1. (2005). Methods of testing cement. Determination of strength. British Standards Institution, UK.

BS EN 13925-1. (2003). Non-destructive testing. X-Ray diffraction from polycrystalline and amorphous materials. British Standards Institution, UK.

BS 1881-119. (2011). Testing concrete - Method for determination of compressive strength using portions of beams broken in flexure (equivalent cube method). British Standards

Institution, UK.

BS 5628-1. (2005). Code of practice for use of masonry. British Standards Institution, UK.

BS 8615-2. (2019). Specification for pozzolanic materials for use with Portland cement High reactivity natural calcined pozzolana. British Standards Institution, UK.

Chen, H., Wang, W., Martin, J. C., Oliphant, A. J., Doerr, P. A., Xu, J. F., DeBorn, K. M., Chen, C., & Sun, L. (2013). Extraction of lignocellulose and synthesis of porous silica nanoparticles from rice husks: a comprehensive utilization of rice husk biomass. *ACS Sustainable Chemistry and Engineering*, *1*(2), 254–259.

Clifford, C. A., Stinz, M., Hodoroaba, V. D., Unger, W. E. S., & Fujimoto, T. (2019). International standards in nanotechnologies. In *Characterization of Nanoparticles: Measurement Processes for Nanoparticles*. Elsevier Inc.

Dabai, M. U., & Muhammad, M. (2017). Studies on the effect of rice straw ash as admixture of ordinary portland cement mortar. *IJISET—International Journal of Innovative Science, Engineering & Technology*, *4*(7), 112–119.

Das, B. B., Gomez, C. P., & Mohapatra, B. G. (2020). Recent developments in sustainable infrastructure. *International Conference on Recent Developments in Sustainable Infrastructure (ICRDSI-2020)*.

Dizaji, H. B., Zeng, T., Hölzig, H., Bauer, J., Klöß, G., & Enke, D. (2022). Ash transformation mechanism during combustion of rice husk and rice straw. *Fuel*, *307*, 121768.

Donatello, S., Tyrer, M., & Cheeseman, C. R. (2010). Comparison of test methods to assess pozzolanic activity. *Cement and Concrete Composites*, *32*(2), 121–127.

Dunuweera, S. P., & Rajapakse, R. M. G. (2018). Cement types, composition, uses and advantages of nanocement, environmental impact on cement production, and possible solutions. *Advances in Materials Science and Engineering*, *2018*.

El-Sayed, T. A., Erfan, A. M., & Abd El-Naby, R. M. (2017). Influence of rice, wheat straw ash and rice husk ash on the properties of concrete mixes. *Jokull*, *67*(5), 103–119.

Embong, R., Shafiq, N., Kusbiantoro, A., & Nuruddin, M. F. (2016). Effectiveness of low-concentration acid and solar drying as pre-treatment features for producing pozzolanic sugarcane bagasse ash. *Journal of Cleaner Production*, *112*, 953–962.

Farirai, F., Daramola, M. O., & Mupa, M. (2020). *Production of nano silicon particles from sugarcane bagasse ash for solar cell application*. University of the Witwatersrand, Johanesburg.

Golewski, G. L. (2018). Evaluation of morphology and size of cracks of the interfacial transition zone (ITZ) in concrete containing fly ash (FA). *Journal of Hazardous Materials*, *357*, 298–304.

Goodman, B. A. (2020). Utilization of waste straw and husks from rice production: a review. *Journal of Bioresources and Bioproducts*, *5*(3), 143–162.

Gun, M., Arslan, H., Saleh, M., Yalvac, M., & Dizge, N. (2022). Optimization of silica extraction from rice husk using response surface methodology and adsorption of safranin dye. *International Journal of Environmental Research*, *16*(2), 1–13.

Gupta, G. K., & Shukla, P. (2020). Lignocellulosic biomass for the synthesis of nanocellulose and its eco-friendly advanced applications. *Frontiers in Chemistry*, *8*(December), 1–13.

He, Z., Zhu, X., Wang, J., Mu, M., & Wang, Y. (2019). Comparison of CO2 emissions from OPC and recycled cement production. *Construction and Building Materials*, *211*, 965–973.

Heikal, M., Abd El Aleem, S., & Morsi, W. M. (2013). Characteristics of blended cements containing nano-silica. *HBRC Journal*, *9*(3), 243–255.

Hela, R., & Orsakova, D. (2013). The mechanical activation of fly ash. *Procedia Engineering*, *65*, 87–93.

Hosseini, S. M., & Aziz, H. A. (2013). Evaluation of thermochemical pretreatment and continuous thermophilic condition in rice straw composting process enhancement. *Bioresource Technology*, *133*, 240–247.

Hu, L., He, Z., & Zhang, S. (2020). Sustainable use of rice husk ash in cement-based materials: Environmental evaluation and performance improvement. *Journal of Cleaner Production*, *264*, 121744.

Ibrahim, A. R., Roy, M. H., Ahmed, Z., & Imtiaz, G. (2010). An investigation of the status of the Malaysian construction industry. *Benchmarking: An International Journal*.

Indriani, D. W., & Wardhani, T. R. (2022). Modeling of extraction of silica rendemen husk rice (Oryza sativa l.) by microwave extraction assisted (MAE) using response surface methodology (RSM). *IOP Conference Series: Earth and Environmental Science*, *963*(1), 012048.

ISO 12677. (2015). Chemical Analysis of Refractory Products by X-Ray Flourescence (XRF) - Fused Cast-Bead Method. International Organization for Standardization.

ISO 25498. (2018). Microbeam Analysis. International Organization for Standardization.

ISO 9277. (2022). Determination of the specific surface area of solids by gas adsorption BET method. International Organization for Standardization.

Izevbekhai, O. U., Gitari, W. M., & Tavengwa, N. T. (2021). Optimization of silica extraction from diatomaceous earth using the central composite design of response surface methodology. *South African Journal of Chemistry*, *75*, 80–90.

Jaya, R. P., Yusak, M. I. M., Hainin, M. R., Mashros, N., Warid, M. N. M., Ali, M. I., & Ibrahim, M. H. W. (2019). Physical and chemical properties of cement with nano black rice husk ash. *AIP Conference Proceedings*, *2151*, 022004.

Jiang, J., Ren, Z., Ma, Z., Zhang, T., Zhang, P., Zhang, D. Z., & Mao, Z. (2020). Mechanical properties and microstructural evolution of TA15 Ti alloy processed by selective laser melting before and after annealing. *Materials Science and Engineering A*, *772*(October 2019), 138742.

John, J. P. (2020). Parametric studies of cement production processes. *Journal of Energy*, *2020*, 1–17.

Kalakada, Z., Doh, J. H., & Chowdhury, S. (2022). Glass powder as replacement of cement for concrete–an investigative study. *European Journal of Environmental and Civil Engineering*, *26*(3), 1046–1063.

Kamaruddin, M. A., Yusoff, M. S., Rui, L. M., Isa, A. M., Zawawi, M. H., & Alrozi, R. (2017). An overview of municipal solid waste management and landfill leachate treatment: Malaysia and Asian perspectives. *Environmental Science and Pollution Research*, *24*(35), 26988–27020.

Kang, S. H., Kwon, Y. H., Hong, S. G., Chun, S., & Moon, J. (2019). Hydrated lime activation on byproducts for eco-friendly production of structural mortars. *Journal of Cleaner Production*, *231*, 1389–1398.

Karim, M. R., Zain, M. F. M., Jamil, M., Lai, F. C., & Islam, M. N. (2012). Strength of mortar and concrete as influenced by rice husk ash: a review. *World Applied Sciences Journal*, *19*(10), 1501–1513.

Kasaniya, M., Thomas, M. D. A., & Moffatt, E. G. (2019). Development of rapid and reliable pozzolanic reactivity test method. *ACI Materials Journal*, *116*(4), 145–154.

Katare, V. D., & Madurwar, M. V. (2020). Design and investigation of sustainable pozzolanic material. *Journal of Cleaner Production*, *242*, 118431.

Kauldhar, B. S., & Yadav, S. K. (2018). Turning waste to wealth: a direct process for recovery of nano-silica and lignin from paddy straw agro-waste. *Journal of Cleaner Production*, *194*, 158–166.

Khan, K., Ullah, M. F., Shahzada, K., Amin, M. N., Bibi, T., Wahab, N., & Aljaafari, A. (2020). Effective use of micro-silica extracted from rice husk ash for the production of high-performance and sustainable cement mortar. *Construction and Building Materials*, *258*, 119589.

Khorsand, H., Kiayee, N., & Masoomparast, A. H. (2013). Optimization of amorphous silica nanoparticles synthesis from rice straw ash using design of experiments technique. *Particulate Science and Technology*, *31*(4), 366–371.

Kramar, S., & Ducman, V. (2018). Evaluation of ash pozzolanic activity by means of the strength activity index test, frattini test and DTA/TG analysis. *Tehnicki Vjesnik*, *25*(6), 1746–1752.

Kumar, B., & Pandey, A. (2014). Perspectives on use of rice straw ash for partial replacement of OPC in rigid pavements.

Kusbiantoro, A., Embong, R., & Shafiq, N. (2017). Adaptation of eco-friendly approach in the production of soluble pozzolanic material. *International Journal of Design and Nature and Ecodynamics*, *12*(2), 246–253. h

Lal, D., Chatterjee, A., & Dwivedi, A. (2019). Investigation of properties of cement mortar incorporating pond ash – an environmental sustainable material. *Construction and Building Materials*, *209*, 20–31.

Librea, J. T., Dacanay, F. D., Martin, Z. Z., & Diaz, L. L. (2019). Effect of water and acid pre-treatment on the physicochemical properties of rice husk for silica extraction. *IOP Conference Series: Materials Science and Engineering*, *540*(1), 012007.

Lu, P., & Hsieh, Y. Lo. (2012). Highly pure amorphous silica nano-disks from rice straw. *Powder Technology*, *225*, 149–155.

M.Z, Rosmiza, Rose, R. A. C., Mapjabil, J., & Marzuki, M. (2019). The potential of rice straw in agricultural activities in the MADA Region of Kedah, Malaysia. *International Journal of Asian Social Science*, *9*(4), 295–303.

Madurwar, M. V., Ralegaonkar, R. V., & Mandavgane, S. A. (2013). Application of agro-waste for sustainable construction materials: a review. *Construction and Building Materials*, *38*(2), 872–878.

Mahmuda, A. F., Tjaronge, M. W., & Amiruddin, A. A. (2020). The potential utilization of rice straw ash as cement replacement in mortar material. *IOP Conference Series: Earth and Environmental Science*, *419*(1), 012037.

Mangi, S. A., Ibrahim, M. H. W., Jamaluddin, N., Arshad, M. F., Memon, S. A., & Shahidan, S. (2019). Effects of grinding process on the properties of the coal bottom ash and cement paste. *Journal of Engineering and Technological Sciences*, *51*(1), 1–13.

Mast, J., Verleysen, E., Hodoroaba, V. D., & Kaegi, R. (2019). Characterization of nanomaterials by transmission electron microscopy: measurement procedures. In *Characterization of Nanoparticles: Measurement Processes for Nanoparticles*. Elsevier Inc.

Miller, S. A., Cunningham, P. R., & Harvey, J. T. (2019). Rice-based ash in concrete: a review of past work and potential environmental sustainability. *Resources, Conservation and Recycling*, *146*, 416–430.

Mohamad Bohari, A. A., Skitmore, M., Xia, B., Teo, M., Zhang, X., & Adham, K. N. (2015). The path towards greening the Malaysian construction industry. *Renewable and Sustainable Energy Reviews*, *52*, 1742–1748.

Mohamad Bohari, A. A., Skitmore, M., Xia, B., & Zhang, X. (2016). Insights into the adoption of green construction in Malaysia: The drivers and challenges. *Proceedings of the 7th Asia-Pacific International Conference on Environment-Behaviour Studies*, *1*(4), 45–53.

Morsy, M. I., & Rashwan, M. A. (2015). Replacement effect of cement by rice straw ash on cement mortar properties. *Misr Journal of Agricultural Engineering*, *32*(4), 1685–1708.

Muhammad, N. Z., Keyvanfar, A., Shafaghat, A., Majid, M. Z. A., Mirza, J., MCcaffer, R., & Aliyu, M. M. (2020). Optimization of nano silicon for integral mixing in cement mortar: a response surface methodology approach. *AIP Conference Proceedings*, *2284*(1), 020009.

Munshi, S., Dey, G., & Prasad Sharma, R. (2013). Use of rice straw ash as pozzolanic material in cement mortar. *IACSIT International Journal of Engineering and Technology*, *5*(5), 603–606.

Munshi, S., & Sharma, R. P. (2016). Experimental investigation on strength and water permeability of mortar incorporate with rice straw ash. *Advances in Materials Science and Engineering*, *2016*.

Munshi, S., & Sharma, R. P. (2018). Investigation on the pozzolanic properties of rice straw ash prepared at different temperatures. *Materials Express*, *8*(2), 157–164.

Munshi, S., & Sharma, R. P. (2019). Utilization of rice straw ash as a mineral admixture in construction work. *Materials Today: Proceedings*, *11*, 637–644.

Nagashree, B., Kishore, V., & Malathi, M. (2017). Studies on geopolymerisation Reaction using synthesised activators. *International Journal of Innovative Research in Science, Engineering and Technology*, *6*(11).

Naveed, S. K., & Sharma, T. (2020). Utilization of rice straw ash in mortar mixes : a review. *International Research Journal of Engineering and Technology (IRJET)*, *7*(2), 1156–1160.

Nayak, P. P., & Datta, A. K. (2021). Synthesis of SiO2-nanoparticles from rice husk ash and its comparison with commercial amorphous silica through material characterization. *Silicon*, *13*(4), 1209–1214.

Nazopatul, P. H., Irmansyah, & Irzaman. (2018). Extraction and characterization of silicon dioxide from rice straw. *IOP Conference Series: Earth and Environmental Science*, *209*(1), 012013.

Obi, F. O., Ugwuishiwu, B. O., & Nwakaire, J. N. (2016). Agricultural waste concept , Generation , utilization and management. *Nigerian Journal of Technology (NIJOTECH)*, *35*(4), 957–964.

Oladosu, Y., Rafii, M. Y., Abdullah, N., Magaji, U., Hussin, G., Ramli, A., & Miah, G. (2016). Fermentation quality and additives: a case of rice straw silage. *BioMed Research International*, *2016*.

Olonade, K. A., Jaji, M. B., & Adekitan, O. A. (2017). Experimental comparison of selected pozzolanic materials. *African Journal of Science, Technology, Innovation and Development*, *9*(4), 381–385.

Onat, N. C., & Kucukvar, M. (2020). Carbon footprint of construction industry: a global review and supply chain analysis. *Renewable and Sustainable Energy Reviews*, *124*, 109783.

Pandey, A., & Kumar, B. (2019a). Effects of rice straw ash and micro silica on mechanical properties of pavement quality concrete. *Journal of Building Engineering*, *26*, 100889.

Pandey, A., & Kumar, B. (2019b). Preliminary study of cement paste admixed with rice straw ash, microsilica and rice straw ash-microsilica composite. *International Journal of Recent Technology and Engineering*, *7*(5), 302–307.

Parande, A. K., Stalin, K., Thangarajan, R. K., & Karthikeyan, M. S. (2011). Utilization of agroresidual waste in effective blending in portland cement. *International Scholarly Research Notices*, *2011*.

Philip, A., & Mathew, A. (2016). Experimental study on mechanical properties of geopolymer concrete using GGBS. *International Journal of Science and Research (IJSR)*, *5*(5), 2465–2468.

Pontes, J., Santos Silva, A., & Faria, P. (2013). Evaluation of pozzolanic reactivity of artificial pozzolans. *Materials Science Forum*, *730*, 433–438.

Qudoos, A., Kim, H. G., Atta-ur-Rehman, Jeon, I. K., & Ryou, J. (2019). Influence of the particle size of wheat straw ash on the microstructure of the interfacial transition zone. *Powder Technology*, *352*, 453–461.

Qudoos, A., Kim, H. G., Atta-ur-Rehman, & Ryou, J. S. (2018). Effect of mechanical processing on the pozzolanic efficiency and the microstructure development of wheat straw ash blended cement composites. *Construction and Building Materials*, *193*, 481–490.

Raheem, A. A., & Kareem, M. A. (2017a). Chemical composition and physical characteristics of rice husk ash blended cement. *International Journal of Engineering Research in Africa*, *32*, 25–35.

Raheem, A. A., & Kareem, M. A. (2017b). Optimal raw material mix for the production of rice husk ash blended cement. *International Journal of Sustainable Construction Engineering & Technology*, *7*(2), 77–93.

Rahmi, Lubis, S., Az-Zahra, N., Puspita, K., & Iqhrammullah, M. (2021). Synergetic photocatalytic and adsorptive removals of metanil yellow using TiO2/grass-derived cellulose/chitosan film composite. *International Journal of Engineering*, *34*(8), 1827–1836.

Rajan, R., Zakaria, Y., Shamsuddin, S., & Hassan, N. F. N. (2020). Morphological and compositional changes exhibited by rice husk when subjected to synergistic thermochemical treatments. *Malaysian Journal of Medicine and Health Sciences*, *16*, 1–7.

Rodier, L., Bilba, K., Onesippe, C., & Arsene, M. . (2017). Study of pozzolanic activity of bamboo stem ashes for use as partial replacement of cement. *Materials and Structures*, *50*(1), 1–14.

Roselló, J., Soriano, L., Santamarina, M. P., Akasaki, J. L., Monzó, J., & Payá, J. (2017). Rice straw ash: a potential pozzolanic supplementary material for cementing systems. *Industrial Crops and Products*, *103*, 39–50.

Rosman, M., Suffian, M. Z. A., Marha, Y. N., Sakinah, M. Z., & Mariam, R. B. R. (2018). Moderating effect of innovation on human capital and small firm performance in construction industry: the Malaysia case. *Journal of Fundamental and Applied Sciences*, *10*(1S), 772–792.

Saad, S. A., Jamaluddin, A. N., Masjuki, S. A., Beddu, S., & Shafiq, N. (2022). Influences of grinding process on the physical and morphological characteristics of ultrafine treated rice husk ash. *GEOMATE Journal*, *23*(97), 74–81.

Saad, S. A., Nuruddin, M. F., Shafiq, N., & Ali, M. (2015). Pozzolanic reaction mechanism of rice husk ash in concrete – a review. *Applied Mechanics and Materials, 773*, 1143–1147.

Saad, S. A., Nuruddin, M. F., Shafiq, N., & Ali, M. (2016). The Effect of incineration temperature to the chemical and physical properties of ultrafine treated rice husk ash (UFTRHA) as supplementary cementing Material (SCM). *Procedia Engineering*, *148*, 163–167.

Sadef, Y., Nizami, A. S., Batool, S. A., Chaudary, M. N., Ouda, O. K. M., Asam, Z. Z., Habib, K., Rehan, M., & Demirbas, A. (2016). Waste-to-energy and recycling value for developing integrated solid waste management plan in Lahore. *Energy Sources, Part B: Economics, Planning and Policy*, *11*(7), 569–579.

Saleh, F., Prayuda, H., Monika, F., & Pratama, M. M. A. (2019). Characteristics comparison on mechanical properties of mortars using agriculture waste as a cement replacement materials. *IOP Conference Series: Materials Science and Engineering*, *650*, 012039.

Samah, M. A. A., Victor, D., Dawda, B., Abd Manaf, L., Ismail, S. N. S., Abd Hamid, K. B., Yunus, K., & Kamarudin, M. K. A. (2018). Composition and generation of municipal solid waste (MSW) in Malaysia: Balakong city case study. *Journal of Chemical Information and Modeling*, *3*, 1325–1331.

Sankar, S., Sharma, S. K., Kaur, N., Lee, B., Kim, D. Y., Lee, S., & Jung, H. (2016). Biogenerated silica nanoparticles synthesized from sticky, red, and brown rice husk

ashes by a chemical method. *Ceramics International*, *42*(4), 4875–4885.

Shamsudin, R., & Vincent, C. J. (2020). Agricultural and food industries in Malaysia. *Advances in Agricultural and Food Research Journal*, *1*(1), 1–4.

Singh, B., Ishwarya, G., Gupta, M., & Bhattacharyya, S. K. (2015). Geopolymer concrete: a review of some recent developments. *Construction and Building Materials*, *85*, 78–90.

Singh, L. P., Karade, S. R., Bhattacharyya, S. K., Yousuf, M. M., & Ahalawat, S. (2013). Beneficial role of nanosilica in cement based materials - a review. *Construction and Building Materials*, *47*, 1069–1077.

Singh, N. B., Kalra, M., & Saxena, S. K. (2017). Nanoscience of cement and concrete. *Materials Today: Proceedings*, *4*(4), 5478–5487.

Singh, N. B., & Middendorf, B. (2020). Geopolymers as an alternative to portland cement: an overview. *Construction and Building Materials*, *237*, 117455.

Subashi De Silva, G. H. M. J., & Priyamali, M. W. S. (2020). Potential use of waste rice husk ash for concrete paving blocks: strength, durability, and run-off properties. *International Journal of Pavement Engineering*, 1–13.

Thakur, M., Sharma, A., Ahlawat, V., Bhattacharya, M., & Goswami, S. (2020). Process optimization for the production of cellulose nanocrystals from rice straw derived α-cellulose. *Materials Science for Energy Technologies*, *3*, 328–334.

Turner, L. K., & Collins, F. G. (2013). Carbon dioxide equivalent (CO2-e) emissions: a comparison between geopolymer and OPC cement concrete. *Construction and Building Materials*, *43*, 125–130.

Uda, M. N. A., Gopinath, S. C. B., Hashim, U., Halim, N. H., Parmin, N. A., Uda, M. N. A., & Anbu, P. (2021). Production and characterization of graphene from carbonaceous rice straw by cost-effect extraction. *3 Biotech*, *11*(5), 1–11.

Uda, M. N. A., Gopinath, S. C. B., Hashim, U., Uda, M. N. A., Parmin, N. A., Halim, N. H., & Anbu, P. (2020). Novelty studies on amorphous silica nanoparticle production from rice straw ash. *IOP Conference Series: Materials Science and Engineering*, *864*(1), 012021.

Umeda, J., & Kondoh, K. (2010). High-purification of amorphous silica originated from rice husks by combination of polysaccharide hydrolysis and metallic impurities removal. *Industrial Crops and Products*, *32*(3), 539–544.

Uwasu, M., Hara, K., & Yabar, H. (2014). World cement production and environmental implications. *Environmental Development*, *10*, 36–47.

Van, V. T. A., Rößler, C., Bui, D. D., & Ludwig, H. M. (2013). Mesoporous structure and pozzolanic reactivity of rice husk ash in cementitious system. *Construction and Building Materials*, *43*, 208–216.

Vargas, P., Restrepo-Baena, O., & Tobón, J. I. (2017). Microstructural analysis of interfacial transition zone (ITZ) and its impact on the compressive strength of lightweight concretes. *Construction and Building Materials*, *137*, 381–389.

Vayghan, A. G., Khaloo, A. R., & Rajabipour, F. (2013). The effects of a hydrochloric acid pre-treatment on the physicochemical properties and pozzolanic performance of rice husk ash. *Cement and Concrete Composites*, *39*, 131–140.

Venkatanarayanan, H. K., & Rangaraju, P. R. (2013). Material characterization studies on low- and high-carbon rice husk ash and their performance in portland cement mixtures. *Advances in Civil Engineering Materials*, *2*(1), 266–287.

Venkatanarayanan, H. K., & Rangaraju, P. R. (2015). Effect of grinding of low-carbon rice husk ash on the microstructure and performance properties of blended cement concrete. *Cement and Concrete Composites*, *55*, 348–363.

Venkatesan, R. P., & Pazhani, K. C. (2016). Strength and durability properties of geopolymer concrete made with ground granulated blast furnace slag and black rice husk ash.

KSCE Journal of Civil Engineering, *20*(6), 2384–2391.

Vieira, A. P., Toledo Filho, R. D., Tavares, L. M., & Cordeiro, G. C. (2020). Effect of particle size, porous structure and content of rice husk ash on the hydration process and compressive strength evolution of concrete. *Construction and Building Materials*, *236*, 117553.

Villca, A. R., Soriano, L., Font, A., Tashima, M. M., Monzó, J., Victoria Borrachero, M., & Payá, J. (2021). Lime/pozzolan/geopolymer systems: performance in pastes and mortars. *Construction and Building Materials*, *276*, 122208.

Wang, W., Martin, J. C., Fan, X., Han, A., Luo, Z., & Sun, L. (2012). Silica nanoparticles and frameworks from rice husk biomass. *ACS Applied Materials and Interfaces*, *4*(2), 977–981.

Wansom, S., Janjaturaphan, S., & Sinthupinyo, S. (2010). Cement and concrete research characterizing pozzolanic activity of rice husk ash by impedance spectroscopy. *Cement and Concrete Research*, *40*(12), 1714–1722.

Wong, Y. S., Kwan, W. H., & Lim, M. (2019). Enhancing pozzolanic properties of rice husk ash using acid leaching treatment. *AIP Conference Proceedings*, *2157*(1), 020027.

Xu, Q., Ji, T., Gao, S. J., Yang, Z., & Wu, N. (2018). Characteristics and applications of sugar cane bagasse ash waste in cementitious materials. *Materials*, *12*(1), 39.

Xu, W., Lo, T. Y., & Memon, S. A. (2012). Microstructure and reactivity of rich husk ash. *Construction and Building Materials*, *29*, 541–547.

Xu, W., Lo, Y. T., Ouyang, D., Memon, S. A., Xing, F., Wang, W., & Yuan, X. (2015). Effect of rice husk ash fineness on porosity and hydration reaction of blended cement paste. *Construction and Building Materials*, *89*, 90–101.

Xu, W., Wei, J., Chen, J., Zhang, B., Xu, P., Ren, J., & Yu, Q. (2018). Comparative study of water-leaching and acid-leaching pretreatment on the thermal stability and reactivity of biomass silica for viability as a pozzolanic additive in cement. *Materials*, *11*(9),

1697.

Yadav, A. L., Sairam, V., Muruganandam, L., & Srinivasan, K. (2020). An overview of the influences of mechanical and chemical processing on sugarcane bagasse ash characterisation as a supplementary cementitious material. *Journal of Cleaner Production*, *245*, 118854.

Yang, H., Monasterio, M., Zheng, D., Cui, H., Tang, W., Bao, X., & Chen, X. (2021). Effects of nano silica on the properties of cement-based materials: a comprehensive review. *Construction and Building Materials*, *282*, 122715.

Yao, X., Xu, K., & Liang, Y. (2016). Comparing the thermo-physical properties of rice husk and rice straw as feedstock for thermochemical conversion and characterization of their waste ashes from combustion. *BioResources*, *11*(4), 10549–10564.

Zahib, Z. M., Kamaruddin, K., & Saman, H. (2018). Strength performance of blended ash based geopolymer mortar. *E3S Web of Conferences*, *34*, 01016.

Záleská, M., Pavlíková, M., Pavlík, Z., Jankovský, O., Pokorný, J., Tydlitát, V., Svora, P., & Černý, R. (2018). Physical and chemical characterization of technogenic pozzolans for the application in blended cements. *Construction and Building Materials*, *160*, 106–116.

Zareei, S. A., Ameri, F., Dorostkar, F., & Ahmadi, M. (2017). Rice husk ash as a partial replacement of cement in high strength concrete containing micro silica: evaluating durability and mechanical properties. *Case Studies in Construction Materials*, *7*, 73–81.

Zolgharnein, J., Shahmoradi, A., & Ghasemi, J. B. (2013). Comparative study of box-behnken, central composite, and doehlert matrix for multivariate optimization of Pb (II) adsorption onto robinia tree leaves. *Journal of Chemometrics*, *27*(1–2), 12–20.

APPENDIX I

LIST OF PUBLICATION AND ACHIEVEMENTS

JOURNAL PUBLICATION

1. Title: Influences of Grinding Process on the Physical and Morphological Characteristics of Ultrafine Treated Rice Husk Ash
   - Published in Geomate Journal in September 2022, volume 23, issue 97, pp 74-81.
   - Retrieved from https://geomatejournal.com/geomate/article/view/3117

CONFERENCES ATTENDED

1. 11th International Conference on Geotechnique, Construction Materials and Environment, 3-5 November 2021, Kyoto, Japan (virtual presentation)
   Title: Grinding Process Influences to the Physical and Morphological Characteristics of Ultrafine Treated Rice Husk Ash (UFTRHA) as Reactive Mineral Additive Construction Material.

2. 10th Awam International Conference on Civil Engineering (AICCE'22), 15-17 February 2022, USM Penang, Malaysia (virtual presentation)
   Title: Compressive Strength Development and Homogeneity of Concrete Incorporating Fly Ash and Used Engine Oil as Chemical Admixture.

3. 1st International Conference on Civil Engineering (ICCE'22), 9-10 August 2022, IIUM Gombak, Selangor (virtual presentation)

Title: Physical and Mechanical Properties of Green Cementless Mortar Incorporating Wastepaper Sludge Ash

Title: Response Surface Methodology Approaches in Producing Amorphous Silica from Rice Straw Ash.

ACHIEVEMENTS

1. Participated in Kulliyyah of Engineering Research, Innovation and Commercialisation Exhibition (KERICE) 2020, 8 December 2020, International Islamic University Malaysia (IIUM) – Awarded with Silver Medal

2. Participated in Innovation Week (InNow 2022), 1-2 November 2022, Universiti Tun Hussein Onn Malaysia (UTHM) – Awarded with Silver Medal

3. Participated in research video competition Kulliyyah of Engineering International Islamic University Malaysia (IIUM) 2022 – Awarded 1st place

4. Participated in Kulliyyah of Engineering Research, Innovation and Commercialisation Exhibition (KERICE) 2022, 22 December 2022, International Islamic University Malaysia (IIUM) – Awarded with Silver Medal